LA-UR-92-331

C.1

LA-UR-92-331

Title: Safety-Related Aspects of Nuclear Fission

Author(s): Andre Michaudon

Submitted to: Workshop on Computation and Analysis of Nuclear Data Relevant to Nuclear Energy and Safety

TABLE OF CONTENTS

SAFETY-RELATED ASPECTS OF NUCLEAR FISSION

Workshop on Computation and Analysis of Nuclear Data
Relevant to Nuclear Energy and Safety
(Trieste, Italy, February 10 - March 13, 1992)

by

A. Michaudon
Los Alamos National Laboratory, Los Alamos, NM, U.S.
and
Institut Laue Langevin, Grenoble, France

ABSTRACT

The subject of this set of lectures is nuclear fission. A brief description of nuclear fission is made at the beginning of these lectures. This description is followed by the study of several aspects of nuclear fission that are related to the safety of nuclear reactors. This study includes the temperature dependence of the reactivity of fast breeders and pressurized-water reactors and the role played in this respect by the low-energy neutron-induced fission cross section of ^{235}U and the fission cross section of ^{239}Pu. Finally, the properties of the fission products are reviewed with the consequences for the knowledge of the decay heat and the delayed-neutron properties.

I. INTRODUCTION

Nuclear fission is certainly one of the most significant scientific discoveries that had a great impact on society because the enormous energy release that this process provides can be used for very important civilian and military applications. The importance of these applications was realized shortly after the discovery of fission in 1938 and stimulated many studies, most of which were kept secret for a long time because of the key role played by fission in nuclear weapons. But fission is also a very complex phenomenon worth studying in itself because it gives access to unusual properties of nuclear matter. The properties of fission were reviewed recently at various conferences held to celebrate the fiftieth anniversary of the

discovery of this nuclear process. The vast amount of information gathered on this occasion can be found in the proceedings of these conferences ([Gau 88], [HKO 89], [BC 89], [Len 89]). Although the properties of nuclear fission are known sufficiently well for the safe production and use of nuclear energy, not all aspects of the process of nuclear fission itself are understood. This still imperfect basic knowledge of fission is due to the extreme complexity of this process, which involves a wide range of deformations of nuclear matter from near sphericity to extreme deformations that culminate in the breaking of the nucleus into two fragments.

These few lectures have the limited goal of focusing only on some safety-related aspects of fission. Nevertheless, Chap. II gives a brief general presentation of fission, with some basic definitions, before treating more specialized aspects of this nuclear process. A somewhat arbitrary selection of these aspects is made in the rest of these lectures. The Doppler effect, which is an important aspect of the safety of fast breeders, is treated in Chap. III. The ^{239}Pu fission cross section, which plays an important role in the safety of fast breeders, is discussed in Chap. IV. The influence of temperature on the reactivity of pressurized-water reactors (PWRs), which depends on the behavior at low neutron energy of the fission cross section and of the number η of fission neutrons per absorbed incident neutron for ^{235}U, is discussed in Chap. V. Some properties of the fission products also play an important role in nuclear safety in case of a shutdown of a nuclear reactor. For this reason, the yields of fission products are discussed first in Chap. VI. Then the decay heat, which is generated in the irradiated nuclear fuel by these fission products when the nuclear reactor is shutdown, is treated in Chap. VII. In the same manner, the properties of delayed neutrons emitted by the fission products are discussed in Chap. VIII. Finally, some conclusions are drawn in Chap. IX.

II. GENERAL DESCRIPTION OF THE FISSION PROCESS

A. Introduction

After more than fifty years of study, many properties of fission have been determined. However, many aspects of this phenomenon still remain unknown. This still imperfect basic knowledge of fission is due to the great complexity of this process, which involves an extreme range of nuclear deformations from near sphericity to the breaking of the fissioning system. Conventional nuclear models commonly used in studies involving nuclear structure and nuclear

reactions were initially developed for relatively small nuclear deformations and, therefore, were not suited for the description of the dramatic rearrangement of nucleons occurring in fission. When similar models were used for the understanding of the experimental fission results, they rarely stemmed from basic nuclear theory but rather were of phenomenological nature. Also, the understanding of fission requires an accurate knowledge not only of the statics but also of the dynamics of this process. Although the statics are now well described by a semiclassical method described below, the dynamics are much more difficult to understand and are still poorly known.

Chapter II briefly introduces the subject of nuclear fission. More details can be found in the numerous books on fission (see [VH 73], [Mic 81], and [Wag 91]). A broad presentation of the various phases of the fission process is first made in Sec. II.B. Then the statics of the phenomenon are described in Sec. II.C with special emphasis on the semiclassical method widely used to obtain the potential-energy surface (PES) and the fission barrier of the fissioning system. The consequences for the fission process of the complex barrier shapes thus obtained are also described in Sec. II.C. The concept of fission channel, which is central to the understanding of fission, is discussed in Sec. II.D.

B. Various Phases of the Fission Process

Ignoring its complexity, the fission of a heavy nucleus in the actinide region can be broadly described as the succession of four different phases:

- formation of the initial state;
- transition from the initial state to scission;
- in-flight de-excitation of the fission fragments, after scission, by prompt processes; and
- de-excitation of the fission products by delayed processes.

1. Formation of the initial state. The nucleus that undergoes fission is called (A_F, Z_F) after its mass and atomic numbers A_F and Z_F, respectively, and the fissioning state in this nucleus is labeled λ_f.

The simplest state λ_f that can be found is the ground state of the nucleus, in which case fission occurs spontaneously without any external interaction; this is spontaneous fission. This type of fission can occur also for relatively long-lived isomeric states. The fissioning state λ_f can also be formed in a nuclear reaction; this is induced fission. In the following, only spontaneous fission or neutron-induced fission are considered.

For neutron-induced fission, with a target nucleus (A,Z) usually in its ground state, the nature of the state λ_f depends on the energy E_n of the incident neutron. At low energy, the neutron-nucleus interaction is dominated by the compound-nucleus (CN) mechanism; the states λ_f are simply the CN states. The excitation energy E^* of a λ_f state formed with an incident neutron of energy E_n is simply

$$E^* = S_n(A_F,Z_F) + E_n\frac{A}{A+1}, \qquad \text{(II.1)}$$

where $S_n(A_F,Z_F)$ is the neutron separation energy in the fissioning nucleus.

Typical values of S_n range from 4.5 MeV to 6.5 MeV for actinides and vary from one nucleus to another because of the odd-even character of Z_F or the neutron number N_F of the fissioning nucleus. This reflects the effect of the pairing force between protons and between neutrons. For example

S_n = 6.5 MeV for ^{236}U (^{235}U + n), and

S_n = 4.8 MeV for ^{239}U (^{238}U + n). (II.2)

This difference in the excitation energy caused by pairing is responsible for the fact that ^{235}U is fissile by slow neutrons, whereas ^{238}U is not.

The spin J of a CN state is determined by the coupling of the spin I of the target nucleus with the orbital angular momentum l and the spin s = ½ of the incoming neutron. For s-wave (l = 0) neutrons, whose contribution is predominant at low energy, the spin J takes the simple form

$$J = \left| I \pm \tfrac{1}{2} \right|, \text{ for } l = 0. \qquad \text{(II.3)}$$

The parity π of the CN state is determined by the parity π' of the target nucleus and the angular momentum l:

$$\pi = \pi' \times (-1)^l . \qquad \text{(II.4)}$$

When E^* is small, fission proceeds essentially through the CN state λ_f. This is the so-called "first chance" fission. At higher energies, the excited nucleus can evaporate one or more neutrons, and the residual nucleus may still have enough excitation energy to fission. This is the second- or third-chance fission if one or two neutrons, respectively, are evaporated before fission. In these cases, fission does not occur from a single initial state but rather through a mixture of states. This multiplicity of initial states renders the analysis of the experimental results more difficult.

2. Transition from the initial state to scission. This transition can be described in terms of three phases with the help of the fission-barrier concept discussed in Sec. II.C. These phases are briefly described below and are illustrated in Fig. II.1 where, for simplicity, the fission barrier is assumed to present only one single hump.

First, the fissioning nucleus undergoes a series of collective oscillations of moderate amplitude in the nuclear potential well.

Secondly, one of the above oscillations causes the system to penetrate the fission barrier by crossing the saddle point where the fission barrier presents a maximum. The penetrability of the fission barrier plays a major role in the fission probability and, consequently, in the fission cross sections. When the excitation energy E^* of the fissioning system is below the barrier height E_f, the fission is said to be subthreshold, e.g., as for the fission of ^{238}U by slow neutrons. Fission is above threshold otherwise, e.g., as for the fission induced by slow neutrons in ^{235}U. Nuclei like ^{238}U (^{235}U) are called nonfissile (fissile) by slow neutrons, or more simply, nonfissile (fissile).

Lastly, the system goes rapidly down the fission barrier toward increasing deformation until it breaks into two fragments at

the scission point. The breaking of the nucleus in more than two fragments at scission is ignored here. In this last and irreversible phase, the dynamical aspects, inertia and dissipation, are important but are also ignored here.

3. In-flight de-excitation of the fission fragments after scission by prompt processes. This phase corresponds to the mutual Coulomb repulsion of the two primary fragments formed at scission and to the prompt de-excitation of these fragments by neutron or γ-ray emission, or both, until they reach a quasi-stable state that can be either their ground state or an isomeric state.

When the fission fragments are formed at scission, they are no more subjected to the short-range nuclear attraction, and they repel each other by the long-range electrostatic force. After full acceleration, the fragments acquire a total kinetic energy E_K^T that is the sum of their Coulomb energy V_c and prescission energy E_K^{sc} at scission. This leads to the following expression:

$$E_K^T = E_K^{sc} + V_c + \Delta E_K^R, \qquad \text{(II.5)}$$

where ΔE_K^R is the small recoil energy of the fragments caused by the emission of neutrons and photons during the fragment in-flight de-excitation process.

Just before scission, the fragments are kept elongated by the nuclear force. But immediately after scission, the fragments are no more forced to be strongly deformed because of the suppression of the nuclear attraction. Consequently, their deformation becomes close to that of their ground state. The deformation energy D_{sc} that is liberated in this manner adds to the excitation energy E_{sc}^* acquired by the nuclear system at scission as a consequence of dissipation during the descent to scission. Therefore, the total excitation energy E_T^* of both fragments just after scission is

$$E_T^* = D_{sc} + E_{sc}^* . \qquad \text{(II.6)}$$

Experimentally, it is not possible to have access to the scission properties because the experimental quantities that are determined are not E_K^{sc} or E_K^{sc} but E_T^* and E_K^T. This is why the

knowledge of the properties of the fissioning system at scission is so elusive.

The mass numbers A_i' of the primary fragments obey the following relation:

$$A_F = A_1' + A_2' . \qquad \text{(II.7)}$$

This relation assumes no particle emission at scission.

Each excited fission fragment de-excites in flight preferentially by neutron evaporation if the excitation energy of the fragment is above the neutron emission threshold and by γ-ray emission if the excitation energy is or falls below this threshold. Prompt fission neutrons are emitted after about 10^{-17} s and prompt γ-rays after about 2×10^{-14} s, as illustrated in Fig. II.2. Each fragment i emits ν_{pi} prompt neutrons. The total number of prompt neutrons emitted by both fragments is ν_p:

$$\nu_p = \nu_{p1} + \nu_{p2} . \qquad \text{(II.8)}$$

In these conditions, the mass numbers A_i of the secondary fragments i, after prompt-neutron emission, are given by the following relations:

$$A_i' = A_i + \nu_{pi} , \text{ and} \qquad \text{(II.9)}$$

$$A_F = A_1 + A_2 + \nu_p . \qquad \text{(II.10)}$$

In neutron-induced fission, an interesting parameter to consider is η, the average number of prompt neutrons emitted per absorbed incident neutron. The value of η is given by the following expression:

$$\eta = \overline{\nu_p} \times \frac{\sigma_{nf}}{\sigma_{nf} + \sigma_{n\gamma}} , \qquad \text{(II.11)}$$

where $\overline{\nu_p}$ is the average of prompt neutrons per fission, whereas σ_{nf} and $\sigma_{n\gamma}$ are the fission and capture cross sections, respectively.

During the process of prompt de-excitation, the fission fragments are called secondary fragments. At the end of prompt de-

excitation, when the secondary fragments are at rest in the physical medium surrounding the fissioning system, these fragments are called fission products.

4. De-excitation of the fission products by delayed processes. The delayed decay processes are governed by the weak interaction or by slow γ-ray transitions and correspond to times longer than about 1 ms. The fission products are located away from the line of β stability on the neutron-rich side, even after prompt neutron emission because of the curvature of this β stability line for heavy nuclei. Therefore, the fission products are still unstable and decay by β^- emission toward the line of β stability. The β^- emission is usually followed by γ-ray emission because the residual nucleus is generally left in an excited state after β-ray emission. The emission of delayed β-rays and γ-rays is at the origin of the decay heat discussed in more detail in Chap. VII.

Note that the de-excitation of the fission fragments by prompt-neutron emission discussed in Sec. II.3 does not occur because the fragments are neutron rich but because neutron evaporation is much faster than either charged-particle emission, which is hampered by the Coulomb barrier, or γ-ray emission.

In a pure β-ray decay, the transition is isobaric because the nucleon number is not modified by this decay. One can therefore talk about "mass chains" of fission products. Up to seven β-rays can be emitted by the fission products produced in the thermal-neutron-induced fission of ^{235}U. In a few cases, the residual nucleus following β^- decay can be excited above the neutron-emission threshold, and then it decays primarily by neutron emission. This origin of delayed neutrons is discussed in more detail in Chap. VIII. In case of delayed-neutron emission, the mass number is not conserved in the decay of the fission fragment.

The total number of neutrons ν emitted per fission is the sum of the number ν_p of prompt neutrons and the number ν_d of delayed neutrons:

$$\nu = \nu_p + \nu_d. \qquad \text{(II.12)}$$

The prompt decays of the fission fragments and the delayed decays of the fission products are illustrated in Fig. II.3.

The total energy release in fission is the sum of the total kinetic energy of the fission fragments and of the energy of the radiations emitted in the prompt and delayed processes, including the energy carried away by neutrinos, which play no role in nuclear energy. For thermal-neutron-induced fission of ^{235}U, the total fission energy is about 202 MeV, about 170 MeV is for the kinetic energy of the fission fragments, 11.7 MeV is for prompt radiation, and 21.3 MeV is for delayed radiation (including 8.6 MeV of neutrino energy).

C. Potential-Energy Surface and Fission Barriers

1. Introduction. The statics of fission are governed by the variation of the total energy (also called the potential energy) of the fissioning system as a function of deformation in the transition from the initial state to scission. The determination of this potential energy necessitates the knowledge of the shape of the system defined with a set $\{s\}$ of shape parameters s_i in number n:

$$\{s\} = s_1, s_2, s_3, ..., s_n. \qquad (II.13)$$

The choice of $\{s\}$ depends on the shape of the system that strongly varies from the initial state to scission. For small deformations, a spherical harmonic expansion of the nuclear shape is adequate, but for largely deformed states, especially at scission, other shape parameterizations are necessary, sometimes with two centers.

The plot of the potential energy $V(\{s\})$ as a function of n deformation parameters in an (n+1)-dimensional space is the PES. The motion of the fissioning nucleus on the PES is the fission path. The PES can be represented by contour plots as a function of two shape parameters only, as in Fig II.4. The PES can also be represented more simply as a function of one single shape parameter s_1, usually elongation, whereas the other shape parameters are adjusted to minimize $V(\{s\})$. The variation of $V(\{s_1\})$ with s_1 is the fission barrier. An illustration of the fission barrier for ^{240}Pu is given in Fig. II.4.

The exact calculation of the PES is a very difficult problem especially for very large deformations and is still a challenge for the theorists. The various models used in these calculations can be

classified in three categories: macroscopic, semiclassical or hybrid, and microscopic. These models are briefly reviewed below.

2. Macroscopic models. In these models, the nucleus is treated as a bulk of incompressible nuclear matter with a sharp or a diffuse boundary. The motion of the nucleons inside the nucleus is ignored. An example of such models is the liquid-drop model (LDM) in which the nucleus is represented as a drop of incompressible and positively charged liquid. The variation of $V(\{s\})$ with the shape of the drop is the result of the interplay between the Coulomb energy $E_c(\{s\})$ and the surface tension $E_s(\{s\})$. For a spherical drop of radius R_0, these energies are called E_c^0 and E_s^0, respectively, and are given by the following expressions:

$$E_c^0 = \frac{3(Ze)^2}{5R_0} = a_c Z^2 A^{-\frac{1}{3}}, \text{ and} \qquad \text{(II.14)}$$

$$E_s^0 = \tau S_N = a_s A^{\frac{2}{3}}. \qquad \text{(II.15)}$$

In these expressions, τ is the surface energy per unit area, S_N is the nuclear area, Ze is the electric charge of the drop, and a_c and a_s are the coefficients of the Coulomb and the surface terms, respectively, in the Weizsäcker mass formula.

The energy $V(\{s\})$ is sometimes expressed in terms of the dimensionless parameter $\zeta(\{s\})$ defined as

$$\zeta(\{s\}) = \frac{E_s(\{s\}) + E_c(\{s\}) - E_s^0 - E_c^0}{E_s^0}. \qquad \text{(II.16)}$$

For small deformations of quadrupole nature, described in terms of a spherical-harmonics expansion, the parameter $\zeta(\{s\})$ can be expressed as

$$\zeta(\{s\}) = \frac{1}{2\pi}(1 - x)\sum_{\mu} |\alpha_{2\mu}|^2, \qquad \text{(II.17)}$$

where $\alpha_{2\mu}$ is the coefficient of the spherical harmonics $Y_{2\mu}$, and x is one-half the ratio of the Coulomb to the surface energies at sphericity:

$$x = \frac{E_c^0}{2E_s^0} = \frac{a_c}{2a_s} \times \frac{Z^2}{A}. \qquad \text{(II.18)}$$

The parameter x defined by Eq. II.18 is called the fissility parameter and its value is determined by that of the ratio $\frac{2a_s}{a_c}$, which is about 50. Therefore, x is smaller than 1 for all known nuclei, and the energy V({s}) increases with deformation for these nuclei, at least for small deformations.

At large deformation, there is a point in the PES where V({s}) is stationary as a function of all deformation parameters s_i:

$$\frac{\delta V(\{s\})}{\delta s_i} = 0, \quad \text{for all } s_i s. \qquad \text{(II.19)}$$

This point presents a maximum for the variation of V({s}) as a function of the elongation parameter but a minimum as a function of the other shape parameters. If the PES is drawn as a function of two shape parameters, one of which being the elongation, then the shape of the PES looks like a saddle, hence the name of saddle point given to this extremum (see Fig. II.5).

The difference between V({s}) at the saddle point and at sphericity is the fission barrier height E_f. The value of this height is about 6 MeV for ^{236}U, which is a small difference between the increase of E_s (about 100 MeV) and the decrease of E_c (about -100 MeV) between the saddle point and sphericity. This point illustrates the difficulty in obtaining reliable values of E_f, which is very sensitive to model calculations.

3. Semiclassical models. These models are a combination of macroscopic models and quantal corrections that take into account the shell structure of the nucleons in the nucleus. This method has been in use for a long time for small deformations but was extended with great success to large deformations by Strutinsky [Str 66]. Calculations with the semiclassical models are made under the assumptions that most of the potential energy is $V_M\{[s\})$ as given by the macroscopic model and that the quantum nature of the nucleus modifies this energy by a small shell-energy correction $\Delta E_{sh}(\{s\})$ determined by the single-particle density $g_F(\{s\})$ at the Fermi surface. Under these conditions,

$$V(\{s\}) = V_M(\{s\}) + \Delta E_{sh}(\{s\}). \qquad \text{(II.20)}$$

Because $g_F(\{s\})$ varies with deformation, the correction $\Delta E_{sh}(\{s\})$ oscillates along the fission path. The result of this combination is a double-hump fission barrier for actinide nuclei (see Fig. II.6).

A double-hump barrier shape has important consequences for the fission process (see [Mic 73], [Mic 76], and [BL 80]). Some of these consequences are briefly listed below.

a. Fission isomers. These are in fact shape isomers in the second well of the fission barrier. They can de-excite by spontaneous fission by tunneling through the outer barrier, and they have a shorter fission half-life than the ground state in the first well because they tunnel only through the outer barrier and at a higher energy. Since the historic discovery of the ^{242}Am fission isomer in Dubna [Pol+ 62], many other fission isomers have been identified. A list of these isomers is given in Fig. II.7.

b. Vibrational resonances. They are caused by vibrational levels in the second well of the fission barrier. A famous example is given by the subthreshold resonance at a neutron energy of about 715 keV in the neutron-induced fission of ^{230}Th ([Blo 89]). High-resolution measurements and a detailed analysis of this resonance now show that this resonance is caused by a shallow third well in the fission barrier (see Fig. II.8).

c. Intermediate structure in the subthreshold fission cross sections. This effect came also as a surprise in measurements of the ^{237}Np neutron-induced fission cross section below the fission threshold, which is at 750-keV incident neutron energy. In the resonance region, fission resonances appear much greater than those predicted by conventional fission-barrier penetrations, and they are grouped in clusters much more widely spaced than the resonances observed in the total cross section (see Fig. II.9). This effect, which was observed later in other nonfissile nuclei, such as ^{240}Pu, is now currently interpreted in terms of CN states in the second well of the fission barrier.

An extension toward extreme deformations (beyond the second saddle point up to scission) of the PES calculations with the semiclassical method shows the existence of valleys that can influence the fission properties (see [Mic 88]). An example of the

effect of such valleys is the bimodal fission observed for heavy actinides (from ^{258}Fm to ^{268}[104]), which are formed in heavy-ion reactions ([Hul+ 86]). These fission modes can be interpreted as the effect of two valleys beyond the saddle point. One valley leads to a compact scission configuration with fission fragments of a high kinetic energy, whereas the other valley leads to a more elongated scission configuration with fission fragments of lower kinetic energy. Another example is provided by the variation from resonance to resonance of the total kinetic energy of the fission fragments in the fission induced in ^{235}U by resonance neutrons ([Ham+ 89]).

4. Microscopic models. In these models, the nucleus is studied as a many-body problem of an ensemble of nucleons moving in a self-consistent Hartree-Fock field with possible extensions. This method should provide the most accurate knowledge of the fissioning system. But the complexity of the effective nucleon-nucleon interaction (that must be derived phenomenologically) and the great number of nucleons in a heavy nucleus make the calculations very difficult and lengthy.

The first microscopic calculations carried out with this method employed the Skyrme interaction ([Flo+ 74]). Great progress has been made since then thanks to the use of more realistic nucleon-nucleon interactions and powerful computers (see [BGG 89] for a review).

An example of the results obtained with this method for the PES of ^{240}Pu is given in Fig. II.10. The two families of shapes that appear in the fission and the fusion valleys, separated by a barrier, can explain several aspects of fission such as the transition of the fissioning state from an elongated shape (in the fission valley) to scission (in the fusion valley) when the barrier between these two valleys vanishes. Another aspect of fission is the so-called cold fission in which the fission fragments are formed with a small excitation energy at scission. This PES provides an explanation of this phenomenon as a transition from the fission valley to the fusion valley at a fairly high energy by tunneling through the barrier between these two valleys.

D. Fission Channels

The concept of fission exit channels is central to a good understanding of fission and has greatly evolved since the discovery of fission ([Mic 88]).

In any nuclear reaction, an exit channel is a given set of reaction products, each one in a well-defined quantum state when these products are no more subject to a mutual nuclear interaction. For fission, this definition would mean that the number of fission exit channels is extremely large as a consequence of the great variety of fission fragments emitted in many possible quantum states. This concept is at variance with several fission properties. For example, the fission widths of the low-energy neutron resonances for fissile nuclei exhibit large fluctuations from resonance to resonance. These fluctuations are incompatible with the predictions of statistical nuclear theory ([PT 56]), according to which large width fluctuations are associated with a small number of exit channels. Also, asymmetries in the shape of fission resonances are observed and interpreted in terms of resonance-resonance interference that can exist only if the number of exit channels is small.

This apparent inconsistency between the conventional concept of fission channel and the analysis of experimental fission results was explained by Bohr's fission channel theory ([Boh 56]), which postulates that the fission channels are the transition states at the top of the fission barrier, supposedly single humped at the time of the theory. The fissioning nucleus is almost cold at the saddle point for low-energy fission. Consequently, the transition states (hence the fission channels) are small in number.

The barrier shape now proves to be much more complex, essentially as a consequence of shell effects at all deformations discussed in Sec. C.3; therefore, the concept of fission channels must be reconsidered. For example, with a double-humped barrier, one has to take into account the transition states on top of both barrier humps; the relative effects of those two categories of states depend, among other factors, on the relative heights of the two humps. Also, because the Class-II states in the second well play the role of doorway states in the fission exit channels as in the intermediate structure effect in the fission cross sections (σ_{nf}) below the fission threshold, they influence those fission channels. Lastly, calculations of the PES beyond the most deformed saddle point show the existence of valleys that may affect the fission properties and may possibly play the role of fission channels.

Therefore, the fission channels now appear as a combination of all these aspects whose interplay depends on the fission parameter

under study; this interplay varies with neutron energy and from nucleus to nucleus and is the focus of many experimental studies.

Some effects of the fission channels may show up in σ_{nf} as in the large fluctuations of the fission widths, in the intermediate structure in subthreshold σ_{nf}, or in the vibrational resonances (see Sec. C.3). Other fission channels (such as the possible fission valleys beyond the most deformed saddle point) will have no effect on σ_{nf} but may influence scission variables and, consequently, fragment properties like mass distribution, kinetic energy, or excitation energy observed through the emission of evaporated neutrons or γ-rays. For this reason, a complete study of the fission channels requires the knowledge of the properties of the fission process itself in addition to that of the shape of σ_{nf}. An attempt to present a more coherent description of fission exit channels was recently made by Weigmann and Hambsch ([WH 91]) who analyzed the data on fragment kinetic energy in the ^{235}U resonances in terms of the transition states (assumed to behave as doorway states in the fission exit channels) and the so-called Brosa channels, which correspond to valleys in the PES at extreme deformations.

The effects of the fission channels on the fission properties and on σ_{nf} are best seen when the excitation energy is near the fission threshold because these channels are small in number and have a greater observable effect when the energy of the fissioning system is as close as possible to the barrier. When the excitation energy increases, the number of channels also increases and their individual effects become relatively smaller. The contributions and properties of the individual fission channels are therefore more difficult to detect and to disentangle one from the other.

III. DOPPLER EFFECT FOR LIQUID-METAL FAST BREEDER REACTORS

A. Introduction

The cross sections are usually calculated in the center-of-mass system, whereas the measurements are made in the laboratory system. But the atoms of the sample used in the measurements are never at rest because they are always subjected to the zero-point motion $\frac{1}{2}\hbar\omega$ of the harmonic oscillator even if the sample is at the extreme temperature T = 0 K. The atomic motion in the sample modifies the incident-neutron velocity relative to the interacting nucleus and, consequently, the observed cross section for a given

neutron energy determined in the laboratory system. This is the so-called Doppler effect in the neutron cross-section measurements. The Doppler effect, which is temperature dependent, is particularly important for the neutron resonances that are broadened by the atomic thermal motion. If the sample is in the form of a solid, which is generally the case, binding effects are present between the atoms and their environment. These solid-state effects can also modify the observed cross sections, especially at low neutron energies. The Doppler and solid-state effects in the cross sections are discussed in Sec. III.B.

The variation in the shape of the observed cross sections as a function of temperature induces a temperature dependence in the reactivity of fission reactors. The Doppler broadening of the resonances plays an important role in the variation with temperature of the reactivity of large fast power reactors. This Doppler effect for liquid-metal fast breeder reactors (LMFBR) is considered in Sec. III.C.

B. Doppler Broadening of Neutron Resonances

1. Introduction. The effect of Doppler broadening can be simply illustrated in the case of a single neutron resonance whose intrinsic shape, in the absence of any experimental effect, is described by the Breit-Wigner single-level formula

$$\sigma_{int}(x) = \frac{\sigma_0}{1 + x^2}, \qquad \text{(III.1)}$$

where $x = \frac{2(E_n - E_0)}{\Gamma}$ is expressed in terms of the incident-neutron energy E_n, the resonance energy E_0, and the total width Γ of the resonance.

The gas model discussed in Sec. B.2 is a good approximation of the effect of the motion of the atoms in the sample in whatever form the sample is. When the sample is a solid, the effect of the crystalline binding on the observed resonance shape is discussed in Sec. B.3.

2. Gas model. In the gas model, the nuclei are assumed to be in single atoms in equilibrium at temperature T. This model thus ignores the complex motions that could be associated with vibrations and rotations of molecules.

The cross section for an incident neutron of velocity v_n in the laboratory system hitting a target nucleus in the gas depends on the relative velocity of the neutron and the target nucleus. The observed cross section in the laboratory system is therefore the average over the velocity distribution of the atoms in the gas.

The velocity distribution of the atoms in the gas model is given by the well-known Maxwell law. For a gas of atoms of mass number A at room temperature, the velocity v_A of the atoms is much smaller than the velocity v_n of epithermal neutrons. The neutron velocity relative to that of an atom before the nuclear interaction takes place can therefore be considered as equal to the neutron velocity v_n in the laboratory system as modified by a correction to first order in v_A/v_n. In these conditions, the observed cross section at a given neutron energy E_n in the laboratory system is equal to the true cross section $\sigma(E_n)$ at this energy (as if the target nucleus were at rest), folded into a Gaussian having a standard deviation σ_D given by the following relation:

$$\sigma_D = \sqrt{\frac{2E_n \times k_B \times T}{A}}\,, \qquad \text{(III.2)}$$

where k_B is the Boltzmann constant. This effect is called Doppler broadening and, traditionally, neutron spectroscopists express this effect in terms of a so-called Doppler width Δ, which is defined as

$$\Delta = \sigma_D \times \sqrt{2}\,. \qquad \text{(III.3)}$$

For a medium-mass nucleus (A = 100) in a gas at room temperature (T = 300 K), the Doppler width is equal to

$$\Delta(\text{eV}) = 0.032 \times \sqrt{E_n(\text{eV})}\,. \qquad \text{(III.4)}$$

When the cross section has the shape of a single-level Breit-Wigner formula, given by Eq. III.1, the result of folding this shape with the Gaussian defined above is the the function $\Psi(\beta,x)$, which is defined as

$$\Psi(\beta,x) = \frac{1}{\beta\sqrt{\pi}} \int_{-\infty}^{+\infty} \frac{1}{1+y^2} \exp\left(-\frac{(x-y)^2}{\beta^2}\right) dy \,, \qquad \text{(III.5)}$$

where $\beta = \frac{2\Delta}{\Gamma}$. The function $\Psi(\beta,x)$ is available from tabulations. The Breit-Wigner shape is modified by the Doppler effect mostly in the regions where this shape deviates most from linearity near the peak and in the wings but not too far from the resonance center. The shape is almost not modified far away in the wings (see Fig. III.1). The area under a resonance remains unchanged if the shape of this resonance is modified by Doppler broadening. These considerations must be kept in mind for understanding resonance self-shielding, which plays an important role in the Doppler effect for LMFBRs discussed in Sec. III.C.

3. Solid-state effects. When the atom is bound in a crystal, the interaction of the incident neutron with a free nucleus is not valid, and one must consider the interaction of the neutron with the crystal as a whole. This process was studied comparatively early in nuclear physics by Lamb who demonstrated that the target nucleus bound in a crystal lattice can lead to the process of recoilless absorption of the neutron by the nucleus ([Lam 39]). This recoilless absorption predicted by Lamb was actually discovered much later for γ-rays by Mössbauer and named after him. This effect was also observed for neutrons as a shape distortion of the 6.68-eV resonance in ^{238}U ([Mic+ 62], [JL 62]), but it was much weaker than that for γ-rays because the nucleus recoil energy is smaller for γ-rays than for neutrons. Also for neutrons, Lamb concluded that the gas model is still adequate in most cases (in the weak-coupling cases) provided that the temperature used in the model, called the effective temperature T_{eff}, is modified from the true sample temperature T by taking into account the phonon density of states f(E) in the sample. The expression for T_{eff} then reads

$$k_B T_{eff} = \int_0^{+\infty} E\, f(E) \coth\left(\frac{E}{2k_B T}\right) dE \,. \qquad \text{(III.6)}$$

The Debye model, which is a measure of the mean energy of the spectrum of phonons in the sample and which assumes a quadratic phonon energy dependence ($f(E) \propto E^2$), is often used in the derivation of T_{eff}. In this case, a plot of the ratio

$$\frac{T_{eff}}{T} = f(\frac{\theta_D}{2T}) \qquad \text{(III.7)}$$

as a function of the Debye temperature θ_D is given in Fig. III.2. The plot in Fig. III.2 shows that the Doppler broadening always exists, even at T = 0 K, as mentioned above.

Approximate expressions for $f(\frac{\theta_D}{2T})$ can be used ([NP 60], such as:

$$f(x) = 1 + x^2/5 \ , \qquad \text{for } x = \frac{\theta_D}{2T} < 2, \text{ and} \qquad \text{(III.8)}$$

$$f(x) = (3x/4)[\ 1 + \pi^4/30x^4\ ] \ , \qquad \text{for } x = \frac{\theta_D}{2T} > 2. \qquad \text{(III.9)}$$

The rest of this report assumes that the weak-coupling case, defined as $\Delta + \Gamma \gg 2\ k_B\theta_D$ with the Debye model, always applies and, consequently, that the gas model can be used but with some care about the calculation of the effective temperature (see Sec. C.4).

C. Doppler Effect for Liquid-Metal Fast Breeder Reactors

1. Introduction. The Doppler effect in LMFBRs is an important aspect of safety and was considered very early in the history of fast reactors ([Bet 57]). There was some concern at that time that small reactors with a high concentration of fissile material could have a positive Doppler effect. But, as interest shifted toward larger reactors with a high fertile-to-fissile ratio (and, consequently, with a softer spectrum), the presence of a negative Doppler coefficient in reactors such as the LMFBRs provides safety in their operation ([Soo 62] and [HO 70]).

The Doppler effect in a fission reactor is a change in the reactivity coefficient k resulting from an arbitrary change in temperature T.

The Doppler coefficient is the derivative $\frac{dk}{dT}$ that varies approximately as T^{-1} and, for this reason, is usually displayed as $T \times \frac{dk}{dT}$.

2. Energy self-shielding. In a LMFBR, the Doppler effect is the consequence of the variation with temperature of the fission and capture rates and of leakage. In such fission reactors the Doppler effect plays a role only at relatively low energies, below about 25 keV. Because of the large size of the reactor and of the shape of the spectrum, the leakage is small below 25 keV and therefore plays a minor role in the Doppler effect, which is thus dominated by the opposite variations with temperature of the fission and capture rates. These variations cause a change in η, the number of fission neutrons per absorbed neutron, and the Doppler effect can then be written as follows:

$$\text{Doppler effect} = \text{Change in } \eta \times \frac{\text{Number of neutrons below 25 keV}}{\text{Total number of neutrons}} . \quad \text{(III.10)}$$

The change in η is governed by the change in self-shielding with Doppler broadening.

Self-shielding plays an important role in reactor physics and was calculated for many reactor configurations using several methods. In the following, self-shielding is discussed in the extreme simplified case of a homogeneous reactor medium and for narrow isolated resonances of the Breit-Wigner type without overlap. This report further assumes that the neutron flux is not modified by the resonances.

3. Single-level approximation. In the vicinity of a resonance, the probability $P_{abs}(E_n)$ that a neutron of energy E_n is absorbed in a nuclear reaction in the reactor medium is given by the following equation:

$$P_{abs}(E_n) = \frac{\Sigma_{ra}}{\Sigma_p + \Sigma_{ra}} , \quad \text{(III.11)}$$

where $\Sigma_{ra} = N_a \sigma_0 \psi(E_n)$ is the macroscopic resonant absorption cross section (with microscopic cross section given by Eq. III.1) for isotope, a, which is present in the medium with a number of atoms/cm^3 equal to N_a. $\Sigma_p = N_s \sigma_s + N_a \sigma_{pa}$ is the macroscopic potential scattering cross section for elements s and a, which have microscopic scattering cross sections σ_s and σ_{pa} and the number of atoms/cm3 equal to N_s and N_a, respectively.

When integrated across the resonance, this neutron absorption probability is equal to

$$\int_{-\infty}^{+\infty} P_{abs}(E_n)\, dE_n = \int_{-\infty}^{+\infty} P_{abs}(x)\, dx = \int_{-\infty}^{+\infty} \frac{N_a \sigma_0 \psi(x)}{N_a \sigma_0 \psi(x) + \Sigma_p} dx . \quad \text{(III.12)}$$

In this equation, the limits of integration are extended to $-\infty$ and $+\infty$ to make the calculations easier without introducing appreciable errors in the results.

In the infinite dilution approximation, in which N_a goes to zero, the integrated absorption probability is equal to

$$\int_{-\infty}^{+\infty} P_{abs}(x)\, dx = \frac{\pi N_a \sigma_0}{\Sigma_p} = \pi \zeta, \quad \text{for small } N_a \text{ values,} \quad \text{(III.13)}$$

with

$$\zeta = \frac{N_a \sigma_0}{\Sigma_p} . \quad \text{(III.14)}$$

The integrated absorption probability given by Eq. III.12 for any arbitrary value of N_a can then be written as

$$\int_{-\infty}^{+\infty} P_{abs}(x)\, dx = \frac{\pi N_a \sigma_0}{\Sigma_p} \times f_H(\beta,\zeta) , \quad \text{(III.15)}$$

where $f_H(\beta,\zeta)$ is the energy self-shielding factor for homogeneous mixtures defined as

$$f_H(\beta,\zeta) = \frac{1}{\pi} \int_{-\infty}^{+\infty} \frac{\psi(x)}{1 + \zeta\psi(x)} dx . \quad \text{(III.16)}$$

Graphs of $f_H(\beta,\zeta)$ are plotted in Fig. III.3 as a function of $\zeta\psi_0$, where ψ_0 is the maximum value of the function ψ at the resonance energy.

In this formalism, the Doppler coefficient is simply the derivative $df_H(\beta,\zeta)/dT$, which can be calculated from the temperature dependence of $df_H(\beta,\zeta)$ through the parameter β. In the extreme condition $\zeta\psi_0 \rightarrow 0$ (case of infinite dilution), the Doppler coefficient vanishes because the integrand in Eq. III.16 is the ψ function whose integral is independent of the temperature. At the other extreme, when $\zeta\psi_0 \rightarrow \infty$ (a case of very strong shielding), the Doppler coefficient also vanishes because the integrand in Eq. III.16 becomes a constant. This latter case can be understood physically from the fact that the Doppler broadening does not modify the resonant cross section far away in the wings of the resonance. Therefore, the Doppler effect presents a maximum for intermediate values of the parameter $\zeta\psi_0$.

For small values of the parameter $\zeta\psi_0$, a power series expansion of the function $f_H(\beta,\zeta)$ leads to a temperature dependence of this function proportional to $T^{\frac{1}{2}}$ and, therefore, to a Doppler coefficient that is proportional to $T^{\frac{3}{2}}$. This situation applies to small self-shielding as for fissile elements at intermediate energies down to about 1 keV or less. For large values of the parameter $\zeta\psi_0$, a power series expansion of the function $f_H(\beta,\zeta)$ can be made. This function varies between $T^{\frac{1}{2}}$ (Doppler coefficient proportional to $T^{\frac{3}{2}}$) and T (Doppler coefficient independent of the temperature). This last case corresponds to extreme self-shielding, which is met only for a few strong resonances at low energy.

4. Solid-state effects. As discussed in Sec. B.3, the gas model can be used in calculating the Doppler effect, but great care has to be given to the determination of the effective temperature used in the calculation of the Doppler width.

When the sample is of monoatomic material like a metal, the Debye model usually applies, and the Debye temperature can be easily derived from specific heat measurements. But the effective temperature is more difficult to determine when the sample is of multiatomic compounds like uranium oxides. The specific heat measurement gives a global Debye temperature averaged over all the atoms of the compound but not that of the particular isotope whose resonances are studied. It has been shown that the phonon spectrum of the uranium atoms in uranium oxides is much softer than that of the oxygen atoms and that the high Debye temperature

deduced from specific heat measurements comes essentially from oxygen.

A variety of studies are aimed at the correct determination of T_{eff} for uranium in uranium oxides. Among these studies, the transmission measurements of UO_2 at temperatures of 1,100 K and 1,800 K from which a Debye temperature of 250 K was deduced ([HS 79]) can be mentioned. By comparison, the Debye temperature of oxygen in the same compound is as high as about 730 K. But the behavior of T_{eff} with temperature is not very well understood. Further measurements are needed to provide better determinations of the Doppler broadening of uranium resonances in compounds used as fuels over wide ranges of temperatures from room temperature to above melting ([Row 88]).

5. Doppler coefficient in liquid-metal fast breeder reactors. In more realistic calculations, one has to sum the effects of the resonances from different isotopes and, for each isotope, the possible contributions of different spin states and angular momentum values. Overlap between resonances has to be considered, particularly for resonances of different isotopes (as for fissile and fertile isotopes) because no repulsion exists between levels of different isotopes (as well as between levels of different spin states in the same isotope). Also, the use of the single-level formalism is sometimes not appropriate to describe some cross sections, as the fission cross sections (see Chap. IV). But the use of more sophisticated formalisms, such as the multilevel formalisms, does not bring about a major change in the Doppler coefficient.

In LMFBRs, the Doppler effect is dominated by the negative contribution of the ^{238}U s-wave capture resonances up to about 10 keV (90% of the ^{238}U component). The Doppler effect caused by ^{239}Pu is a balance between the fission and capture contributions, which are about equal below 750 eV. Above this energy, the fission component becomes more important. The relative contributions of the Doppler coefficient in a typical LMFBR are as follows ([Row 88]):

^{238}U capture	- 92
^{239}Pu fission	+ 12
^{239}Pu capture	- 9
^{240}Pu capture	- 5
Fe capture	- 7

The large s-wave resonances that account for most of the total cross sections of sodium and the constituents of steel are too broad to be affected by the Doppler effect. Most of the Doppler effect in iron comes from the narrow 1.15-keV p-wave resonance in ^{56}Fe.

D. Conclusion

This brief review of Doppler broadening shows that its accurate knowledge is important for safety in LMFBRs. Although the Doppler coefficient for these reactors is mainly determined by capture in the ^{238}U resonances, fission in ^{239}Pu resonances also plays an important role up to an energy of a few keV. This is the reason why the properties of the ^{239}Pu resonances need to be known experimentally up to the maximum possible energy compatible with the experimental resolution.

IV. FISSION CROSS SECTION OF ^{239}Pu

A. Introduction

In addition to ^{235}U, used as a fuel, and to ^{238}U, used as a fertile element and sometimes as a fuel as in fast breeders, ^{239}Pu is present in nuclear reactors either because it is part of the fuel at the loading stage or because it is the result of the irradiation of ^{238}U during the operation of the reactor, or both. The ^{239}Pu resonances play an important role in the Doppler effect of fast power reactors, as discussed in Chap. III. But the ^{239}Pu fission cross section is also important for safety for other reasons illustrated by the two examples given below ([SD 91]).

One important safety aspect of reactors is the void coefficient ρ_v. The water-void coefficient has an uncertainty of 30 to 40% for the undermoderated reactors, whereas the sodium-void coefficient has an uncertainty of 20 to 30% for the fast breeders. A reduction of 5% in the uncertainty on σ_{nf} for ^{239}Pu below 1 keV leads to a reduction of 30% in the uncertainty on ρ_v.

Another important safety aspect of nuclear reactors is the antireactivity coefficient ρ_c of the control system of a large breeder. This coefficient is known to $\pm 12\%$. A reduction of 5% in the uncertainty on σ_{nf} for ^{239}Pu above several keV leads to a reduction of 30% in the uncertainty on ρ_c.

These examples show that σ_{nf} for ^{239}Pu plays an important role for safety in nuclear reactors. Taking into account the facts given above, σ_{nf} for ^{239}Pu will be considered in the following below 1 keV (in the resolved-resonance region) and above 1 keV.

B. Fission Cross Section of ^{239}Pu Below 1 keV

1. General behavior of the ^{239}Pu fission cross section. The ^{239}Pu is a fissile nucleus because the excitation energy E^* in the compound nucleus ^{240}Pu, which is just above the neutron separation energy $S_n = 6.53$ MeV in ^{240}Pu for small incident neutron energies, is above the barrier height $E_{fA} = 5.78$ MeV. This illustration of the neutron-pairing effect is discussed in Chap. II.

The measurements of σ_{nf} for ^{239}Pu are difficult because the half-life $\tau_{1/2}$ of ^{239}Pu is rather short ($\tau_{1/2} = 2.4 \times 10^4$ years), creating a large source of α-rays in the fission detector. Though the energy of these α-rays is small compared with the average energy of a fission fragment, the piling up of α-ray pulses can easily simulate a fission fragment pulse, thus causing a large background in the experiment. This effect seriously limits the quantity of ^{239}Pu that can be used in a fission detector. The early experiments were made with slow fission detectors (therefore with small amounts of ^{239}Pu) and neutron sources of small intensities. These measurements nevertheless demonstrated that σ_{nf} for ^{239}Pu was composed of resonances, but the quality of the measurements was not good enough to separate these resonances above a few eV or a few tens of eV ([RP 56]).

During the last two or three decades, great improvements have been made both in building fission detectors containing large quantities of ^{239}Pu (up to about 1 g) and in operating more intense neutron sources. The neutron time-of-flight method is used almost exclusively in this energy range. An illustration of the improvement in the measurements of σ_{nf} for ^{239}Pu is given in Fig. IV.1. It was possible also to make some fission cross-section measurements at the liquid-nitrogen temperature to reduce the Doppler effect. All these measurements demonstrate the existence of resonances at an energy much higher than a few tens of eV. In fact, the best measurements can now separate most of the resonances up to about 1 keV (see Sec. B.2.b). These data provide a good base for the analysis of a large number of resonances and for the study of their properties.

2. Analysis of the ^{239}Pu fission cross section

a. Single-level analysis. In the resolved-resonance region, the simplest analysis assumes that the cross section is composed of a sum of isolated resonances. This is called the single-level formalism. Each resonance i is then described by a single-level Breit-Wigner formula

$$\frac{\sigma_{0f}^{i}}{1 + x_i^2}, \qquad \text{(IV.1)}$$

where σ_{0f}^{i} is the peak fission cross section at the center of the resonance, and x_i is given by

$$x_i = \frac{E_n - E_0^i}{\frac{\Gamma^i}{2}}, \qquad \text{(IV.2)}$$

where E_n is the incident neutron energy, E_0^i is the resonance energy, and Γ^i is the total width of the resonance. The total width itself is the sum of all the partial widths, which, for fission resonances at low energy, are the neutron width Γ_n^i, the radiative-capture width Γ_γ^i, and the fission width Γ_f^i:

$$\Gamma^i = \Gamma_n^i + \Gamma_\gamma^i + \Gamma_f^i. \qquad \text{(IV.3)}$$

For the scattering and the total cross sections, one must include also a resonance-potential interference term of the form $\frac{x}{1 + x^2}$. The effect of this term, which is weak for a fissile nucleus, is ignored in the rest of this paper.

The peak fission cross section σ_{0f}^{i} is related to the peak value σ_0^i in the total cross section (ignoring potential scattering) by the following relation:

$$\sigma_{0f}^{i} = \sigma_0^i \frac{\Gamma_f^i}{\Gamma^i}. \qquad \text{(IV.4)}$$

The area A_f^i under a fission resonance i is simply given by

$$A_f^i = \frac{\pi}{2} \sigma_{0f}^{i} \Gamma^i. \qquad \text{(IV.5)}$$

A useful relationship between some of these parameters is given by the following expression:

$$\sigma_0^i \Gamma^i = \frac{4\pi}{k_n^2} g^i \Gamma_n^i , \qquad \text{(IV.6)}$$

where k_n is the wave number of the incoming neutron, and g^i is the statistical factor expressed in terms of the spin I of the target nucleus and the spin J^i of the resonance. For a resonance induced by s-wave neutrons, this statistical factor reads

$$g^i = \frac{2J^i + 1}{2(2I + 1)} . \qquad \text{(IV.7)}$$

Therefore, an s-wave resonance is determined by the energy E_0^i; the various partial widths Γ_n^i, Γ_γ^i, and Γ_f^i, thus adding to the total width Γ^i; and the spin J^i. The parity π of an s-wave resonance is the same as that of the target nucleus. From now on, the suffix i will be dropped unless absolutely necessary.

These relations demonstrate that all these parameters cannot be determined by the fission cross section alone. Another cross section is needed, which is usually the total cross section σ_{nt}. Even with these two cross sections, the spin J cannot be determined except under very favorable conditions ([Mic 67]).

A standard single-level analysis of a resonance will first require an area analysis of the resonance. This is the simplest analysis that can be made because for thin samples the area is independent of the Doppler effect and of the resolution function. One then obtains $\sigma_0\Gamma_f$ and $\sigma_0\Gamma$ (and consequently $g\Gamma_n$) for the fission and the total cross sections, respectively. A shape analysis of one of these cross sections (or of both of them) can be made if the experimental conditions are sufficiently good and well known. One then obtains the total width. The fission width is derived simply from Γ, $\sigma_0\Gamma_f$, and $\sigma_0\Gamma$. Another piece of information is needed to obtain the capture and the neutron widths, such as a scattering measurement. A scattering measurement, however, is difficult to carry out in the case of a fissile nucleus because the neutron widths are small (as a consequence of the small level spacing) and because the scattering measurement is also sensitive to the fission neutrons, which are emitted in larger

numbers than the scattered neutrons are. The product $\sigma_0\Gamma_n$ is obtained from an area analysis of a scattering resonance. Used in conjunction with Γ and $\sigma_0\Gamma$, the parameters g (and consequently J), Γ_n, and Γ_γ are then obtained ([Tro+ 70]). When the spin J is not known, the statistical factor g is usually taken as equal to $\frac{1}{2}$. An example of the single-level analysis of the ^{239}Pu cross sections is given in [Der+ 67].

b. Multilevel analysis. The single-level analysis briefly described above is only an approximation because in a nucleus like ^{239}Pu, the resonances are closely spaced and each of them cannot be analyzed as if the other resonances did not exist. The parameters obtained from the single-level analysis are usually a good approximation of the true parameters, but the cross sections cannot be accurately reproduced with this formalism. On several occasions, the measured fission resonances have not always been symmetric (see for example [SS 58] for the ^{235}U resonances). The asymmetry may be caused by missed levels (see Sec. B.3), by the interference effect with other resonances, or by both effects. Sometimes the difference between the measured and the calculated cross sections can be accounted for by adding a residual cross section to the calculated cross section, but this method is not very satisfactory.

A better and more physical method involves the calculation of cross sections with a more realistic formalism (called multilevel formalism) that takes into account all the existing resonances and their possible interactions. This is a very stringent requirement because all these resonances are not known. If the resonances were known, the exact calculations would still be very long, even with present-day computing capabilities.

One multilevel formula ([FPW 54]) used extensively provides a good approximation when the spacings of the resonances are much greater than their widths. This formula gives the cross section σ_{nc} for a reaction with entrance and exit channels, respectively. This cross section is the square of the sum of complex amplitudes, one for each resonance i:

$$\sigma_{nc} \sim \left| \sum_i \frac{\gamma_n^i \gamma_c^i}{E_0^i - E_n - \frac{i}{2}\Gamma^i} \right|^2 , \qquad \text{(IV.8)}$$

where γ_n^i and γ_c^i are the reduced widths for the resonance i and for the channels n and c, respectively. In this formula, as in the rest of this section, we assume that the cross section is calculated for one spin state only. In this respect, the summation in Eq. IV.8 runs over resonances i of the same spin state J. The experimental results are usually obtained at low energy (where the contribution of only s-wave neutrons is important) and with unpolarized targets and unpolarized neutrons. In this case, one must of course fit the experimental data by adding the cross sections calculated for the two spin states $J^+ = I + \frac{1}{2}$ and $J^- = I - \frac{1}{2}$.

Though approximate, Eq. IV.8 clearly shows that the squares of the diagonal terms correspond to single-level Breit-Wigner formulas. But, in addition, there are cross terms that represent the effect of interference between resonances. This formalism is very useful, but it is derived with the assumption that the level spacings between resonances are large compared with their widths. This assumption is usually not valid for fissionable nuclei for which the widths of the neutron resonances are comparable with their spacings. One has then to use more exact multilevel formalisms.

Essentially three formalisms are used for the cross sections of fissionable nuclei. These formalisms are all derived from the R-matrix (**R**) theory of Wigner and Eisenbud ([WE 47], [Wig 46]). They are described in some detail by Moore ([Moo 70]).

The Adler-Adler formalism ([AA 63]) is derived from the Kapur-Peierls formalism and gives a cross section that is composed of Breit-Wigner single-level terms (including the resonance-potential interference terms). This formalism is attractive because of the simplicity of the expressions for the cross sections. But the parameters used in the formalism can be related with difficulty with those of **R**.

In contrast, the two other formalisms developed by Vogt ([Vog 58]) and by Reich and Moore ([RM 58]) are more complicated, but their cross sections are expressed directly in terms of **R**. Both these formalisms express the cross section σ_{nc} for a given spin in terms of the collision matrix (**U**) for the same spin:

$$\sigma_{nc} = \frac{\pi}{k_n^2} \left| \delta_{nc} - U_{nc} \right|^2. \qquad \text{(IV.9)}$$

In the Vogt formalism, the number of levels is limited but not the number of exit channels. The terms of the matrix **U** can then be expressed as

$$U_{nc} = e^{\,i\,(\varphi_n + \varphi_c)} \left(\delta_{nc} + i \sum_{ij} \left(\Gamma_n^i\right)^{\frac{1}{2}} \left(\Gamma_c^j\right)^{\frac{1}{2}} A_{ij} \right), \qquad \text{(IV.10)}$$

where φ_n and φ_c are the phase factors in the entrance and the exit channels, respectively, whereas A_{ij} is the term of matrix (**A**), which is defined by its inverse:

$$(A^{-1})_{ij} = (E_0^i - E_n)\, \delta_{ij} - \frac{i}{2} \sum_c \left(\Gamma_c^i\right)^{\frac{1}{2}} \left(\Gamma_c^j\right)^{\frac{1}{2}}. \qquad \text{(IV.11)}$$

In these equations, the summation runs over all exit channels c. Also, the square roots $\left(\Gamma_c^i\right)^{\frac{1}{2}}$ and $\left(\Gamma_c^j\right)^{\frac{1}{2}}$ of the widths are proportional to the reduced widths for exit channel c and can take positive or negative values. Because the Vogt formalism considers a limited number of resonances, the inversion of the matrix $\mathbf{A}^{-1}$ can be accomplished. If the off-diagonal elements vanish, this formalism gives a sum of Breit-Wigner one-level formulas, as expected. In evaluating the importance of the off-diagonal elements, one has to distinguish between elastic scattering, capture, and fission exit channels. The contribution of elastic scattering is small because the neutron widths are small. The contribution of capture is also small because there is a great number of capture exit channels with fluctuations in the signs of their reduced widths so that all the contributions of the capture channels finally add to a very small value. The case of fission is different because the fission widths are large and the number of fission exit channels is small, as demonstrated by the large fluctuations of the fission widths. Therefore, the off-diagonal terms of **A** can be expressed simply as

$$(A^{-1})_{ij} = -\frac{i}{2} \sum_{c=f} \left(\Gamma_c^i\right)^{\frac{1}{2}} \left(\Gamma_c^j\right)^{\frac{1}{2}} = -\frac{i}{2}\, g_f^i . g_f^j \qquad (\text{for } i \neq j), \qquad \text{(IV.12)}$$

where the summation runs over all fission channels. This summation can also be considered as the scalar product of two fission vectors g_f^i and g_f^j in a fission-vector space with components $\left(\Gamma_c^i\right)^{\frac{1}{2}}$ and $\left(\Gamma_c^j\right)^{\frac{1}{2}}$ and

with lengths $|g_f^i|^2 = \Gamma_f^i$ and $|g_f^j|^2 = \Gamma_f^j$. Therefore, the Vogt formalism provides a good physical description of the fission process in the resonances.

The Reich-Moore formalism, like the Vogt formalism, makes use of the same collision matrix. This matrix **U**, expressed in terms of **R**, reads

$$\mathbf{U} = \omega \frac{1 + i(\mathbf{BRB} + \mathbf{C})}{1 - i(\mathbf{BRB} + \mathbf{C})} \omega . \qquad \text{(IV.13)}$$

In Eq. IV.13, the diagonal matrices ω, **B**, and **C** depend on the external nuclear region. This is in contrast to the matrix **R**, which describes the intrinsic nuclear properties of the levels and is given by the expression

$$\mathbf{R} = \sum_i \frac{\gamma^i \times \gamma^i}{E_0^i - E_n} , \qquad \text{(IV.14)}$$

where $\gamma^i \times \gamma^i$ is the direct product of the vectors γ^i whose components are the reduced widths γ_c^i. This means that the matrix element R_{nc} for entrance and exit channels n and c, respectively, reads

$$R_{nc} = \sum_i \frac{\gamma_n^i \times \gamma_c^i}{E_0^i - E_n} . \qquad \text{(IV.15)}$$

Reich and Moore calculate **U** assuming that the number of fission channels ν_f is small but that the number of levels can be large in contrast to the Vogt formalism. The matrix **R** is then partitioned such that indices ranking from 1 to $m = 1 + \nu_f$ correspond to the neutron entrance channel and the fission channels and that indices greater than m correspond to the capture channels. After some calculations, in which the usual assumption is made that the reduced widths γ_c^i for the capture channels have random signs and exhibit random variations from one channel to the other, the matrix **U** becomes an $m \times m$ matrix given by the following expression:

$$\mathbf{U} = \omega \frac{1 + i(\mathbf{BR'B} + \mathbf{C})}{1 - i(\mathbf{BR'B} + \mathbf{C})} \omega , \qquad \text{(IV.16)}$$

where all the matrices are m × m. This is the same expression as Eq. IV.13, with the exception that the matrix **R** is now replaced by the slightly modified matrix **R'**:

$$\mathbf{R}' = \sum_i \frac{\gamma^i \times \gamma^i}{E_0^i - E_n - \frac{i}{2}\Gamma_\gamma^i} \quad , \qquad \text{(IV.17)}$$

where Γ_γ^i is the total capture width for level i.

The Reich-Moore formalism is now widely used in the calculation of fission cross sections, especially in the evaluated data files. This is because the calculations need to invert m × m matrices, with small m, whereas the rank of matrices to be inverted in the Vogt formalism corresponds to the number of levels that can be quite large.

In the rest of this section, we illustrate how the Reich-Moore formalism was recently used to obtain the best possible set ([DSP 90]).

The measurements considered in this analysis were obtained after 1970 and are given in Table IV.1.

Some of these measurements were carried out at low temperature to reduce the Doppler effect, such as those of Blons ([Blo 73]) for the fission cross section and those of Harvey et al. ([Har+ 88]) for the total cross section (transmission). All together, these measurements provide a data base of more than 80,000 data points.

These data were fitted with the SAMMY Code ([Lar 89]), which can calculate the cross sections with the Reich-Moore formalism. Only s-wave resonances with spins $J^\pi = 0^+$ and $J^\pi = 1^+$ were considered in the analysis. The average fission widths for these two spin states differ by about 2 orders of magnitude because the 0^+ transition state is below the neutron separation energy and is therefore fully open, whereas the 1^+ transition state is above the neutron separation energy and is partially closed. During the fitting procedure, one fission channel was assumed for the 1^+ resonances, but two fission channels were used for the 0^+ resonances for reasons discussed in Sec. B.3.c. The Bayesian approach was used in the fitting

procedure so that the various experimental parameters could be adjusted and optimized within given constraints.

Input resonance parameters below 660 eV (including their spins) came from a previous analysis ([Der 73]). Above 660 eV, the input spins were chosen according to the widths of the resonances, broad (narrow) resonances were given spin 0 (1), and the other input parameters were chosen by inspection of the data. Great care was given to background corrections and to the normalization of the data. A single correlated SAMMY fit that covered all the selected data and the entire energy range was not possible. Instead, the fits were separated into several energy intervals, and each fit included all the resonance parameters.

Examples of fits to the data are given in Fig IV.2 for the 50- to 100-eV and 800- to 900-eV intervals. The transmission results illustrate the effects of the resolution and the sample temperature at high energy. For the fission cross section, the results of Blons [Blo 73] have a better resolution and a reduced Doppler effect than those of Weston and Todd [WT 84], but the latter have better statistical accuracy and lower background.

The average fission cross sections over 100-eV intervals obtained from the above fits are given in Table IV.2, where they are compared with those obtained from the data by Blons ([Blo 73]) and Weston and Todd ([WT 84]) and from the evaluated data file given in ENDF/B-VI (Standards Subcommittee) ([Car+ 87]). Note the good agreement between the SAMMY fits and the data by Weston and Todd; however, both the SAMMY fits and the data by Weston and Todd are somewhat below the data by Blons and the ENDFB/B-VI evaluated data.

The properties of the resonance parameters as obtained in this analysis are discussed in Sec. B.3.

3. Properties of the ^{239}Pu neutron resonance parameters

a. Level spacings. The average spacing of the observed resonances can be easily obtained from a plot of the cumulative sum of observed resonances as a function of energy as in Fig. IV.3. This plot is approximately linear up to 480 eV with an average spacing of 2.4 eV. But even in this limited interval, where the plot is linear, it is shown later in this paper that levels are certainly missed. The slope

of this plot, which decreases gradually above 480 eV, shows that the proportion of missed levels increases gradually with energy above 480 eV.

The level-spacing distribution for levels situated below 480 eV is shown in Fig. IV.4 where it is compared with an uncorrelated superposition of two families of resonances, each of which corresponds to a given spin and parity state (0^+ or 1^+) and obeys the Wigner level repulsion law. This superposition assumes three times as many 1^+ resonances as 0^+ ones in agreement with the $(2J + 1)$ law. The agreement between the measured and calculated distribution is quite good, even above 480 eV (not shown here) where a larger proportion of the levels is missed. Thus, the lack of levels is not necessarily caused by small spacings missed because of unseen level overlap but rather by unseen small resonances distributed at random (also see the next section). The level-spacing distribution for each spin state does not totally agree with a Wigner law, which suggests that some spins have been misassigned.

b. Neutron widths. The average neutron widths are generally expressed in terms of the strength function S_0. More exactly, one considers for each resonance the reduced neutron width Γ_n^0 defined as

$$\Gamma_n^0 = \frac{\Gamma_n}{\sqrt{E_n}} . \qquad \text{(IV.18)}$$

Then, assuming that the strength function is spin independent, one can write

$$S_0 = \frac{1}{2} \frac{\sum 2\, g\, \Gamma_n^0}{E_n} , \qquad \text{(IV.19)}$$

where $2g\Gamma_n^0$ is obtained from an area analysis of the resonance in the total cross-section measurement, and the sum runs over all resonances analyzed below energy E_n.

One then obtains the following value for the resonances analyzed below 1 keV:

$$S_0 = (1.145 \pm 0.082)\ 10^{-4} . \qquad \text{(IV.20)}$$

This value is not very sensitive to missed levels because most of them are small, as discussed below.

The integral distribution of the reduced neutron widths for the resonances analyzed below 480 eV is shown in Fig. IV.5. No level was detected with a reduced neutron width smaller than $2g\Gamma_n^0 =$ 0.0028 meV. This histogram shows an absence of small reduced neutron widths when compared with a Porter-Thomas distribution, which is an indication that small levels are missed. This Porter-Thomas distribution gives a good fit to the data above $2g\Gamma_n^0 =$ 0.01 meV but comprises 221 resonances instead of the 201 resonances analyzed. The average level spacing deduced from this Porter-Thomas distribution is 2.17 eV instead of 2.4 eV for the observed resonances. But the proportion of missed levels depends, for example, on the threshold above which the reduced neutron widths are analyzed. A systematic study of the number of resonances below 300 eV, which need to be included in the Porter-Thomas distribution to fit the data above a given threshold, has been made as a function of this threshold. Above a threshold of about $2g\Gamma_n^0 =$ 0.16 meV, the analysis is consistent with an average level spacing as low as 1.91 eV. Thus, about 25% of the resonances may have been missed in the measurements, though they were carried out under optimal experimental conditions. All the missed resonances may not necessarily be small; some of them may be rather large.

The same study was made for resonances of a given spin, but the results are not reported here.

c. Fission widths. The analysis described in Sec. B.3.b confirms that the fission widths are very different for the $J^\pi = 0^+$ and 1^+ resonances. This analysis was carried out in the intervals 0 to 480 eV and 0 to 1 keV. The integral distribution of the fission widths for the resonances analyzed below 480 eV is plotted in Fig. IV.6. It shows very clearly the existence of two families interpreted as belonging to the two spin states $J^\pi = 0^+$ and $J^\pi = 1^+$. The parameters of the χ^2 distributions used to fit the data for the two 0- to 480-eV and 0- to 1-keV energy intervals are given in Table IV.3. A constant value of 3 meV was subtracted from all the fission widths to account for the $n(\gamma,f)$ process ([FS 74]). This value is very small compared with the average width of the 0^+ resonances, but it is not negligible compared with that of the 1^+ resonances.

The 1^+ family of resonances is consistent with one partially closed fission channel (N_{eff} = 0.1) and corresponds, in fact, to subthreshold fission. The 1^+ transition state was postulated by Griffin to result from the coupling of two octupole vibrations called the mass-asymmetry and bending modes. This analysis confirms that this 1^+ transition state is located about 200 keV above the neutron separation energy in ^{240}Pu.

The properties of the 0^+ family of resonances (N_{eff} = 2.6 and ν_f = 1.5) show that more than one fission channel is needed to fit the 0^+ fission cross section. The analysis described in Sec. B.2.b uses two fission channels and gives a good fit to the data, but an even better fit would certainly be obtained with more than two fission channels and would have a better physical basis.

d. Capture widths. The capture widths can easily be extracted from the widths Γ, Γ_f, and $2g\Gamma_n$ obtained from the analysis described in Sec. B.2.b. Even if the spin is not known, an approximate value of $g = \frac{1}{2}$ is taken to extract the neutron width, as mentioned in Sec. B.2.a. This does not cause a great uncertainty in the derivation of the capture width because the neutron width is usually small compared with the total width. The errors associated with the determination of Γ_γ are fairly large because these widths are obtained by the difference between other widths. The width Γ_γ was determined for 64% of the resonances analyzed below 1 keV and fluctuations as large as 40% are observed in these Γ_γ values. These fluctuations are not believed to be physically significant but are simply an illustration of the uncertainties associated with the determination of Γ_γ. The Γ_γ values are believed to be reliable only below 500 eV, with an average value of $\langle\Gamma_\gamma\rangle$ = 41.14 meV.

C. Fission Cross Section of ^{239}Pu Above 1 keV

The ^{239}Pu fission cross section below 1 keV, as presented in Sec. B.2.b, seems to be very good. This analysis is in good agreement with a relatively new measurement ([WT 84]) but below other values such as those of Blons ([Blo 73]) or those of the ENDF/B-VI subcommittee on standards. This analysis is also in agreement with integral measurements made with thermal neutrons.

The situation involving the ^{239}Pu fission cross section above 1 keV is not as good as below 1 keV. The measurements of Weston and Todd ([WT 84]), which are quite satisfactory below 1 keV, are below the values of the ENDF/B-VI subcommittee on standards by about 4% in the range 100 eV to 1 keV (Fig. IV.7). But these ENDF/B-VI values lead to an underprediction of k_{eff} by 1% ([Alt+ 74]). Therefore, what appears to be the most reliable microscopic measurement of σ_{nf} for Pu^{239} tends to pull this cross section down, whereas integral measurements tend to pull it up. Moreover, another measurement of σ_{nf} for Pu^{239} carried out at LANL in the MeV region ([Lis+ 88]) shows a fission cross section much higher than the values of the ENDF/B-VI subcommittee on standards (see Fig. IV.8).

In order to resolve these discrepancies especially between 1 eV and 100 keV, an international group has been set up jointly by the Nuclear Energy Agency Nuclear Data Committee (NEANDC) and by the Nuclear Energy Agency Committee on Reactor Physics (NEACRP). This group has started a very comprehensive study of the ^{239}Pu cross sections, including the analysis of recent experimental results that could not be taken into account in previous evaluations, new theoretical calculations of microscopic cross sections, and simulations of results on several integral measurements.

V. REACTIVITY TEMPERATURE COEFFICIENT IN PRESSURIZED-WATER REACTORS

A. Introduction

The variation of reactivity with temperature is very important for the safety of fission reactors. This subject was already discussed for fast power reactors in Chap. III, where the effect of Doppler broadening on self-shielding was presented. This subject is also important for PWRs for which the effect of temperature is important for different reasons. In PWRs, the spectrum of thermal neutrons is too low in energy to cover neutron resonances. But a change in temperature induces a change in the thermal neutron energy spectrum and, consequently, a change in the fission rates because the cross sections change with energy in that energy range.

Over the years, a disagreement about the reactivity temperature coefficient (RTC) has emerged. This coefficient, which must be negative for safety reasons, must be known to about ±1 pcm/°C (1 pcm = 10^{-5}). The value of this RTC is systematically

overestimated in the calculations compared with experimental results coming from the operation of PWRs, as well as from integral experiments (such as CREOLE and GEDEON) ([BGT 83],[ST 88]). The disagreement between the experimental values (called E) and the calculated values (called C) of the RTC for integral experiments is

$$E - C = (4.2 \pm 2.0)\ \text{pcm/°C} . \qquad (V.1)$$

The data coming from the PWRs are more difficult to interpret. But many analyses show that the calculated value of the RTC seems to be systematically 1 to 3 pcm/°C above the experimental value that corresponds to the domain of operation of PWRs (about 300°C).

Reducing the difference between the calculated and the experimental values to therefore obtain a more negative RTC in the calculations required a modification of the shapes of the ^{235}U cross sections in the thermal energy range ([GMS 84], [San 87]). The shapes of the ^{235}U cross sections at low energy have been a puzzle for a long time (see for example [SS 58]). To explain their behavior, one had to postulate the existence of "negative-energy resonances" that modified the cross sections at small "positive" energies. Negative-energy resonances correspond to compound-nucleus states with energies situated below the neutron separation energy. The existence of two such negative-energy resonances was assumed to obtain calculated values of the RTC that agreed with the experimental values. However, the resonance parameters (below) are different from those used previously:

$E_0^1 = -0.80$ eV $\Gamma_f^1 = 230$ meV

$\Gamma_\gamma^1 = 31$ meV $(g\Gamma_n^0)_1 = 0.34$ meV

$E_0^2 \simeq 0$ $\Gamma_f^2 = 10$ meV

$\Gamma_\gamma^2 = 40$ meV $(g\Gamma_n^0)_2 = 1.6 \times 10^{-4}$ meV

As can be seen, the negative-energy resonance at - 0.8 eV is shifted at lower energy (by 0.25 eV) compared with previous values, and a small resonance dominated by capture is added at 0 energy. This causes σ_{nf} to level at a lower value and η to drop at very low energies. In addition to these negative-energy resonances, a series of other negative-energy regularly spaced resonances (picket-fence model) was taken into account in the calculations ([San 91]).

In the next two sections, we shall compare the values of σ_{nf} and η for ^{235}U calculated with the inclusion of these two resonances with recent measurements of these two quantities.

B. Shape of the ^{235}U Fission Cross Section at Low Energy

The calculated shape of σ_{nf} for ^{235}U as obtained with the parameters given in Sec. A is plotted in Fig. V.1. It is below the previously assumed shape as given in ENDF/B-V at very low energies (below about 0.01 meV) and more in accordance with a 1/v behavior.

A recent measurement, made at Geel, settled this question ([WD 86]). In what follows, we give a brief description of this experiment.

The Geel linear accelerator, called GELINA, was used as a pulsed neutron source to carry out this measurement by the time-of-flight (TOF) method with a flight path length of 8.2 m. Neutron production at low energy was increased by slowing down the primary neutrons in a liquid-methane moderator cooled to 77 K. The ^{235}U fission events were detected with surface-barrier detectors from a thin deposit of 53 $\mu g/cm^2$ of $^{235}UF^4$ mounted back to back with a thin layer (25 $\mu g/cm^2$) of ^6LiF in a vacuum chamber. The $^6Li(n,\alpha)t$ has a perfect 1/v cross section that was used to obtain the shape of σ_{nf} for ^{235}U. GELINA was operated at the low repetition frequency of 40 Hz to minimize the neutron overlap at such small neutron energies.

The fission data were normalized in two steps to a fission cross-section value of (587.6 ± 2.6) barns for thermal neutrons; the σ_{nf} values are plotted in Fig. V.1. These results agree with previous values above about 10 meV, but at lower energies, they are below the ENBF/B-V values and are consistent with 1/v behavior. They are also in good agreement with the cross section postulated to obtain the RTC more in line with the integral experiments.

Another more exotic experiment was carried out at much lower energies from 6 to 60 μeV ([Wag+ 88]), using the source of very cold neutrons installed at the high-flux reactor of the Institut Laue-Langevin (ILL) ([Mic 87]). This experiment, briefly described below, is still to date the only cross-section measurement made at such a low energy.

The neutrons used in this experiment were produced in the reactor, cooled in a liquid-deuterium moderator at 25 K (where they have wavelengths between 20 and 600 Å), and then further decelerated in a set of vertical and curved neutron guides having excellent reflectivity. The integrated neutron flux at the exit of these neutron guides was about 1.2×10^9 neutrons/cm^2/s. Although this neutron source is continuous, the TOF method was used to obtain the measurements made on a 0.581-m flight path, using a very slow chopper operated at 300 to 600 rotations per minute. The measurements were made by detecting the fission fragments originating from a thin ^{235}U layer and the alpha particles or tritons emitted from a thin ^{6}LiF layer. Those two layers were placed inside a vacuum chamber, and the events were detected with solid-state detectors. The raw neutron spectrum obtained with the ^{6}LiF layer is plotted in Fig. V.2 with the shape of σ_{nf} for ^{235}U. Apparently, there is no detectable deviation of the cross section from a 1/v law over the whole energy range of the measurement. This behavior of the cross section is in agreement with the low-energy part of the Geel results.

C. Shape of η for ^{235}U at Low Energy

For the same reasons as for the measurement of σ_{nf} for ^{235}U at low energies, the Central Bureau for Nuclear Measurements (CBNM) undertook two measurements (one at Geel and one at the ILL) to obtain more precise information about the behavior of η for ^{235}U at low energy. We give a brief description of these two experiments below ([Wei+ 90]).

The measurement at Geel was made by the TOF method, using GELINA (equipped with a liquid-methane moderator cooled down to 77 K) as a pulsed neutron source operated at a repetition frequency of 40 Hz. At a TOF distance of 8.8 m, a "black" metallic sample of uranium enriched in ^{235}U was used. Essentially all the incident neutrons were absorbed in the sample at least below 100 meV. The measurement involved detection of the fission neutrons emitted from the sample. The spectrum of the incident neutrons was determined by a thin flux monitor. This gave, by definition, a measurement of η. The fission neutrons were detected with a thick NE213 liquid scintillator used with the pulse-shape-discrimination (PSD) method to remove the pulses given by γ-rays. Precautions, which were needed to reduce the background especially above 20-meV incident neutron energy, were taken by placing a beryllium

filter across the incident beam to reduce the neutron flux above 6.8 meV and by placing a ^{6}Li sleeve around the uranium sample.

The results obtained from this measurement after a thorough analysis of the data are shown on Fig. V.3. Good agreement can be seen with the shape deduced from integral measurements.

Another measurement using the same method was made at the ILL where a more suitable source of subthermal neutrons was available. The experiment was carried out at the end of a neutron guide that views the heavy-water moderator of the high-flux reactor. A double chopper located at the end of the neutron guide provides a source of monochromatic neutrons. The first chopper provides a pulsed white source of neutrons, whereas the second chopper provides slices of a band of neutron energies in this white spectrum. The two choppers are operated at slightly different velocities so that their relative phase and, consequently, the selected neutron energy are varied continuously. This arrangement provides a more controlled background. The results obtained from this measurement are displayed in Fig. V.4 where they are notably in agreement with those obtained at Geel and from the integral measurements.

VI. FISSION-PRODUCT YIELDS

A. Introduction

Fission yields must be known to thoroughly understand the delayed effects in fission, such as the decay heat that follows the shutdown of a reactor (see Chap. VII) and the delayed-neutron emission that plays an important role in the kinetics of a fission reactor (see Chap. VIII).

The physical phenomena associated with the formation of fission fragments were already discussed in broad terms in Chap. I. More specific properties of fission products produced after prompt neutron emission are considered in Sec. VI.B. The measurements and the calculations of the fission-fragment yields are described in Secs. VI.C and VI.D, respectively.

Users of data on fission-fragment yields can find the relevant information in complete computerized libraries, which contain yields for all significant fission products and for all the important fissioning systems. The libraries that can be used are listed below:

- the U.K. adjusted library UKFYA2 (now included in JEF2),
- a U.S. library at Los Alamos National Laboratory,
- a French library,
- a Chinese library, and
- a Japanese library.

All these libraries are in the ENDF/B-VI format and are discussed in detail in [Jam 87] and [JMW 90].

B. General Properties of the Yields of the Fission Products

1. Definitions of fission-product yields. A great variety of fission products, about 1,300, can be formed over many fission events. A fission-product yield is the probability that a given fission product is formed in one single fission event. This probability varies as a function of the fissioning system (A_F, Z_F) and its excitation energy. A detailed discussion of the yields of the fission products requires some definitions of these yields.

The most elementary fission-product yield is the independent yield IN = Y_i = Y(A,Z,I) of a given nuclear species i = (A,Z,I) having mass and atomic numbers A and Z, respectively, produced in a state I, which is either its ground state or an isomeric state.

For some measured yields, one obtains the yield $Y_i(q, E)$ of a given fission fragment i produced in an ionic-charge state q with an energy E. Summation over all possible charge states and integration over the energy must be made to obtain the IN (see Sec. VI.C).

The mass-number yield Y(A) is the summation, for a given A, of the INs over all possible values of Z and states I:

$$Y(A) = \sum_{Z,I} Y(A,Z,I). \qquad \text{(VI.1)}$$

In a similar manner, the atomic-number (also called charge or element) yield Y(Z) for a given value of Z is obtained by summing the INs over all possible values of A and I:

$$Y(Z) = \sum_{A,I} Y(A,Z,I). \qquad \text{(VI.2)}$$

The yields Y_i, Y(A), and Y(Z) are defined at the time of the formation of the primary fission products immediately after prompt-neutron emission but before their β decay has started ($\simeq$ 1 ms).

The cumulative yield $Y_c(A,Z,I)$ for a given nuclear state i is the sum of the independent yield Y_i and of all the subsequent yields Y_j of chain members j that decay to the nuclear state i.

The chain yield Y(A) for a given mass number A is the sum of all cumulative yields ending with stable end products having the same A.

The fractional independent and cumulative yields for a given fission product i having mass number A are obtained by dividing the independent and cumulative yields Y_i and Y_c, respectively, by the chain yield for the same mass number A.

The ternary yield is the cumulative yield of a light charged particle (^{4}He, ^{3}H, ^{14}C, etc.)

There are essentially three general methods used to derive a yield Y:

- direct determination relative to one fission event,
- determination relative to the yield Y_{ref} of a reference fission product, and
- determination of a "ratio of ratio," $(Y/Y_{ref})_a$ relative to $(Y/Y_{ref})_b$, where the subscripts a and b refer to different fissioning systems or to the same fissioning system but at different energies.

An illustration of the yields Y_i, Y(A), and Y(Z) is given in Fig. VI.1 for the thermal-neutron-induced fission of ^{235}U.

2. Mass distribution of the fission fragments. The chain yield for neutron-induced fission of ^{235}U is plotted in Fig. VI.2 for several incident neutron energies. This yield is very asymmetric for thermal neutrons. The most probable yield of asymmetric fission at the peaks of the mass distribution is about 600 times more abundant than the yields for symmetric fission in the valley of this distribution. This result is the consequence of shell effects that give extra stability and

yield to the heavy fragment around the doubly closed shell Z = 50 and N = 82. Confirmation of this interpretation is given by the variation of the mass distribution as a function of the mass A_F of the fissioning system. As illustrated in Fig. VI.3, the average mass $\langle A_H \rangle$ of the heavy-fragment group remains constant when A_F is changed, whereas the average mass $\langle A_L \rangle$ of the light-fragment group increases linearly with A_F. Therefore, the mass increase of the fissioning system goes to the light fragment, not to the heavy fragment, which is stabilized by the closed shells both in neutrons and in protons. When the atomic number Z_F of the fissioning system is equal to 100 (twice the magic number 50), then the mass distribution becomes symmetric when the neutron number N_F of the fissioning system is equal to or exceeds 158. The transition from symmetric to asymmetric fission is very rapid, as can be seen in Fig. VI.4.

The asymmetry in the fragment-mass distribution for most actinides at low excitation energy is caused by shell effects, as discussed above. Shell effects decrease with increasing excitation energy. As a consequence, the mass asymmetry in the fission fragments should also decrease with excitation energy. This effect is actually observed, for example, in the fission induced in ^{235}U by neutrons of various energies, as illustrated in Fig. VI.2 where symmetric fission, which is very low for thermal neutrons, increases with incident neutron energy.

3. Charge distribution of the fission fragments. An illustration of the charge distribution of the fission fragments is given in Fig. VI.5. The locations of the fission products obtained in the light group for thermal-neutron-induced fission of ^{233}U are plotted on a (Z,N) chart. An examination of the locations of these fission products shows that their proton-to-neutron ratio Z/N is, on the average, slightly greater than the ratio Z_F/N_F of the fissioning system even with the correction made for prompt-neutron emission. The fission fragments are in fact situated between the line of β stability and the line of unchanged-charge distribution $Z_{UCD}(A)$, defined by

$$\frac{Z_{UCD}(A)}{A + \overline{\nu_p(A)}} = \frac{Z_F}{A_F}, \qquad \text{(VI.3)}$$

where $\overline{\nu_p(A)}$ is the average number of prompt neutrons emitted by the fragment of mass number A.

Because of charge conservation, heavy fragments have, on the average, a proton number smaller than Z_{UCD}.

More quantitatively, the isobaric charge distribution P(Z) can be adequately described by a Gaussian of the following form:

$$P(Z) = \frac{1}{\sigma_Z(A)\sqrt{2\pi}} \exp \frac{-[Z - Z_p(A)]^2}{2\sigma_Z^2(A)}, \qquad \text{(VI. 4)}$$

where $Z_p(A)$ is the most probable charge and $\sigma_Z(A)$ is the standard deviation of the distribution. An example of isobaric charge distribution is given in Fig. VI.6. The charge $Z_p(A)$ is usually expressed as the difference $\Delta Z_p(A)$ (the charge shift) between $Z_p(A)$ and $Z_{UCD}(A)$:

$$\Delta Z_p = Z_{UCD} - Z_p. \qquad \text{(VI.5)}$$

The charge shift ΔZ_p varies from fragment to fragment but is, on the average, equal to 0.5 (-0.5) for a heavy (light) fragment.

The width parameter σ_Z also varies from fragment to fragment but, on the average, increases slightly with A_F from about 0.5 for thorium to 0.65 for californium.

There is an odd-even effect in the charge yields Y(Z) whereby fragments with even-Z values are formed with larger yields than those having odd-Z values. This odd-even effect, which decreases with increasing excitation energy and mass of the fissioning system, has been extensively studied to pinpoint possible viscosity effects in fission ([BR 89]).

C. Measurements of the Yields of the Fission Fragments

1. Introduction.

Several methods can be used to obtain experimentally the fission-fragment yields:

- direct γ-ray spectroscopy,
- radiochemistry, and
- physical measurements on fission fragments in flight.

These methods have been reviewed several times ([Den 83]). In the following, the principles of the first two methods are briefly summarized (Secs. VI.C.2 and VI.C.3), and a few examples of fission-

fragment spectrometers for in-flight measurements are given in Sec. VI.C.4.

2. Method of direct γ-ray spectroscopy. In this method, the fissile sample is irradiated for a given period of time, and the spectrum of γ-rays emitted by the fission products is subsequently measured as a function of time with a high-resolution γ-ray spectrometer. Each γ-ray is the signature of the decay of a specific fission product whose γ-ray activity can then be measured as a function of time. The method, though simple in its principle, is sometimes difficult to apply because the numerous components are often difficult to disentangle, one from the other, in the complex spectra. Also, γ-rays emitted by low-yield fission products cannot usually be seen. The analysis of the measured spectra requires a knowledge of the decay properties of the fission products. For these reasons, the accuracy of the method is limited to 5% at best.

3. Radiochemical methods. In radiochemical methods, several techniques can be used. The classical manual-radiochemical-separation technique was widely used in the early days of fission studies. This technique can be applied when the decay time of the fission product is long enough, and it can be very successful for the determination of extremely low yields, down to the 10^{-13} level. The classical radiochemical method can be improved by the use of fast, automatic separation techniques, which make it possible to extend the range of measurements to fission products with shorter lifetimes. On-line separation techniques are also frequently used, such as the emanation technique for rare gases. Another radiochemical method makes use of mass separation with a chemically selective ion source. The product spectrum thus obtained is much simpler than the original one because mass separation excludes a number of chemical elements. The mass separators using this technique include OSIS (Soreq, Israel), OSTIS at the ILL (Grenoble, France), and OSIRIS (Studsvick, Sweden).

4. Physical measurements of the fission fragments in flight. Physical methods usually involve making measurements on the fission fragments after prompt neutron emission and after full (or almost full) acceleration by their mutual Coulomb field. But these fragments are not slowed down, except for the possible small energy loss in the sample (usually thin) where they are emitted. The fission fragments are then analyzed by a high-resolution spectrometer,

which selects their mass (and possibly their charge). The independent yield for these mass and charge numbers can then be measured. Two such spectrometers, LOHENGRIN, installed at the ILL high-flux reactor, and HIAWATHA, installed at the Illinois Advanced TRIGA Reactor (Urbana, Illinois, U.S.), are briefly described below.

The LOHENGRIN spectrometer analyzes, outside the reactor (with a very small solid angle), the recoiled fission fragments emitted from a sample located inside the reactor in a thermal-neutron flux of 5×10^{14} n/cm2/s ([Mol+ 75]). The spectrometer uses a combination of electrostatic and magnetic deflections of the fission-fragment beam, as illustrated in Fig. VI.7. For a given set of electric and magnetic fields (U and B, respectively) and for a given value of the ratio A/q (q is the ionic charge of the fragment), the deflected particles are located on a parabola. The ratio of energy to ionic charge E/q of the fragment varies along the parabola. Therefore, at a given location in space, where the fragments are detected, and for a set of values for U and B, the fragments are selected according to their A/q and E/q values. The total energy E of the fragments is measured with an ionization chamber. The three parameters, A, E, and q, are then known, and the yield Y(A) can be determined by summation over all possible values of E and q obtained from other similar measurements. A mass-resolving power of $A/\delta A \geq 400$ (where δA is the mass resolution) is currently obtained for fragments of the light group. The nuclear charge can also be determined, for example, by the energy loss ΔE of the fragment in a passive (solid) absorber placed across the fission-fragment beam in front of the ionization chamber or by an active (gaseous) absorber, which is a part of the chamber itself. In both cases, the nuclear charge can be obtained from the measured ΔE value, which is dependent on the nuclear charge. An example of charge determination obtained with the passive-absorber method is given in Fig. VI.8. Charge determination with an active absorber is less precise because the resolution of a gaseous absorber is not as good as that for a solid absorber. Another method uses a Frisch-grid ionization chamber to detect the fission fragment, which subsequently provides a measurement of the nuclear charge. The shape in time of the signal given by such a chamber is similar to a Bragg curve and is therefore dependent on the nuclear charge, which can subsequently be determined ([Oed+ 83]).

In the same manner as for the LOHENGRIN spectrometer, the HIAWATHA spectrometer analyzes, outside the reactor, the fission fragments emitted from a sample located inside the reactor in a thermal-neutron flux of 4×10^{12} n/cm^2/s ([DW 77]). The mass of a fission fragment is determined by a TOF measurement of the time t it takes the fragment to traverse a distance d and of the kinetic energy E of this fragment. The experimental arrangement is sketched in Fig. VI.9. The energy E is measured with a 2 to 4% resolution with a surface-barrier detector at the end of the flight length. But to achieve a better resolution, the TOF instrument is preceded by an electrostatic analyzer, which can provide a more precise measurement (about 0.3%) of E/q. Because the charge q is an integer, the final energy resolution is also about 0.3%. The overall mass resolution obtained with this spectrometer is $\delta A \simeq 0.5$. As for LOHENGRIN, summation over E and q is required to obtain the mass yield Y(A). No measurements of the nuclear charge with HIAWATHA has been reported.

A great number of fission-fragment yields have been measured, but an experimental effort is still necessary

- in the symmetric fission region,
- for neutron-induced fission at different neutron energies, and
- for fissile nuclei having an odd nuclear charge number.

D. Calculations of Fission-Fragment Yields

Independent yields have been measured for only a small fraction of the large number ($\simeq$ 1,000) of fission fragments, even for the best-known fissioning systems. For example, about 220 INs have been measured for the thermal-neutron-induced fission of ^{235}U and 140 for the thermal-neutron-induced fission of ^{239}Pu. Calculations that can supplement the known INs for these fissioning systems and that can predict the INs for other systems for which the yield data are scarce or even nonexistent are therefore essential. Such calculations are based on models that use systematic trends of the parameters derived from available data. The same situation also applies, to some extent, to other yields, such as the mass and the charge yields.

The mass yields are better known than the other yields especially for the fission fragments situated at the peaks of the

asymmetric mass division. One of the first methods used to calculate the mass yields for a large number of fissioning systems involved fitting the available data with a sum of five Gaussian curves, two complementary pairs for the light- and heavy-fragment peaks, and one single curve for symmetric fission. The parameters used in these calculations were either obtained directly by fitting the available data or were extrapolated from these data ([MCT 74], [Dic 87a]).

More sophisticated models, called the Z_p and the A'_p models, were developed by Wahl ([Wah 88]). These models are an extension of the model using the five Gaussian curves discussed above. The Z_p model assumes a Gaussian charge dispersion about the most probable Z_p value for a primary fragment of mass A. In the same manner, the A'_p model assumes a Gaussian mass distribution about the most probable A'_p value for a fragment of mass A' (A' is the mass number of the fission fragment before prompt-neutron emission). The parameters used in the equations that define the mass and charge distributions are derived globally by least-squares fits to the available data. These data are evaluated for the light and heavy fragments and treated together by the least-squares method. Model parameters are derived preferentially for the heavy fragment, with complementary values used for the the light fragment, because of the stability of the heavy-fragment group for different fissioning systems. Yields are also modulated to take into account pairing effects both in neutrons and in protons. The average values of the number of prompt neutrons emitted by each fragment are estimated empirically from experimental data.

These models have been used by Wahl ([Wah 88]) to calculate the fission-fragment yields for eight different fissioning systems from the fast-neutron-induced fission of ^{232}Th to the spontaneous fission of ^{252}Cf. An illustration of such calculations is given in Figs. VI.10 and VI.11 for the charge and the mass yields, respectively, of the thermal-neutron-induced fission of ^{235}U. As can be seen from Fig. VI.11, the A'_p model involves the summation (for each mass number) of the independent yields obtained from the isotopic mass distributions for various charge numbers. These figures show a very good agreement of the calculations with the data. Yet, some areas of discrepancies can exist for low yields near symmetric fission or in the wings of the asymmetric mass division. These models are also used in calculations for evaluated data files such as JEF2 and ENDF/B-

VI. Similar calculations could be extended to other systems if new measured yields are made available, as discussed in Sec. VI.C.

VII. DECAY HEAT

A. Introduction

As discussed in Chap. VI, the fission products after prompt-neutron evaporation are still away from the line of β stability on the neutron-rich side. Therefore, they are generally unstable and decay by β-ray emission with lifetimes that are long compared with the fast processes governed by the strong interaction. The residual nucleus obtained by β-ray decay is generally formed in an excited state that decays by γ-ray emission. In some cases, the residual nucleus can also decay by neutron emission discussed in Chap. VIII. The β-rays and the γ-rays emitted over long periods of time in the decay of the fission products dissipate heat in the irradiated fuel. This is the so-called decay heat, though a more precise expression should be "decay heat rate" or "decay power" because the decay heat is in fact a power dissipated in the sample.

Another source of decay heat, different from that of the fission products but usually much smaller at least for short cooling times, comes from the actinides formed during the operation of the reactor, especially for high burnups. The contribution of the actinides to the decay heat is difficult to measure and is usually calculated. This aspect of decay heat is ignored in this chapter.

The decay heat generated by the fission products is a very important parameter in nuclear safety. It is possible to stop the fission process in a nuclear reactor; however, it is not possible to stop the generation of decay heat, which must be removed by very reliable cooling devices to avoid serious consequences such as the melting of the fuel.

The decay heat must be known for different time scales and for different purposes. A time scale from a fraction of a second to a few days following fission (short cooling times) is applicable to the so-called in-core utilization (or burnup) and to the consequences of a loss-of-coolant accident (LOCA). This time regime is relevant to safety and is the only one considered in this chapter. Longer time scales are relevant to the storage of the irradiated fuel either onsite or offsite (for example, for reprocessing).

The decay heat dissipated in an irradiated fuel depends on the history of the operation of the reactor before its shutdown and any possible modification of the fission-product inventory by neutron radiative capture. This aspect is considered here only for integral experiments discussed in Sec. VII.B.

The basic decay-heat data that are required include the average energies $\langle E_\beta \rangle$ and $\langle E_\gamma \rangle$ that correspond to the energies released by the β-rays and the γ-rays, respectively, and possibly the energy spectra for these radiations as a function of time following one fission event. The decay power m(t) produced at a time t after a fission event is called the decay-heat burst function, which is the sum of the burst functions b(t) and g(t) that correspond to the β-rays and γ-rays, respectively.

The decay heat can be obtained from calculations or from measurements. The summation method, which is used extensively in the calculations, has made great progress and is preferable, whenever possible, because it is based on the contributions of individual fission products. The origin of the decay heat can therefore be identified more precisely, and the knowledge of the decay heat can then be more easily extrapolated to different fissioning systems. But the measurements remain indispensable, which was the case in the early studies of decay heat because the fission-product data were scarce at that time, especially for short-lived ones with more energetic radiation releases. But measured data on decay heat are still very useful because they provide a verification of the calculations and can therefore establish confidence in the validity of these calculations.

Measurements of decay properties of individual fission products also play an important role as basic ingredients in calculations using the summation method (see Sec. VII.C).

The measurements and calculations of the decay heat and fission-product decay properties are discussed in more detail in Secs. VII.B and VII.C, respectively.

B. Measurements

Measurements of decay heat following fission were made in the 1940s shortly after the discovery of fission as part of the Plutonium

Project. Details of the first decay-heat measurements made in 1942 and 1943 are given by Borst ([Bor 51]). The decay-heat measurements that have been carried out since this early work have been reviewed many times (see [Sch 79], [Tob 80], and [Dic 87a]). In the following, we review briefly the various methods used to measure the decay heat, and we describe some recent work in this field.

In the experimental determinations of the decay heat, a fissile sample is first irradiated for a given time in a known neutron flux; the irradiated sample is then rapidly removed from the irradiation position (usually with a fast pneumatic device), and the residual heat produced in the sample is subsequently measured as a function of the cooling time following the end of the irradiation.

The spectrum of the neutrons used for the irradiation depends on the future use of the decay heat results, e.g., whether it is for light-water reactors or for fast breeders.

The burst function m(t) can be obtained directly from the measurement if a short and intense neutron burst is produced for the irradiation of the sample. Although such neutron bursts are sometimes available, e.g., with the GODIVA fast-pulsed ^{235}U critical assembly at the Los Alamos National Laboratory, they are very difficult to produce. In practically all cases, the sample is irradiated during a time I that cannot be neglected, and the result of the measurement is not directly m(t) but, rather, a quantity M(I,t) given by the following expression:

$$M(I,t) = \int_{t}^{I+t} m(\tau)\, d\tau \,. \qquad \text{(VII.1)}$$

In a subsequent analysis of the results, the quantity M(I,t), usually obtained for several values of I, is frequently transformed into the burst function m(t). Direct comparisons between different M(I,t) results can nevertheless be made without using the burst function m(t) provided that consistent M(I,t) values are used in the comparisons.

The number of fissions that took place in the sample during the irradiation must also be determined to obtain the decay heat per fission.

Since the pioneering measurements mentioned above, the techniques for the experimental determination of the decay heat have varied considerably from integral to microscopic measurements.

Calorimetry is an integral method that was widely used in early measurements. Still in use, it can give the total decay heat in a single measurement. But this method is usually not suitable for short cooling times because the time constant of the calorimeter is generally too long. Calorimeters can be designed to have a smaller heat capacity with a time constant less than 1 s. But these calorimeters have small dimensions and cannot totally absorb the hard γ-rays that are emitted by the sample. The measured decay heat is then underestimated. To compensate for that, γ-ray detectors can be placed around the calorimeter to detect hard γ-rays that may escape the calorimeter. A separation between the contributions from β-rays and γ-rays can sometimes be achieved by using absorbers.

A major step forward toward more sophisticated decay-heat measurements was made with the radiation-spectrometry method that uses counters, especially scintillators, to detect and to measure separately the γ-rays or β-rays or both. These detectors can provide the spectrum of the radiation emitted from the sample. Most measurements of the radiation responsible for the decay heat are made on the ensemble of all fission products accumulated from many fissions, or aggregate fission products (AFP), present in the irradiated sample. The average energies, $\langle E_\beta \rangle$ or $\langle E_\gamma \rangle$ or both, can easily be derived from the spectrum measurements of the β-rays or the γ-rays or both, respectively. Because of the fast response of these detectors, the decay heat can be measured for very short cooling times. In most cases, only the γ-rays are detected because they can escape the irradiated sample much more easily than β-rays, which have a short range in the sample. Yet the γ-ray spectra are also difficult to measure for short-lived fission products, not only because of the short half-life of these products but also because large energies are involved in the decay of short-lived products with the consequence that the spectra extend over a large energy range and are very complex and that many γ-ray lines are often missed in the measurements. The β-rays can be measured with thin samples if the

fission cross section or the neutron flux or both for the irradiation are large enough.

It is also possible, with more sophisticated techniques, to measure the radiation emitted by individual fission products. For example, the fission product responsible for the emission of a particular measured radiation can be identified from a specific γ-ray transition emitted by this fission product or its daughter. Many decay properties of fission products were also obtained as a spin off of the increased use of on-line isotope separation techniques developed for nuclear astrophysics, which make use of these data for tests of models for nucleosynthesis. Though not made for fission studies, these results could be used for the knowledge of fission-product properties. All the results on these fission-product properties can be used directly or indirectly in the calculations of the decay heat, as discussed in Sec. VII.C.

Most of the experimental studies on the decay heat are now carried out in Sweden and in Japan. In the following, we describe briefly the methods used in these two countries.

In the measurements made in Japan at the National Engineering Research Laboratory (NERL, often called YAYOI in the literature) the decay heat was determined for the AFPs produced in fission induced by fast neutrons in ^{233}U, ^{235}U, ^{239}Pu, ^{238}U, natU, and ^{232}Th for a time scale between 10 to 10^5 s ([AA 82]). The samples were irradiated at the center of the grazing hole of the YAYOI reactor where the neutron spectrum is similar to, though a little softer than, a fission-neutron spectrum. Both the β- and γ-ray spectra were measured for the fission of ^{233}U, ^{235}U, and ^{239}Pu, but only the γ-ray spectra were measured for the fission of ^{232}Th, natU, and ^{238}U. For these last isotopes, as compared with the fissile ones, the fission rate is smaller. Larger samples had to be used with the consequence that β-rays could not be measured. Irradiation times of 10 s and 100 s were used for the γ-decay measurements and slightly longer times of 10 s, 60 s, and 300 s were used for the β-decay measurements. The number of fissions that took place in the sample during irradiation was measured from the activity of ^{97}Zr, which was also formed during the irradiation. The γ-ray spectrum was measured between 0.1 and 5 MeV with a NaI scintillator, which had a diameter and a length of 76.2 mm and was properly shielded against β-rays. The β-ray spectrum was measured between 0.3 and 8 MeV with a plastic

scintillator having a well shape with external diameter and length of 50.82 mm and a hole of 16 mm in diameter and 20 mm in depth. The average energies $<E_\beta>$ or $<E_\gamma>$ were obtained by integrating these spectra at different cooling times and normalizing them to the number of fission events. These results are discussed in Sec. VII.C.

In a measurement made in Sweden at the Studsvick Neutron Research Laboratory (SNRL), the decay heat was measured for the AFPs produced in the thermal-neutron-induced fission of ^{235}U and ^{239}Pu and for the fast-neutron-induced fission of ^{238}U ([Joh 88]). Both the β-ray and the γ-ray decay heat were measured separately for ^{235}U and ^{239}Pu, but only the γ-ray decay heat was measured for ^{238}U. The neutrons were produced with the 6-MeV proton beam accelerated by a Van de Graaff accelerator. For the ^{235}U and ^{239}Pu measurements, the fast neutrons produced from the bombardment of a thick ^{9}Be target by the proton beam were thermalized in a big block of paraffin. For the ^{238}U measurements, fast neutrons of 2.3 MeV were produced with the T(p,n) reaction by bombarding a thin tritium target with the proton beam. Irradiation times varied from 4 s to 120 s for ^{235}U, from 4 s to 870 s for ^{238}U, and from 20 s to 870 s for ^{239}Pu. The number of fissions was determined with fission ionization chambers for ^{235}U and ^{239}Pu and from well-known γ-ray lines from fission products for ^{238}U. The β-ray spectrum was measured for ^{235}U and ^{238}U from 400 keV to 3 MeV with a Si(Li) detector. The β-ray spectrum could not be measured for the thick ^{238}U samples, which had to be used because the $^{238}U(n,f)$ cross section and the neutron flux were too low at 2.3 MeV. The γ-ray spectrum was measured for the three nuclei from 40 keV and 6 MeV with a NaI (Tl) crystal having a diameter and a length of 12.5 cm. The results from this work are discussed in Sec. VII.C

In another measurement, also made in Sweden, the spectra of β-rays and γ-rays were directly determined for each of 112 fission products ([Rud+ 88], [Rud+ 90]). This microscopic method was already used in an earlier work for the determination of the antineutrino spectrum emitted by a reactor ([AR 82]) and is based on simultaneous measurements of the β-rays emitted by a mixture of fission products and specific γ-rays emitted by the daughter nuclei. The spectra of the β-rays emitted by these fission products are measured without any knowledge of the spectrum of the corresponding γ-rays, except for the specific γ-rays, which are labels

of the β-ray emitters. The fission products were obtained partly with ISOLDE (CERN, Switzerland) and partly with OSIRIS (Studsvick, Sweden). In both cases, the β-rays were measured with two different detectors, depending on the energy range. Above 500 keV, the detector was a telescope consisting of a thin plastic detector (for the measurement of an initial energy loss ΔE) in coincidence with a 15-mm-thick germanium detector (for the measurement of the residual energy). Below 1,500 keV, a Si(Li) detector was used. The 500- to 1,500-keV overlap region was used to adjust the two spectra relative to each other. In addition to the β-ray detector, a high-resolution Ge(Li) detector was used for the detection of γ-rays, thus permitting the identification of the β-ray emitters. In a subsequent analysis of the data, the spectra of β-rays was obtained for individual fission products in the 80 to 100 mass range (light-fragment group) and in the 130 to 150 mass range (heavy-fragment group). The $\langle E_\beta \rangle$ energies were derived from these spectra and used in the summation method to calculate the β-ray decay heat. The results obtained in this manner for 112 fission products with half-lives between a fraction of a second and a few hours can account for 50 to 60% of the β-ray heat for cooling times shorter than 100 s. If the contribution of long-lived fission products with well-known decay schemes is added to these experimental results, then about 90% of the β-ray decay heat can be determined. Measurements of γ-ray spectra were also carried out in a similar manner with OSIRIS by replacing the β-ray detector by a γ-ray detector. The results of this work are discussed in Sec. VII.C.

C. Calculations

The decay heat can, in principle, be determined by the microscopic method in which the yields and decay properties of the fission products are known. The overall decay-heat power P(t) from the AFPs formed in the fission of a given fissioning system can then be determined by the summation method, which simply involves adding the contributions of all the fission products i:

$$P(t) = \sum_i N_i(t)\, E_i\, \lambda_i\,, \qquad \text{(VII.2)}$$

where $N_i(t)$ is the number of fission products i present at time t, E_i is the energy released in the decay of fission product i, and λ_i is the decay constant of fission product i. The energy E_i can be either the β-decay energy $E_{i\beta}$, the γ-decay energy $E_{i\gamma}$, or the sum of the two

energies $E_{i\beta} + E_{i\gamma}$. This expression is exact, and the uncertainty in the calculation of P(t) comes from the uncertainties in the quantities used in the summation.

In addition to the yields, discussed in Chap. VI, the decay properties that need to be known for each fission product are the half-life $\tau_{\frac{1}{2}}$ (or decay constant λ), the various decay modes and their probabilities, and the average energies (with possibly the energy spectrum) of the emitted radiations. The total energy release Q_β in the β decay is also useful to know.

The decay properties cannot be measured for all fission products. Therefore, an experimental data base must be supplemented with calculations that make partial use of these measured data. These calculations are especially needed for short-lived fission products for which measurements are notoriously difficult. Models, like the gross theory of β decay ([TYK 73]), which assumes that the β strength function $S_\beta(E)$ varies smoothly from nucleus to nucleus, were developed for such calculations. But as evident by the growing body of measured decay properties, this assumption is not always justified, and more sophisticated models that take into account the specific properties of the nuclei ([Kla 83]) are now used.

The data for decay-heat predictions were the subject of a recent meeting ([Nea 87]). The proceedings of this meeting provide a wealth of information that are used in this chapter and are supplemented, when necessary, with more recent results.

The present knowledge of the half-lives seems satisfactory for most calculations of the decay heat. Some gaps in measured values exist for elements from Y through Pd and from La through Sm, as well as for the Ni and Co isotopes, but these nuclei do not play a major role in the decay heat. The unmeasured half-lives can be calculated with the theory of weak interactions (see [Kra 87]).

The population of fission-product isomers is a challenging problem that is not completely resolved, even for the most important ones: ^{96}Y, ^{98}Nb, ^{99}Nb, and ^{100}Nb.

The knowledge of Q_β is very useful for the calculation of the decay properties of fission products (especially for short-lived ones) and also for the verification of the energy balance in the β decay

$$Q_\beta = \langle E_\beta \rangle + \langle E_\gamma \rangle + \langle E_{\bar{\nu}} \rangle , \qquad \text{(VII.3)}$$

where $\langle E_{\bar{\nu}} \rangle$ is the average energy of the antineutrinos emitted in the β decay.

There are much fewer measurements on Q_β than on the half-lives. Therefore, the determination of Q_β values relies heavily on calculations that make use of mass evaluations. These mass evaluations become less precise away from the line of β stability. A review of the various mass evaluations is under way, but the 1988 "Midstream" evaluation ([WAH 88]) is widely used at the present time.

The average energies $<E_\beta>$ and $<E_\gamma>$ are usually deduced from β-ray and γ-ray spectra, respectively. The γ-ray spectra are more easily measured than the β-ray ones and are therefore widely used in the calculations. The calculations of the β-ray and γ-ray spectra rely extensively on the Evaluated Nuclear Structure Data File (ENSDF), supplemented by experimental results.

A comparison of the values of Q_β, $<E_\beta>$, and $<E_\gamma>$ coming from various sources can be found in [Rei 87].

The calculations of the decay heat with the summation method, using both experimental and theoretical data on the decay properties of the fission products, have been greatly developed. These calculations can now provide a good description of the decay heat for several fissioning systems. These calculations are currently compared with results of integral measurements. The quantities most used in the decay-heat comparisons are the burst functions m(t), b(t), and g(t). These burst functions vary approximately as t^{-1}, and for this reason they are often multiplied by t in the comparison plots for convenience. Discrepancies between calculations and measurements indicate that the microscopic data files may be deficient, at least for some fission products. Only a few of the innumerable comparisons are briefly described below.

The β-ray decay heat for the fission induced in ^{235}U and in ^{239}Pu by thermal neutrons was determined, for example, from an integral measurement described above ([Joh 88]) and from calculations using the summation method with the β-ray spectra measured for individual fission products described above ([Rud+ 88]) and was supplemented by the evaluated data of JEF-1 for some unmeasured β-ray energies of fission products. The summation method also made use of the fission-product yields from a data file essentially based on JEF-1. The comparison between the two sets of data is plotted in Fig. VII.1 for the fission of ^{235}U. The integral data are composed of a mixture of results obtained with irradiation times of 4 s (for short cooling times) and 120 s (for long cooling times). These integral results were not analyzed to obtain the burst function b(t), but the summation method took into account the effect of the irradiation times in the comparison. As can be seen in Fig VII.1, excellent agreement exists between the integral and the calculated results for the fission of ^{235}U. A similar agreement is obtained for the fission of ^{239}Pu. Although a good agreement is also obtained in similar comparisons using other data files in the summation method, disagreement can show up with some data files as illustrated in Fig. VII.2, which shows the interest of integral measurements for the test of fission-product data files.

The comparison between the results of the summation methods and integral experiments is illustrated for fission induced in ^{235}U by thermal neutrons in Figs. VII.3, VII.4, and VII.5 for the β-, γ-, and total-decay heat, respectively. In this comparison, the results of the summation method come from the evaluated file ENDF/B-VI ([RE 90]), and the results of the integral experiment are those from YAYOI ([AA 82]) described in Sec. VII.B. The various contributions to the summation method are also given in Figs. VII.3 through VII.5. The data used in these contributions correspond to

(a) average energies obtained from decay schemes constructed from spectroscopic investigations ([KE 91]),

(b) direct experimental determinations of the β-ray and γ-ray energies measured at Studsvick ([Rud+ 90]),

(c) average energies from gross beta theory supplemented by incomplete experimental information ([KE 91]), and

(d) average energies from gross beta theory ([KE 91]).

Note that the ENDF/B file contains data on as many as about 891 fission products of which 127 are stable and 168 are formed in isomeric states. Among the 764 unstable fission products, only 510 have some measured spectra or average energies. Theoretical calculations are needed to obtain the spectra and energies for most remaining unstable fission products and to supplement the incomplete measured spectra for 115 nuclei in the set of 510 fission products. In some cases, only the half-life of the fission product is known and sometimes the half-life is not known at all. Thus, the experimental data base for fission products is incomplete; therefore, calculated data with theoretical models are essential for a complete data file that can be used for accurate decay-heat calculations with the summation method.

An illustration of the importance of supplementing the measured data with calculated data in decay-heat calculations using the summation method is given in Fig. VII.6 for the γ-ray decay-heat burst function for the fission of ^{238}U induced by fast neutrons. The integral data comes from the YAYOI experiments. The summation method was used in the calculated results of versions IV, V, and VI of ENDF/B plotted in Fig. VII.6. The improvement in the results of the summation method is obvious when going from ENDF/B version IV to VI. This improvement comes mainly from the use of more model calculations to supplement the experimental data base.

Another effect worth mentioning is the critical role played by a few selected isotopes such as ^{102}Tc, which decays to ^{102}Ru. The γ-ray energy emitted in the decay of ^{102}Tc is poorly known, and values ranging from 80 keV to 1.2 MeV have been used in different evaluated-data files. Theoretical calculations are also imprecise. For example, a new improved theory called QRPA ([MBK 89]) cannot calculate transitions to levels located below the pairing gap in doubly even nuclei such as ^{102}Ru. The effect of using different γ-ray energies in the decay of ^{102}Tc is illustrated in Fig. VII.7 for the γ-ray decay-heat burst function for the fission induced in ^{239}Pu by fast neutrons ([RE 91]). Clearly, high γ-ray energies for the decay of ^{102}Tc are in better agreement with the integral data than are low energies.

VIII. DELAYED NEUTRONS

A. Introduction

The emission of delayed neutrons following fission was detected in 1939 shortly after the discovery of fission ([RMW 39]). The properties of these neutrons must be known with great precision because they play an important role in the kinetic behavior of any chain-reacting system during its normal mode of operation ([Kee 65]).

The physics of delayed-neutron emission in fission is briefly described in Sec. VIII.B, and recent results on delayed-neutron properties are given in Sec. VIII.C.

B. Physics of Delayed-Neutron Emission

The mechanism whereby a delayed neutron is emitted after fission is illustrated in Fig VIII.1. When a fission product decays by β-ray emission, the residual (or daughter) nucleus is generally left in an excited state. The excited daughter nucleus decays itself by γ-ray emission if the excitation energy is below the neutron-emission threshold. But, in a few cases, if the excitation energy of the daughter nucleus can be high enough to exceed the neutron separation energy S_n, the daughter nucleus decays preferentially by neutron emission because the neutron width Γ_n is greater than the capture width Γ_γ. This neutron decay of the daughter nucleus (called the neutron emitter) is fast, as is any emission governed by the strong interaction, but the β decay of the parent nucleus (called the delayed-neutron precursor) is slow because it is governed by the weak interaction. Therefore, the β decay of the precursor, not the decay of the emitter, is responsible for the relatively long emission time of the delayed neutron after fission. Consequently, the delayed-neutron emission rate follows that of the β decay of the delayed-neutron precursor.

Delayed-neutron emission can occur not only from fission products but also from other nuclei such as those formed in some heavy-ion reactions. Delayed-neutron emission is considered here for several types of fissioning systems: (1) spontaneous fission (S) and (2) fission induced by thermal neutrons (T), by fast neutrons (F), or by high-energy neutrons (H). Fast neutrons do not have a well-defined energy; they correspond generally to a fission-neutron spectrum, sometimes degraded in energy in the medium where the

fission takes place. High-energy neutrons have an energy in the neighborhood of 14 MeV.

A complete determination of delayed-neutron emission in fission requires the identification of the delayed-neutron precursors and of their properties, which are yield Y, half-life $\tau_{\frac{1}{2}}$ or decay constant λ, delayed-neutron emission probability P_n, and the energy spectrum χ_d of the emitted neutrons. But these detailed microscopic data are never completely available from experiments. They must therefore be supplemented by model calculations and from results of more global (or macroscopic) measurements that give the overall delayed-neutron properties, which are essentially the average total number $\overline{\nu_d}$ of delayed neutrons per fission (also called the absolute delayed-neutron yield), the time dependence $n_d(t)$ of the delayed neutron activity, and the energy spectrum of the delayed neutrons at various times after fission. All these results are usually tested against integral data.

Two important delayed-neutron precursors are ^{87}Br and ^{137}I with daughter nuclei ^{87}Kr and ^{137}Xe, respectively. The $\tau_{\frac{1}{2}}$ values for these precursors are 55.6 s for ^{87}Br and 22 s for ^{137}I. Neutron emission from ^{87}Kr and ^{137}Xe is possible because their neutron numbers are 51 and 83, respectively. These numbers are equal to a magic number (50 or 82) plus 1 with the consequence that this extra nucleon is loosely bound and the S_n value is small (5.5 MeV and 3.6 MeV for ^{87}Kr and ^{137}Xe, respectively). Information on delayed-neutron precursors has greatly improved over the last 15 years through measurements and also through model calculations, and the number of delayed-neutron precursors that can now be taken into account to predict delayed-neutron properties can be very large. Fig. VIII.2 presents a review of the location of delayed-neutron precursors on an (N,Z) chart with their relative contributions to the absolute delayed-neutron yield and with an indication of the experimental data available for each of them. Most delayed neutrons are emitted from odd-Z precursors. Recent model calculations of delayed-neutron properties include as many as 271 delayed-neutron precursors though many of them play a minor role ([BE 89]).

The neutron activity $n_d(t)$ can be derived from the individual properties of the delayed-neutron precursors by the summation method:

$$n_d(t) = \sum_k \lambda_k P_{nk} Y_k e^{-\lambda_k t} . \qquad \text{(VIII.1)}$$

In this expression, the summation is made over all delayed-neutron precursors k with a yield Y_k, a neutron-emission probability P_{nk}, and a decay constant λ_k. But the neutron activity $n_d(t)$ can be adequately described in terms of neutron groups much smaller in number than the large quantity of precursors used in the summation method. The most common description of $n_d(t)$ is made with a sum of a few exponentials, each one corresponding to a neutron group:

$$n_d(t) = \sum_i a_i e^{-\lambda_i t} . \qquad \text{(VIII.2)}$$

The parameters a_i and λ_i in Eq. VIII.2 are determined by fitting measured aggregate data on delayed-neutron emission following a fission pulse and on saturation irradiation experiments in critical assemblies. Satisfactory fits to the data are obtained with only six groups. An example of the half-lives obtained from these fits, weighted over nine different types of fission, are given in Table VIII.1. Other six-group decay constants can be used, but the consequences of the differences in these constants on calculated reactor kinetics are not very important. This separation into six groups is rather artificial and has no real physical basis, though the two first groups given in Table VIII.1 must be strongly influenced by the contributions of ^{87}Kr and ^{137}I. Six delayed-neutron groups are sufficient for most reactor kinetics studies. Sometimes, for certain kinetics studies, the number of groups actually used is even smaller than six, and the six-group data are frequently consolidated into two or three reduced groups.

The average total number of delayed neutrons $\overline{\nu_d}$ can also be expressed relative to the average total number of fission neutrons $\overline{\nu}$, which is then called β, the delayed-neutron fraction:

$$\beta = \frac{\overline{\nu_d}}{\overline{\nu}} . \qquad \text{(VIII.3)}$$

The average number of delayed neutrons can also be expressed for each temporal group i:

$$\beta = \sum_i \beta_i \ . \qquad \text{(VIII.4)}$$

The fractional group abundance α_i is sometimes used and is defined for each temporal group as

$$\alpha_i = \frac{\beta_i}{\beta} \ . \qquad \text{(VIII.5)}$$

The neutron activity $n_{di}(t)$ for each temporal group i is then given by

$$n_{di}(t) = a_i e^{-\lambda_i t} = \sum_k \alpha_{ki} \lambda_k P_{nk} Y_k e^{-\lambda_k t} \ . \qquad \text{(VIII.6)}$$

The summation is made on delayed-neutron precursors having decay constants λ_k satisfying the condition

$$\lambda_i < \lambda_k < \lambda_{i+1} \ . \qquad \text{(VIII.7)}$$

C. Recent Results on Delayed-Neutron Properties

1. Introduction. The most important data on delayed neutrons are their absolute yields $\overline{\nu_d}$ discussed in Sec. VIII.C.2. The delayed-neutron properties such as yields and spectra in the various temporal groups are discussed in Sec. VIII.C.3. The results presented below use extensively, among other references, recent delayed-neutron data ([Bla+ 90]). The test of these data against integral experiments is not treated here.

2. Absolute delayed-neutron yields. Measurements of the yields $\overline{\nu_d}$ have been made for 16 nuclei ranging from ^{232}Th to ^{252}Cf. An illustration of the results is given in Fig. VIII.3 for the neutron-induced fission of ^{235}U. The dispersion of the results plotted in Fig. VIII.3 indicates that the quoted uncertainties are probably underestimated.

For the thermal-neutron induced fission of ^{235}U and ^{239}Pu, the simple mean of the best available experimental results and evaluations is given below:

$\overline{\nu_d}(^{235}U) = 0.0166 \pm 3\%$ and

$\overline{\nu_d}(^{239}Pu) = 0.00654 \pm 4\%$.

For the fast-neutron fission of ^{238}U, long-standing discrepancies exist among the reported values of $\overline{\nu_d}$. A new and more accurate measurement of this parameter is therefore very desirable. Meanwhile, the following range of values are recommended:

$\overline{\nu_d}(^{238}U) = 0.043$ to 0.047.

For the less important actinides, the evaluation of Tuttle ([Tut 79]) is recommended.

The summation method can be very useful in obtaining $\overline{\nu_d}$ values, but the accuracy is about 8 to 10%, roughly twice that for direct measurements. This relatively large uncertainty is mainly due to the fission yields rather than to the P_n values. This method is very useful for nuclei for which no direct measurements have been made. Also, this method can give other information, such as the neutron spectra and the time dependence of the various delayed-neutron properties (see Sec. VIII.C.3).

Three major evaluation efforts use this method to calculate the $\overline{\nu_d}$ values:

- ENDF/B-VI in the U.S. ([BE 89]),
- JEF-2 in Europe ([NGS 91], [Bla 91]), and
- Soviet work.

For example, a set of $\overline{\nu_d}$ values for 43 fissioning systems was obtained with this method for ENDF/B-VI using as many as 271 delayed-neutron precursors in the summation procedure ([BE 89]). These results are given in Table VIII.2 and. are compared with those coming from the evaluation by Tuttle ([Tut 79]). There is an overall agreement between the two sets of results but the summation method gives systematically higher (smaller) values for the light (heavy) fissioning systems than those of the Tuttle evaluations. For

the thermal-neutron-induced fission of ^{235}U and ^{239}Pu, the summation method also gives higher results than the recommended values, which are in better agreement with those of the Tuttle evaluation ([Tut 79]). This shows the limitations of the summation method, which is not as reliable and accurate as the precise measurements or evaluations based on such measurements.

An illustration of the relative importance of the delayed-neutron precursors in the absolute yields, as obtained in the calculations by the summation method for JEF-2, is given in Table VIII.3.

The absolute delayed-neutron yields are sometimes needed for high-A actinides like ^{243}Am for which there are no direct measurements and for which the microscopic data base is too incomplete for the summation method to be used. In such cases, it is possible to derive a $\overline{\nu_d}$ value by using the semiempirical $\overline{\nu_d}$ dependence on the parameter $(3Z_F\text{-}A_F)$, as pointed out by Keepin ([Kee 65]), or on the parameter $(3Z_F\text{-}AF)A_F/Z_F$, as used more recently by Tuttle ([Tut 79]) and illustrated in Fig. VIII.4. Those two dependencies give very close values of $\overline{\nu_d}$ for ^{243}Am [$(1 \pm 0.1) \times 10^{-3}$ and 9.45×10^{-3}, respectively)] in fair agreement with more recent values, such as that of $\overline{\nu_d} = 9.1 \times 10^{-3}$ adopted for JEF-2. This example shows that these empirical laws, though not having any real physical basis, can be very useful for the prediction of average delayed-neutron yields for poorly known actinides.

Very few data are available about a possible $\overline{\nu_d}$ dependence on the energy of the incident neutrons. It is known that $\overline{\nu_d}$ depends mainly on odd-odd fission yields that vary with excitation energy, but this variation seems to be quite weak below 2-MeV neutron incident energy.

3. Delayed-neutron properties in the temporal groups. The experimental determination of the (α,λ) parameters (fractional abundances and half-lives) and the spectra for the six usual temporal groups is very difficult, and, consequently, only a few data are available for a small number of nuclei.

Measurements before 1986 were made for ^{238}U (groups 1-5) and for ^{235}U and ^{239}Pu (groups 1-4). More recent measurements

were made for the six groups at Lowell ([Sha+ 88], [Cou+ 89], [Tan+ 86]) and Birmingham ([Wea+ 87]) for ^{235}U, ^{238}U, and ^{239}Pu.

The most complete data base for the temporal description of delayed-neutron emission is obtained by the summation method ([BE 89]). Good agreement is obtained between these data and the direct measurements when a comparison is possible. This agreement gives confidence that the data base obtained for 43 fissioning systems by the summation method is reliable.

An example of the comparison of the delayed-neutron activity $n_d(t)$ calculated from the six-group parameters obtained by the summation method with a direct measurement of this neutron activity is given in Fig. VIII.5 for the fast-neutron fission of ^{235}U. The (α,λ) parameters used in the calculated results for this comparison are given in Table VIII.4.

Delayed-neutron spectra can easily be obtained from this method for each group and for each fissioning system. These calculated spectra can be compared with measured spectra obtained at Lowell for ^{235}U and for eight successive time intervals between 0.17 s and 85.5 s. Good agreement is obtained for the average energies for all eight temporal groups (Table VIII.5). These average energies are in the 400- to 500-keV range, thus demonstrating that delayed neutrons are, on the average, much softer than prompt fission neutrons that have an energy of about 2 MeV. Satisfactory agreement is also obtained for the spectra, as illustrated in Fig. VIII.6 for the delay interval 3 (0.79 s to 1.25 s).

IX. CONCLUSION

This presentation of some aspects of fission illustrates the interplay that can exist between fundamental and applied approaches to a scientific subject. Many fission studies were stimulated by applications such as the safety of nuclear reactors. The need for better knowledge of fission properties for applications was often substantiated by integral experiments. The analysis of some of these integral experiments could even predict some microscopic fission properties such as the behavior of the low-energy cross sections of ^{235}U. But confidence in integral experiments is greatly enhanced if they can be explained on a sound microscopic data base. I sincerely hope that such a fruitful interplay can continue in the future.

ACKNOWLEDGEMENTS

The author is greatly indebted to Dr. J. Blachot for many useful comments in the course of the writing of this report and to Grace Hollen for her very efficient help in editing the manuscript.

REFERENCES

[AA 63] "Neutron Cross Sections in Fissile Elements," D. B. Adler and F. T. Adler, Proceedings of the Conference on Breeding, Economics, and Safety in Large Fast Power Reactors, Argonne, Illinois, U.S., October 7-10, 1963, Argonne National Laboratory report ANL-6792 (1963).

[AA 82] "Measurements of Fission-Product Decay Data Heat for Fast Reactors," M. Akiyama and S. An, in *Nuclear Data for Science and Technology*, Proceedings of the International Conference, Antwerp, Belgium, September 6-10, 1982, K. H. Böckhoff, Ed. (D. Reidel Publishing Company, Boston, Massachusetts, U.S., 1983), p. 237.

[Alt+ 74] "ENDF-202: Cross-Section Evaluation Working Group Benchmark Specifications," Brookhaven National Laboratory report BNL-19302, ENDF-202 (1974).

[AR 82] "Average Beta-Ray Energies of Short-Lived Fission Products," K. Aleklett and G. Rudstam, Nucl. Sci. Eng. **80**, 74 (1982).

[BBB 89] "Méthodes de Mesure des Produits de Fission: Etat Actuel des Connaissances," J. P. Bocquet, J. Blachot, and R. Brissot, unpublished report (1989).

[BC 89] "50 Years With Nuclear Fission," Proceedings of an International Conference, Gaithersburg, Maryland, U.S., April 25-28, 1989, J. W. Behrens and A. D. Carlson, Eds. (American Nuclear Society, Inc. La Grange Park, Illinois, U.S., 1989).

[BE 89] "Delayed Neutron Data and Group Parameters for 43 Fissioning Systems," M. C. Brady and T. R. England, Nucl. Sci. Eng. **103**, 129 (1989).

[Bet 57] "On the Doppler Effect in Fast Reactors," H. A. Bethe, Report No. APDA-119 (Atomic Power Development Associates, Inc., and Cornell University, Ithaca, New York, U.S., 1957).

[BGG 89] "Constrained Hartre-Fock and Beyond," J. F. Berger, M. Girod, and D. Gogny, Proceedings of the International Conference on Fifty Years Research in Nuclear Fission, Berlin, Germany, April 3-7, 1989, Nucl. Phys. A **502**, 85c (1989).

[BGT 83] "Besoins en Données Nucléaires pour les Réacteurs à Neutrons Rapides," J. Bouchard, C. Golinelli, and H. Tellier, in *Nuclear Data for Science and Technology*, Proceedings of the International Conference, Antwerp, Belgium, September 6-10, 1982, K. H. Böckhoff, Ed. (D. Reidel Publishing Company, Boston, Massachusetts, U.S., 1983), p. 21.

[BL 80] "The Double-Humped Fission Barrier," S. Bjørnholm and J. E. Lynn, Rev. Mod. Phys. **52**, No. 4, 725 (1980).

[Bla 91] "Delayed-Neutron Yields for 39 Fissile Systems," J. Blachot, Paper presented at the International Conference on Nuclear Data for Science and Technology, Jülich, Germany, May 13-17, 1991 (to be published).

[Bla+ 90] "Status of Delayed-Neutron Data," J. Blachot, M. C. Brady, A. Philip, R. W. Mills, and D. R. Weaver, Report Nos. NEACRP-L-323 and NEANDC-299 'U,' (Nuclear Energy Agency, OECD, Paris, France, 1990).

[Blo 73] "High Resolution Measurements of Neutron-Induced Fission Cross Sections for ^{233}U, ^{235}U, ^{239}Pu, and ^{241}Pu Below 30 keV," J. Blons, Nucl. Sci. Eng. **51**, 130 (1973).

[Blo 89] "A Third Minimum in the Fission Barrier," J. Blons, Proceedings of the International Conference on Fifty Years Research in Nuclear Fission, Berlin, Germany, April 3-7, 1989, D. Hilscher, H. J. Krappe, and W. von Oertzen, Eds., Nucl. Phys. A **502**, 121c (1989).

[Boh 56] "On the Theory of Nuclear Fission," A. Bohr, Proceedings of the International Conference on Peaceful Uses of Atomic Energy, Geneva, Switzerland, 1955 (United Nations, New York, 1956), Vol. II, p. 151.

[Bor 51] "Estimates of the Amount of Radiation and of the Accompanying Energy Liberation from Fission Products," L. B. Borst, Paper No. 34 in *Radiochemical Studies: The Fission Products*, National Nuclear Energy Series (McGraw-Hill, New York, U.S., 1951), Div. IV, Vol. 9.

[BR 89] "Mass, Energy and Nuclear Charge Distribution of Fission Fragments," J. P. Bocquet and R. Brissot, Invited Paper, International Conference on Fifty Years Research in Nuclear Fission, Berlin, Germany, April 3-7, 1989, Nucl. Phys. A **502**, 609c (1989).

[Car+ 87] "Results of the ENDF/B-VI Standards Evaluation," A. Carlson et al., National Bureau of Standards, Private Communication to C. Dunford, August 31, 1987.

[Cou+ 89] "Composite Delayed-Neutron Spectra of Fissionable Isotopes," G. Couchell, P. Bennett, E. Jacobs, D. Pullen, W. Schier, M. Villani, R. Tanczyn, M. Haghighi, and Q. Sharfuddin, Proceedings of an International Conference, Gaithersburg, Maryland, April 25-28, 1989 (American Nuclear Society, La Grange Park, Illinois, U.S., 1989), Vol. 1, p. 399.

[Den 83] "Independent Yield Evaluations," H. O. Denschlag, NEANDC Specialists Meeting on Yields and Decay Data of Fission Product Nuclides, Brookhaven National Laboratory, Upton, Long Island, New York, U.S., October 24-27, 1983, R. E. Chrien and T. W. Burrows, Eds., Brookhaven National Laboratory Report BNL-51778, p. 7.

[Der 73] "Etude des Sections Efficaces de Réaction des Neutrons de Résonances avec ^{239}Pu," H. Derrien, Thesis, Orsay Série A, No. 1172, University of Paris Sud, Orsay, France (1973).

[Der+ 67] "Sections efficaces totale et de fission du ^{239}Pu, Etude statistique des paramètres de résonances," H. Derrien, J. Blons, C. Eggermann, A. Michaudon, D. Paya, and P. Ribon, Proceedings of the International Conference on Nuclear Data for Reactors, Paris, France, October 17-21, 1966 (IAEA, Vienna, Austria, 1967), Vol. II, p. 195.

[Dic 87a] "Review of New Integral Determinations of Decay Heat," J. K. Dickens, Proceedings of a Specialist's Meeting on Data for Decay Heat Predictions, Studsvick, Sweden, September 7-10, 1987, Report Nos. NEACRP-302 'L' and NEANDC-245 'U' (OECD, 1987), p. 199.

[Dic 87b] "Fission Product Yields for Fast-Neutron Fission of $^{243, 244, 246, 248}$Cm," J. K. Dickens, Nucl. Sci. Eng. **96**, 8 (1987).

[DSP 73] "The Accurate Fission Cross Section of ^{235}U from 0.002 to 0.15 eV and Its Reference Value at 2,200 m/s," A. Deruytter, J. Spaepen, and P. Pelfer, J. Nucl. En. **27**, 645 (1973).

[DSP 90] "R-Matrix Analysis of ^{239}Pu Neutron Cross Sections in the Energy Range Up to 1,000 eV," H. Derrien, G. de Saussure, and R. B. Perez, Nucl. Sci. Eng. **106**, 434 (1990).

[DW 72] "Measurement and Normalization of the Relative ^{239}Pu Fission Cross-Section in the Low Resonance Region," A. J. Deruytter and C. Wagemans, J. Nucl. Energy **96**, 318 (1972).

[DW 77] "HIAWATHA, a Fission-Fragment Recoil Mass Spectrometer," G. Dhorio and B. W. Wehring, Nucl. Instrum. Methods **147**, 487 (1977).

[Eng+ 88] "Background Radiation from Fission Pulses," T. R. England, E. D. Arthur, M. C. Brady, and R. J. Labauve, Los Alamos National Laboratory Report LA-11151-MS (1988).

[FGG 75] "The Mass Distribution for Spontaneous Fission of ^{252}Cf," K. F. Flynn, J. E. Gindler, and L. E. Glendenin, J. Inorg. Nucl. Chem. **37**, 881 (1975).

[Flo+ 74] "Hartree-Fock Calculations of the Fission Barriers of Plutonium Isotopes," H. Flocard, P. Quentin, D. Vautherin, M. Veneroni, and A. K. Kerman, Proceedings of the IAEA Symposium on the Physics and Chemistry of Fission, Rochester, New York, U.S., August 13-17, 1973 (IAEA, Vienna, Austria, 1974), Vol. I, p. 221.

[Fly+ 72] "Distribution of Mass in the Spontaneous Fission of ^{256}Fm," K. F. Flynn, E. P. Horwitz, C. A. Bloomquist, R. F. Barnes, R. K. Sjoblom, P. R. Fields, L. E. Glendenin, Phys. Rev. C **5**, 1725 (1972).

[FPW 54] "Model for Nuclear Reactions with Neutrons," H. Feshbach, C. E. Porter, and V. F. Weisskopf, Phys. Rev. **96**, 448 (1954).

[FS 74] "Mesure du Nombre Moyen de Neutrons Prompts et de l'Energie Moyenne des Rayons Gamma Prompts Emis lors de la Fission Induite par Neutrons de Résonances dans ^{235}U et ^{239}Pu," J. Fréhaut and D. Shackleton, Proceedings of the Third IAEA Symposium on the Physics and Chemistry of Fission, Rochester, New York, U.S., August 13-17, 1973 (IAEA, Vienna, Austria, 1974), Vol. II, 201.

[Gau 88] XVIIIth International Symposium on Nuclear Physics: Physics and Chemistry of Fission, Castle Gaussig (near Dresden), Germany, November 21-25, 1988, Report No. ZfK-732 (Zentralinstitut für Kernforschung, Rossendorf bei Dresden, Germany, 1988).

[GMS 84] "Temperature Effect Analysis in LWR Lattices," P. Gaucher, L. Martin-Deidier, and A. Santamarina, Proceedings of the ANS Topical Meeting on Reactor Physics, Chicago, September 1984 (American Nuclear Society, Inc., La Grange Park, Illinois, U.S., 1984), Vol. I, p. 56.

[Gwi+ 71] "Simultaneous Measurement of the Neutron Fission and Absorption Cross Sections of ^{239}Pu Over the Energy Region 0.02 eV to 30 keV," R. Gwin, L. W. Weston, G. de Saussure, R. W. Ingle, J. H. Todd, F. E. Gillespie, R. W. Hockenbury, and R. C. Block, Nucl. Sci. Eng. **45**, 25 (1971).

[Gwi+ 76] "Measurement of the Neutron Capture and Fission Cross Sections of ^{239}Pu and ^{235}U, 0.02 eV to 200 keV, the Neutron Capture Cross Sections of ^{197}Au, 10 to 50 keV, and Neutron Fission Cross Sections of ^{233}U, 5 to 200

keV," R. Gwin, E. G. Silver, R. W. Ingle, and H. Weaver, Nucl. Sci. Eng. **59**, 79 (1976).

[Gwi+ 84] "Measurements of the Neutron Fission Cross Sections of ^{235}U (E_n = 0.01 eV to 30 keV) and ^{239}Pu (E_n = 0.01 to 60 eV)," R. Gwin, R. R. Spencer, R. W. Ingle, J. H. Todd, and S. W. Scoles, Nucl. Sci. Eng. **88**, 37 (1984).

[Hab 89] "Spectroscopy of the Second Minimum," D. Habs, Proceedings of the International Conference on Fifty Years Research in Nuclear Fission, Berlin, Germany, April 3-7, 1989, Nucl. Phys. A **502**, 105c (1989).

[Ham+ 89] "Fission Mode Fluctuations in the Resonances of ^{235}U(n,f)," F. J. Hambsch, H. H. Knitter, C. Budtz-Jorgensen, and J. P. Theobald, Nucl. Phys. A **491**, 56 (1989).

[Har+ 88] "High Resolution Neutron Transmission Measurements on ^{235}U, ^{238}U, and ^{239}Pu," J. A. Harvey, N. W. Hill, F. G. Perey, G. L. Tweed, and L. Leal, in *Nuclear Data for Science and Technology*, Proceedings of the International Conference, Mito, Japan, May 30-June 3, 1988, S. Igarasi, Ed. (Saikon Publishing Company, Ltd., Tokyo, Japan, 1988), p. 115.

[HKO 89] Proceedings of the International Conference on Fifty Years Research in Nuclear Fission, Berlin, Germany, April 3-7, 1989, D. Hilscher, H. J. Krappe, and W. von Oertzen, Eds., Nucl. Phys. A **502** (1989).

[HO 70] "Reactivity Coefficients in Large Fast Power Reactors," H. H. Hummel and D. Okrent (American Nuclear Society, Inc., La Grange Park, Illinois, U.S., 1970).

[Hof 89] "Spontaneous Fission Properties and Lifetime Systematics," D. C. Hoffman, Invited Paper, International Conference on Fifty Years Research in Nuclear Fission, Berlin, Germany, April 3-7, 1989, Nucl. Phys. A **502**, 21c (1989).

[HS 79] "A Study of the Temperature Dependence of the Neutron Transmission of Uranium Dioxide," T. J. Haste and M. G. Sowerby, J. Phys. D: App. Phys. **12**, 1203 (1979).

[Hul+ 86] "Bimodal Symmetric Fission Observed in the Heaviest Elements," E. K. Hulet, J. F. Wild, R. J. Dougan, R. W. Lougheed, J. H. Landrum, A. D. Landrum, M. Schädel, R. L. Hahn, P. A. Baisden, C. M. Henderson, R. J. Dupzyk, K. Sümmerer, and G. Bethune, Phys. Rev. Lett. **56:4**, 313 (1986).

[Jam 87] "A Review of Libraries of Fission Product Yields," M. F. James, Proceedings of a Specialist's Meeting on Data for Decay Heat Predictions, Studsvick, Sweden September 7 -10, 1987, Report Nos. NEANDC-245'U' and NEACRP-302 'L' (1987), p. 69.

[JL 62] "Resonant Absorption of Neutrons by Crystals", H. E. Jackson and J. E. Lynn, Phys. Rev. **127**, 461 (1962).

[JMW 90] "A New Evaluation of Fission Product Yields and the Production of a New Library (UKFA2) of Independent and Cumulative Yields," R. W. Mills, M. F. James, and D. R. Weaver, Report Nos. AEA TRF 1015 (Vol. I), AEA TRF 1018 (Vol. II), and AEA TRF 1019 (Vol. III) (1990).

[Joh 88] "Integral Determination of the Beta and Gamma Heat in Thermal-Neutron-Induced Fission of ^{235}U and ^{239}Pu and of the Gamma Heat in Fast Fission of ^{238}U," P. Johansson, in *Nuclear Data for Science and Technology*, Proceedings of the International Conference, Mito, Japan, May 30-June 3, 1988, S. Igarasi, Ed. (Saikon Publishing Company, Ltd., Tokyo, Japan, 1988), p. 857.

[KE 91] "Augmentation of ENDF/B Fission Product Gamma-Ray Spectra by Calculated Spectra," J. Katakura and T. R. England, Los Alamos National Laboratory report LA-12125-MS (1991).

[Kee 65] "*Physics of Nuclear Kinetics*," G. R. Keepin (Addison-Wesley Publishing Company, Inc., Reading, Massachusetts, U.S., 1965).

[Kla 83] "The Shape of the Beta Strength Function and Consequences for Nuclear Physics and Astrophysics," H.

V. Klapdor, *Progress in Particle and Nuclear Physics* (Pergamon Press, Oxford, 1983), Vol. 10.

[Kra 87] "Beta-Decay Half-Lives of Very Neutron-Rich Nuclei and Their Consequences for the Astrophysical R-Process," K. L. Kratz, Proceedings of the 4th Workshop on Nuclear Astrophysics, Ringberg Castle, Tegernsee, Germany, April 21-24, 1987, W. Hillebrandt, R. Kuhfuβ, E. Müller, and J. W. Truran, Eds., Lecture Notes in Physics (Springer-Verlag, New York, U.S., 1987), Vol. 287, p. 68.

[Lam 39] "Capture of Neutrons by Atoms in a Crystal," W. E. Lamb, Phys. Rev. **55**, 190 (1939).

[Lar 89] "Updated User's Guide for SAMMY: Multilevel R-Matrix Fits to Neutron Data," N. M. Larson, Report No. ORNL/TM-9179/R2, Oak Ridge National Laboratory (1989).

[Len 89] Proceedings of the International Conference on the Fiftieth Anniversary of Nuclear Fission, Leningrad (St. Petersburg), Russia, October 16-20, 1989, Report of the V. G. Khlopin Radium Institute (1989).

[Lis+ 88] "Neutron-Induced Fission Cross Section Ratios for ^{232}Th, ^{235}U, ^{238}U, ^{237}Np, and ^{239}Pu from 1 to 400 MeV," P. W. Lisowski, J. L. Ullmann, S. J. Balestrini, A. D. Carlson, and N. W. Hill, in *Nuclear Data for Science and Technology*, Proceedings of the International Conference, Mito, Japan, May 30-June 3, 1988, S. Igarasi, Ed. (Saikon Publishing Company, Ltd., Tokyo, Japan, 1988), p. 97.

[MBK 89] "Proton-Neutron Quasiparticle RPA and Charge-Changing Transitions," K. Muto, E. Bender, and H. V. Klapdor, Zeitschrift für Physik A **333**, 125 (1989).

[MCT 74] "Prediction of Unmeasured Fission Product Yields," A. R. de L. Musgrove, J. L. Cook, and G. D. Trimble, Proceedings of the Panel on Fission Product Data, Bologna, Italy, 1973, Report No. IAEA-169 (IAEA, Vienna, Austria, 1974), Vol. II, p. 163.

[Mea 88] "The Fission Cross Sections of ^{230}Th, ^{230}Th, ^{233}U, ^{234}U, ^{236}U, ^{238}U, ^{237}Np, ^{239}Pu, ^{242}Pu Relative to ^{235}U at 14.74 Neutron Energy," J. W. Meadows, Ann. Nucl. En. **15**, 421 (1988).

[Mic 67] "Détermination du spin des résonances des noyaux fissiles," A. Michaudon, Invited Paper, Proceedings of a Conference on Nuclear Data for Reactors, Paris, France, October 17-21, 1966 (IAEA, Vienna, Austria, 1967), Vol. II, p. 161.

[Mic 68] "Intermediate Structure in the Fission Cross Sections of ^{237}Np and Possibly of ^{239}Pu," A. Michaudon, Symposium on Nuclear Structure, Dubna, Russia, 1968 (IAEA, Vienna, Austria, 1968), p. 463.

[Mic 73] "Nuclear Fission," A. Michaudon, in *Advances in Nuclear Physics*, M. Baranger and E.Vogt, Eds. (Plenum Press, New York, U.S., 1973), Vol. 6, p. 1.

[Mic 76] "Neutrons and Fission," A. Michaudon, Invited Paper, International Conference on the Interactions of Neutrons with Nuclei, Lowell, Massachusetts, U.S., July 6-9, 1976, Report No. CONF-760715-P1, E. Sheldon, Ed. (University of Lowell, Lowell, Massachusetts, U.S.), Vol. I, p. 641.

[Mic 81] "*Nuclear Fission and Neutron-Induced Fission Cross Sections*," A. Michaudon, Ed., A Nuclear Energy Agency Nuclear Data Committee (OECD) Series on Neutron Physics and Nuclear Data in Science and Technology, A. Michaudon, S. W. Cierjacks, and R. E. Chrien, General Eds. (Pergamon Press, Oxford, England, 1981), Vol. I.

[Mic 87] "A New Intense Source of Very-Cold and Ultra-Cold Neutrons," A. Michaudon, Invited Paper presented at an Advisory Group Meeting on Properties of Neutron Sources, Leningrad (St. Petersburg), Russia, Report No. IAEA-TECDOC-410 (IAEA, Vienna, Austria, 1987), p. 421.

[Mic 88] "Fission Barriers, Fission Channels, Fission Valleys," A. Michaudon, Invited Paper, XVIIIth International

Symposium on Nuclear Physics: Physics and Chemistry of Fission, Castle Gaussig (near Dresden), Germany, November 21-25, 1988, Report No. ZfK-732 (Zentralinstitut für Kernforschung, Rossendorf bei Dresden, Germany, 1988), p. 2.

[Mic 89] "Measurements of Phonon Spectra in Complex Compounds Using Epithermal Neutrons," A. Michaudon, Los Alamos National Laboratory Report LA-UR-89-3923 (1989).

[Mic+ 62] "Etude de l'interaction résonnante de neutrons d'énergie voisine de 6,67 eV avec les noyaux de ^{238}U dans l'oxyde d'uranium à basse température," A. Michaudon et al., C. R. Acad. Sci. **255**, 2086 (1962).

[Mol+ 75] "Analysis of ^{236}U-Fission Products by the Recoil Separator 'Lohengrin'," E. Moll, H. Schräder, G. Siegert, M. Ashgar, J. P. Bocquet, G. Bailleul, J. P. Gautheron, J. Greif, G. I. Crawford, C. Chauvin, H. Ewald, H. Wollninck, P. Armbruster, G. Fiebig, H. Lawin, and K. Sistemich, Nucl. Instrum. Methods **123**, 615 (1975).

[Moo 70] "Low Energy Neutron Spectroscopy Measurements on Fissile Nuclides," M. S. Moore, in *Experimental Neutron Resonance Spectroscopy*, J. A. Harvey, Ed. (Academic Press, Inc., New York, U.S., 1970), p. 347.

[Nea 87] "Data for Decay Heat Calculations," Proceedings of a Specialist's Meeting, Studsvick, Sweden, September, 7-10, 1987 (Nuclear Energy Agency, OECD, Paris, France, 1987).

[NGS 91] "Status of JEF and EFF Projects," C. Nordborg, H. Gruppelaar, and M. Salvatores, International Conference on Nuclear Data for Science and Technology, Jülich, Germany, May 13-17, 1991 (proceedings to be published).

[NP 60] "Effects of Chemical Binding on Nuclear Recoil," M. S. Nelkin and D. E. Parks, Phys. Rev. **119**, 1060 (1960).

[Oed+ 83] "High Resolution Axial Ionization Chamber for Fission Products," A. Oed, P. Geltenbort, F. Gönnenwein, T.

Manning, and D. Souque, Nucl. Instrum. Methods **205**, 455 (1983).

[Pol+ 62] "Spontaneous Fission with an Anomalously Short Period," S. M. Polikanov, V. A. Douin, V. A. Karnaukhov, V. L. Mikeev, A. A. Pleve, N. K. Skolelov, V. G. Subbotin, G. M. Terakopyan, and V. A. Fomichev, Sov. Phys. JETP **15**, 1016 (1962).

[PT 56] "Fluctuations of Nuclear Radiation Widths," C. E. Porter and R. G. Thomas, Phys. Rev. **104**, 483 (1956).

[QRS 79] "A High Resolution Ionization Chamber Tested with Fission Products of ^{235}U," U. Quade, K. Rudolph, and G. Siegert, Nucl. Instrum. Methods **164**, 435 (1979).

[RE 90] "Test of Pre-ENDF/B-VI; Decay Data and Fission Yields," G. Rudstam and T. R. England, Los Alamos National Laboratory Report LA-11909-MS (1990).

[RE 91] "The File of Evaluated Data in ENDF/B," C. W. Reich and T. R. England, Proceedings of the 1991 Annual Meeting of the American Nuclear Society, Orlando, Florida, U.S., June 2-6, 1991 (Transactions of the American Nuclear Society, Report No. TANSAO 63-1-464, 1991), Vol. 63, p. 163.

[Rei 87] "Review of Nuclear Data of Relevance for the Decay Heat Problem," C. W. Reich, in *Data for Decay Heat Calculations*, Proceedings of a Specialist's Meeting, Studsvick, Sweden, September 7-10, 1987, (Nuclear Energy Agency, OECD, Paris, France, 1987), p. 107.

[RM 58] "Multilevel Formula for the Fission Process," C. W. Reich and M. S. Moore, Phys. Rev. **111:3**, 929 (1958).

[RMW 39] "Further Observations of the Splitting of Uranium and Thorium," R. Roberts, R. Meyer, and P. Wang, Phys. Rev. **55**, 510 (1939).

[Row 88] "Nuclear Data for Studies of Reactor Safety and Control and for Criticality Studies," J. Rowlands, in *Nuclear Data for Science and Technology*, Proceedings of the

International Conference, Mito, Japan, May 30-June 3, 1988, S. Igarasi, Ed. (Saikon Publishing Company, Ltd., Tokyo, Japan, 1988), p. 25.

[RP 56] "The Cross Sections of the Plutonium Isotopes," J. F. Raffle and B. T. Price, Proceedings of the International Conference on the Peaceful Uses of Atomic Energy, Geneva, Switzerland, August 8-20, 1955 (United Nations, New York, U.S., 1956), Vol. 4, p. 187.

[Rud+ 88] "Experimental Determinations of the Average Beta and Gamma Energies and Their Use for Decay Heat Predictions," G. Rudstam, P. Aagaard, K. Aleklett, P. I. Johansson, E. Lund, O. Tengblad, B. Jonson, G. Nyman, R. von Dincklage, and P. Hoff, in *Nuclear Data for Science and Technology*, Proceedings of the International Conference, Mito, Japan, May 30-June 3, 1988, S. Igarasi, Ed. (Saikon Publishing Company, Ltd., Tokyo, Japan, 1988), p. 867.

[Rud+ 90] "Beta and Gamma Spectra of Short-lived Fission Products," G. Rudstam, P. I. Johansson, O. Tenglad, P. Aagaard, and J. Eriksen, Atomic Data and Nuclear Data Tables **45**, 239 (1990).

[San 87] "Temperature Effect Analysis in LWR Lattices: Thermal Cross-Section Shapes and Qualification Through French Integral Experiments," A. Santamarina, Proceedings of an IAEA Advisory Group Meeting on Nuclear Data for the Calculation of Thermal Reactor Reactivity Coefficients, Vienna, Austria, December 7-11, 1987 (IAEA, Vienna, Austria, 1987).

[San 91] A. Santamarina, private communication (1991).

[Sch 79] "Evaluations of Decay Heating in Shutdown Reactors," V. E. Schrock, Progr. Nucl. En. **3**, 125 (1979).

[SD 91] "L'évaluation des besoins futurs dans le domaine des réacteurs nucléaires," M. Salvatores and M. Darrouzet, Internal Report (Commissariat à l'Energie Atomique, Paris, France, 1991, unpublished).

[Sha+ 88] "Search for an Energy Dependence in ^{238}U Delayed Neutron Spectra," Q. Sharfuddin et al., Nucl. Sci. Eng. **98**, 341 (1988).

[Soo 62] "*Reactor Handbook*," H. Soodak, Ed. (John Wiley & Sons: Interscience Publishers, New York, 1962), Vol. III, Part A.

[Spe+ 87] "Parameters of the 1.056-eV Resonance in ^{240}Pu and the 2,200-m/s Neutron Total Cross Sections of ^{235}U, ^{239}Pu, and ^{240}Pu," R. R. Spencer, J. A. Harvey, N. W. Hill, and L. W. Weston, Nucl. Sci. Eng. **96**, 318 (1987).

[SS 58] "Slow Neutron Resonances," F. J. Shore and V. L. Sailor, Phys. Rev. **112:1**, 191 (1958).

[ST 88] "The French 'CEA 86' Multigroup Cross Section Library and Its Integral Qualification," A. Santamarina and H. Tellier, in *Nuclear Data for Science and Technology*, Proceedings of the International Conference, Mito, Japan, May 30-June 3, 1988, S. Igarasi, Ed. (Saikon Publishing Company, Ltd., Tokyo, Japan, 1988), p. 47.

[Str 66] V. M. Strutinsky, Yad. Fiz. **3**, 614 (1966); Sov. J. Nucl. Phys. **3**, 449 (1966).

[Tan+ 86] "Composite Delayed Neutron Energy Spectra for Thermal Fission of ^{235}U," R. Tanczyn, Q. Sharfuddin, W. A. Schier, D. J. Pullen, M. H. Haghighi, L. Fisteag, and G. P. Couchell, Nucl. Sci. Eng. **94**, 353 (1986).

[Tob 80] "Decay Heat," A. Tobias, Progr. Nucl. En. **5**, 1 (1980).

[Tro+ 70] "Determination of the Spin of ^{239}Pu Slow-Neutron Resonances," J. Trochon, H. Derrien, B. Lucas, and A. Michaudon, Proceedings of the 2nd International Conference on Nuclear Data for Reactors, Helsinki, Finland, June 15-19, 1970 (IAEA, Vienna, Austria, 1970), Vol. I, p. 495.

[Tut 79] "Delayed-Neutron Yields in Nuclear Fission," R. J. Tuttle, Proceedings of a Consultant's Meeting on Delayed-

Neutron Properties, Vienna, Austria, March 26-30, 1979, International Atomic Energy Agency report No. INDC(NDS)-107/G+Special (IAEA, Vienna, Austria, 1979), p. 29.

[TYK 73] "Beta-Decay Half-Lives Calculated on the Gross Theory," K. Takahashi, M. Yamada, and T. Kondoh, Atomic Data and Nuclear Data Tables **12**, 101 (1973).

[VH 73] "*Nuclear Fission*," R. Vandenbosh and J. R. Huizenga, (Academic Press Publishers, Inc., New York, U.S., 1973).

[Vog 58] "Resonance Theory of Neutron Cross Sections of Fissionable Nuclei," E. Vogt, Phys. Rev. **112:1**, 203 (1958).

[Wag 91] "*The Nuclear Fission*," Cyriel Wagemans, Ed. (CRC Press, Inc., Boca Raton, Florida, U.S., 1991).

[Wag+ 88] "Investigation of the Shape of the $^{235}U(n,f)$ Cross-Section with Very Cold Neutrons," C. Wagemans, A. J. Deruytter, R. Bartélémy, W. Mampe, P. Ageron, and A. Michaudon, in *Nuclear Data for Science and Technology*, Proceedings of the International Conference, Mito, Japan, May 30-June 3, 1988, S. Igarasi, Ed. (Saikon Publishing Company, Ltd., Tokyo, Japan, 1988), p. 131.

[Wah 65] "Mass and Charge Distribution in Low-Energy Fission," A. C. Wahl, Proceedings of the IAEA Symposium on the Physics and Chemistry of Fission, Salzburg, Austria, March 22-26, 1965 (IAEA, Vienna, Austria, 1965), Vol. I, p. 317.

[Wah 88] "Nuclear-Charge Distribution and Delayed Neutron Yields for Thermal-Neutron-Induced Fission of ^{235}U, ^{233}U, and ^{239}Pu and for Spontaneous Fission of ^{252}Cf," A. C. Wahl, Atomic Data and Nuclear Data Tables **39**, 1 (1988).

[Wah 89] "Nuclear-Charge and Mass Distributions from Fission," A. Wahl, Proceedings of the International Conference on Fifty Years with Nuclear Fission, Gaithersburg, Maryland, U.S., April 26-28, 1989 (American Nuclear Society, Inc., La Grange Park, Illinois, U.S., 1989), p. 525.

[WAH 88] "Atomic Masses from (Mainly) Experimental Data," A. H. Wapstra, G. Audi, and R. Hoekstra, Atomic Data and Nuclear Data Tables **39**, 281 (1988).

[WD 86] "Subthermal Fission Cross-Section Measurements," C. Wagemans and A. J. Deruytter, in *Nuclear Data for Basic and Applied Science*, Proceedings of the International Conference, Santa Fe, New Mexico, May 13-17, 1985, P. G. Young, R. E. Brown, G. F. Auchampaugh, P. W. Lisowski, and L. Stewart, Eds. (Gordon and Breach Science Publishers, New York, U.S., 1986), p. 499.

[WE 47] "Higher Angular Momenta and Long Range Interaction in Resonance Reactions," E. P. Wigner and L. Eisenbud, Phys. Rev. **72**, 29 (1947).

[Wea+ 87] "The Variation of Delayed-Neutron Spectra from ^{235}U with Primary Neutron Energy from 0.5 to 2 MeV," D. R. Weaver et al., Proceedings of the Specialist's Meeting on Delayed-Neutron Properties, University of Birmingham, United Kingdom, September 15-19, 1986, D. R. Weaver, Ed. (University of Birmingham, Department of Physics Radiation Center, 1987), p. 165.

[Wei+ 90] "Measurements of η of ^{235}U for Subthermal Neutrons," H. Weigmann, B. Keck, J. A. Wartena, P. Geltenbort, and K. Schreckenbach, Proceedings of the International Conference on the Physics of Reactors: Operation, Design, and Computation, Marseille, France, April 23-27, 1990 (American Nuclear Society, Inc., La Grange Park, Illinois U.S., 1990).

[WH 91] "What is a fission channel?" H. Weigmann and F. J. Hambsch, Invited Paper, Second Seminar on Fission, Pont d'Hoye, Belgium, October 23-25, 1991 (proceedings to be published).

[Wig 46] "Resonance Reactions," E. P. Wigner, Phys. Rev. **70**, 606 (1946).

[WT 84] "Subthreshold Fission Cross Section of ^{240}Pu and the Fission Cross Sections of ^{235}U and ^{239}Pu," L. W. Weston and J. H. Todd, Nucl. Sci. Eng. **88**, 567 (1984).

[WW 58] "*Physical Theory of Neutron Chain Reactors*," A. M. Weinberg and E. P. Wigner (University of Chicago Press, Chicago, Illinois, U.S., 1958).

[YM 91] "Evaluation and Testing of n + ^{239}Pu Data for ENDF/B-VI in the keV and the MeV Regions," P. G. Young and R. E. Macfarlane, Proceedings of the International Conference on Nuclear Data for Science and Technology, Jülich, Germany, 13-17 May 1991 (proceedings to be published).

LIST OF SYMBOLS

a_c	Coefficient of the Coulomb term in the Weizsäcker mass formula.
a_s	Coefficient of the surface term in the Weizsäcker mass formula.
$b(t)$	Decay power produced by β-rays at time t after a single fission event.
f_H	Energy self-shielding factor for homogeneous mixtures.
g	Statistical factor.
$g(t)$	Decay power produced by γ-rays at time t after a single fission event.
k	Reactivity coefficient.
k_n	Neutron wave number.
k_B	Boltzmann constant.
l	Orbital angular momentum.
$m(t)$	Decay power produced at time t after a single fission event.
$n_d(t)$	Delayed-neutron activity at time t after fission.
q	Charge state of a fission fragment.
s	Spin of the incoming particle.
$\{s\}$	Set of shape parameters.
s_i	Shape parameter i.
v_n	Neutron velocity.
v_A	Velocity of nucleus having mass number A.
x	Fissility parameter.
A	Mass number.
A_F	Mass number of the fissioning nucleus.
A_i	Mass number of fission fragment i (i = 1, 2 or L, H) after prompt neutron emission.
A_i'	Mass number of fission fragment i (i = 1, 2 or L, H) before prompt neutron emission.
D_{sc}	Deformation energy at scission.
E_0	Resonance energy.
E^*	Excitation energy.
E_f	Fission barrier height.
E_{fA}	Height of inner fission barrier A.
E_{fB}	Height of outer fission barrier B.
E_n	Neutron kinetic energy.
E_c^0	Coulomb energy at sphericity.
$E_c(\{s\})$	Coulomb energy at deformation {s}.
E_s^0	Surface energy at sphericity.

$E_s(\{s\})$	Surface energy at deformation {s}.
E_K^{sc}	Prescission kinetic energy.
E_K^T	Total kinetic energy of the fission fragments.
E_{sc}^*	Excitation energy at scission.
E_T^*	Total excitation energy of both fission fragments.
E_β	β-ray energy.
E_γ	γ-ray energy.
$E_{\bar{\nu}}$	Antineutrino energy.
I	Spin of target nucleus.
I	Isomeric state of a fission fragment.
J	Spin of the compound nucleus state.
IN_i	Independent yield of fission fragment i.
M(I,t)	Decay power produced at time t after a single fission event and after an irradiation time I.
$N_i(t)$	Number of fission products i present at the time t after fission.
N	Neutron number.
N_a	Number of atoms/cm^3 having absorption cross section σ_a.
N_s	Number of atoms/cm^3 having scattering cross section σ_s.
N_F	Neutron number of the fissioning nucleus.
P(t)	Decay power generated by an aggregate of fission products at a time t after fission.
P_n	Neutron-emission probability of a delayed-neutron precursor.
Q_β	Total energy release in β decay.
R	R matrix.
S_n	Neutron separation energy.
S_N	Nuclear area.
S_0	Strength function for s-wave neutrons.
S_β	Beta strength function.
T	Temperature (in degrees Kelvin).
T_{eff}	Effective temperature (in degrees Kelvin).
U	Collision matrix.
V({s})	Potential energy at deformation {s}.
V_c	Coulomb energy at scission.
$V_M(\{s\})$	Macroscopic potential energy at deformation {s}.
Y_i	Independent yield of fission fragment i.
Y(A)	Chain yield of fission fragments having mass number A.
Y(A, Z, I)	Independent yield of fission fragment having mass number A, atomic number Z, and isomeric state I.
Y(Z)	Elemental yield of fragments having atomic number Z.

Y_c	Cumulative fragment yield.
Z_F	Atomic number of the fissioning nucleus.
$Z_p(A)$	Most probable atomic number of fragments with mass number A.
Z_F	Atomic number of fissioning nucleus.
$Z_{UCD}(A)$	Unchanged charge distribution of fragment with mass number A.
α_i	Fractional group abundance of delayed neutrons.
β	Delayed-neutron fraction.
β	Width parameter of the Doppler broadened function $\psi(\beta,x)$.
β_ι	Delayed-neutron fraction for temporal group i.
γ_c	Amplitude for channel c.
γ_n	Neutron width amplitude.
$\zeta(\{s\})$	Dimensionless value of the deformation energy, at deformation ($\{s\}$), normalized to the potential energy at sphericity.
η	Average number of prompt fission neutrons per absorbed incident neutron.
λ	Decay constant.
λ_f	Initial fissioning state.
ν	Total number of fission neutrons per fission.
ν_f	Number of fission exit channels.
ν_p	Number of prompt fission neutrons per fission.
ν_{pi}	Number of prompt fission neutrons emitted by fragment i.
ν_d	Number of delayed fission neutrons per fission.
$\overline{\nu}$	Average total number of fission neutrons per fission.
$\overline{\nu_p}$	Average number of prompt fission neutrons per fission.
$\overline{\nu_d}$	Average number of delayed neutrons per fission.
$\nu_p(A)$	Number of prompt fission neutrons emitted by fragment of mass number A.
π	Parity of the compound-nucleus state.
π'	Parity of the target nucleus.
ρ_c	Antireactivity coefficient of the control system of a reactor.
ρ_v	Void antireactivity coefficient.
σ_a	Microscopic absorption cross section.
σ_{int}	Intrinsic shape of a resonance.
σ_{nf}	Neutron-induced fission cross section.
$\sigma_{n\gamma}$	Neutron-induced capture cross section.
σ_s	Microscopic scattering cross section.

σ_D	Standard deviation of the Gaussian used in Doppler broadening.
σ_0	Peak cross section of an isolated Breit-Wigner resonance.
σ_{0f}	Peak fission cross section of an isolated Breit-Wigner resonance.
τ	Surface tension per unit nuclear area.
$\tau_{1/2}$	Half-life of a radioactive nucleus.
ψ_0	Value at the peak of the $\psi(\beta,x)$ function.
Γ	Total width of a resonance.
Γ_n	Neutron width.
Γ_n^0	Reduced neutron width.
Γ_f	Fission width.
$\Gamma\gamma$	Radiative capture width.
Δ	Doppler width.
ΔE_K^R	Recoil energy of both fission fragments caused by fast decay processes.
$\Delta E_{sh}(\{s\})$	Shell-energy correction to the macroscopic potential energy at deformation ($\{s\}$).
$\Delta Z_p(A)$	Charge shift, relative to Z_{UCD}, of fragment with mass number A.
Θ_D	Debye temperature.
Σ_{ra}	Macroscopic resonant-absorption cross section.
Σ_p	Macroscopic potential-scattering cross section.

TABLE IV.1

Selection of measurements of ^{239}Pu cross sections*

Reference	Energy Range (eV)	Measurement Characteristics
Gwin et al. ([Gwi+ 71])	0.01 to 0.5	Fission and absorption at 25.6 m
Deruytter and Wagemans ([DW 72])	0.01 to 0.5	Fission at 8 m
Blons ([Blo 73])	40 to 1,000	Fission at 50 m; sample at 77 K
Gwin et al. ([Gwi+ 76])	0.02 to 0.5	Fission and absorption at 40 m
Gwin et al. ([Gwi+ 84])	0.01 to 30	Fission at 21.65 m
Weston and Todd ([WT 84])	9 to 1,000	Fission at 18.9 m
Spencer et al. ([Spe+ 87])	0.01 to 30	Transmission at 18 m
Harvey et al. ([Har+ 88])	0.7 to 30	Transmission at 18 m; samples at 97 K
Harvey et al. ([Har+ 88])	30 to 1,000	Transmission at 80 m; samples at 97 K

*These measurements were used in the analysis of ^{239}Pu resonances discussed in the text ([DSP 90]).

TABLE IV.2

Comparison of the average ^{239}Pu fission cross sections (in barns)*

Energy (eV)	Calculations [DSP 90]	ENDF/B-VI Standards Subcommittee [Car+ 87]	Blons [Blo 73]	Weston and Todd [WT 84]
100 to 200	18.135	18.66 ± 0.13	18.93	18.095
200 to 300	17.312	17.88 ± 0.12	17.79	17.441
300 to 400	8.080	8.43 ± 0.06	8.91	8.130
400 to 500	9.389	9.57 ± 0.07	9.71	9.337
500 to 600	15.062	15.56 ± 0.11	15.51	15.17
600 to 700	4.129	4.46 ± 0.04	4.63	4.192
700 to 800	5.323	5.63 ± 0.04	5.94	5.385
800 to 900	4.729	4.98 ± 0.04	5.11	4.765
900 to 1,000	8.223	8.30 ± 0.07	8.57	8.165
100 to 1,000	10.043	10.39	10.57	10.075

*([DSP 90]).

TABLE IV.3

Parameters of the χ^2 distributions used in the calculations presented in Fig. IV.6*

Spin	N	$\langle\Gamma_f\rangle$	ν_f
0^+	62	3.000	1.3
1^+	154	0.030	1.0

* ([DSP 90]).

N: number of levels used for the normalization of the distribution.

$\langle\Gamma_f\rangle$: average fission width in eV (a value of 3 meV was subtracted from the fission widths to take into account the (n,γf) reaction).

ν_f: number of fission exit channels.

TABLE VIII.1

Average delayed-neutron half-lives*

Group index	Weighted average half-life (s)
1	54.67 ± 0.33
2	21.66 ± 0.25
3	5.42 ± 0.15
4	2.28 ± 0.02
5	0.514 ± 0.013
6	0.191 ± 0.010

*These half-lives were obtained for the six temporal neutron groups in the analysis of the data for many different fissioning systems ([Kee 65]).

TABLE VIII.2

Total delayed-neutron yields*

Type of Fission	$\overline{\nu_d}$ [BE 89]	$\overline{\nu_d}$ [Tut 79]
^{227}Th(T)	1.41 ± 0.26	
^{229}Th(T)	1.82 ± 0.29	
^{232}Th(F)	5.64 ± 0.41	5.31 ± 0.23
^{232}Th(H)	4.16 ± 0.36	2.85 ± 0.13
^{231}Pa(F)	1.60 ± 0.23	1.11 ± 0.11
^{232}U(T)	0.52 ± 0.08	
^{233}U(T)	0.97 ± 0.16	0.67 ± 0.03
^{233}U(F)	0.90 ± 0.12	0.73 ± 0.04
^{233}U(H)	0.70 ± 0.10	0.42 ± 0.03
^{234}U(F)	1.29 ± 0.15	1.05 ± 0.11
^{234}U(H)	0.77 ± 0.11	0.62 ± 0.08
^{235}U(T)	1.78 ± 0.10	1.62 ± 0.05
^{235}U(F)	2.06 ± 0.20	1.67 ± 0.04
^{235}U(H)	1.09 ± 0.13	0.93 ± 0.03
^{236}U(F)	2.32 ± 0.23	2.21 ± 0.24
^{236}U(H)	1.55 ± 0.17	1.30 ± 0.20
^{237}U(F)	3.50 ± 0.28	
^{238}U(F)	4.05 ± 0.29	4.39 ± 0.10
^{238}U(H)	2.76 ± 0.25	2.73 ± 0.08
^{237}Np(F)	1.14 ± 0.12	
^{237}Np(H)	0.97 ± 0.11	
^{238}Np(F)	2.16 ± 0.19	
^{238}Np(F)	0.79 ± 0.09	0.47 ± 0.05

TABLE VIII.2
(continued)

Type of Fission	$\overline{\nu_d}$ [BE 89]	$\overline{\nu_d}$ [Tut 79]
$^{239}Pu(T)$	0.76 ± 0.04	0.63 ± 0.04
$^{239}Pu(F)$	0.68 ± 0.08	0.63 ± 0.02
$^{239}Pu(H)$	0.38 ± 0.06	0.42 ± 0.02
$^{240}Pu(F)$	0.81 ± 0.09	0.95 ± 0.08
$^{240}Pu(H)$	0.51 ± 0.07	0.67 ± 0.05
$^{241}Pu(T)$	1.41 ± 0.09	1.52 ± 0.11
$^{241}Pu(F)$	1.42 ± 0.14	1.52 ± 0.11
$^{242}Pu(F)$	1.43 ± 0.14	2.21 ± 0.26
$^{241}Am(T)$	0.53 ± 0.07	
$^{241}Am(F)$	0.51 ± 0.06	
$^{241}Am(H)$	0.26 ± 0.05	
$^{242m}Am(T)$	0.78 ± 0.09	
$^{243}Am(F)$	0.80 ± 0.09	
$^{242}Cm(F)$	0.14 ± 0.03	
$^{245}Cm(T)$	0.64 ± 0.08	
$^{249}Cf(T)$	0.16 ± 0.03	
$^{251}Cf(T)$	0.75 ± 0.08	
$^{252}Cf(S)$	0.65 ± 0.07	
$^{254}Es(T)$	0.46 ± 0.06	
$^{255}Fm(T)$	0.28 ± 0.04	

*Total delayed-neutron yields $\overline{\nu_d}$ per 100 fissions obtained by the summation method for 43 fissioning systems using 271 precursors ([BE 89]) (column 2) and from the evaluation by Tuttle (column 3), ([Tut 79]). As explained in the text, the symbols T, F, and H used in column 1 refer to fission induced by thermal, fast, and high-energy neutrons, respectively, whereas the symbol S refers to spontaneous fission.

TABLE VIII.3

Delayed-neutron yields per precursor for fission of ^{235}U by fast neutrons*

(1)		(2)	(3)	(4)	(5)	(6)
53	137	2.29E-1	5.4E-3	4.0E-1	3.8E-2	14.0
35	89	1.96E-1	3.3E-3	5.0E-1	4.7E-2	12.0
37	94	1.54E-1	4.2E-3	2.2E-1	4.2E-2	9.4
35	90	1.29E-1	1.7E-3	9.0E-1	4.4E-2	7.9
35	88	1.17E-1	3.0E-3	2.6E-1	1.9E-2	7.2
39	98I	9.04E-2	5.0E-3	9.6E-1	3.0E-2	5.5
53	138	7.77E-2	4.2E-3	3.0E-1	2.2E-2	4.8
33	85	7.71E-2	4.8E-4	2.1E+0	2.5E-2	4.7
37	95	6.04E-2	2.3E-3	2.3E-1	2.0E-2	3.7
53	139	5.93E-2	2.1E-3	4.0E-1	2.0E-2	3.6
35	87	5.24E-2	2.1E-3	6.0E-2	5.4E-3	3.2
37	93	4.75E-2	5.4E-3	4.0E-2	7.3E-3	2.9
39	99	3.58E-2	4.8E-3	3.2E-1	1.0E-2	2.2
35	91	3.24E-2	5.9E-4	3.3E+0	1.2EE-2	2.0
51	135	2.69E-2	6.3E-4	2.0E+0	1.0E-2	1.7
55	143	2.69E-2	4.2E-3	8.0E-2	7.0E-3	1.7
37	96	2.03E-2	5.4E-4	4.0E-1	7.2E-3	1.2
33	86	1.53E-2	1.7E-4	3.5E+0	5.7E-3	0.94
55	144	1.42E-2	1.5E-3	3.2E-1	5.1E-3	0.87
55	145	1.42E-2	3.4E-4	9.0E-1	5.0E-3	0.86
52	136	1.35E-2	4.6E-3	4.0E-1	8.3E-3	0.83
52	137	1.19E-2	1.6E-3	5.0E-1	4.6E-3	0.73
53	140	1.18E-2	4.5E-4	1.0E+0	4.3E-3	0.72
36	93	1.03E-2	1.7E-3	1.1E-1	3.4E-3	0.63
35	92	7.82E-3	8.2E-5	3.0E+0	2.8E-3	0.48
37	97	7.78E-3	1.0E-4	8.0E-1	2.7E-3	0.48
51	136	7.27E-3	7.7E-5	4.0E+1	9.1E-3	0.44
39	100	6.42E-3	2.2E-3	1.9E-1	2.6E-3	0.39
36	94	6.41E-3	4.1E-4	2.2E+0	3.4E-3	0.39

TABLE VIII.3
(continued)

*These delayed-neutron yields, which are included in the JEF-2 evaluated data file, are sorted by importance (only the 29 most important precursors are given) ([Bla 91]):

(1) precursor given by Z,A (I indicates an isomeric state),
(2) value of the delayed-neutron yield for the precursor given in (1),
(3) error (in %) on the cumulative fission yield,
(4) error (in %) on the neutron emission probability P_n,
(5) error (in %) on the delayed-neutron yield given in (1), and
(6) contribution of the delayed-neutron yield given in (1) on the total delayed-neutron yield $\overline{\nu_d}$.

TABLE VIII.4

Delayed-neutron parameters*

	Groups					
	(1)	(2)	(3)	(4)	(5)	(6)
α	0.0350	0.1807	0.1725	0.3868	0.1586	0.0664
λ	0.0133	0.0327	0.1208	0.3028	0.8495	2.8530

*The delayed-neutron parameters (α,λ) for the six temporal groups are obtained by the summation method for the fission of ^{235}U by fast neutrons ([BE 89]).

TABLE VIII.5

Average energy of delayed neutrons at various time intervals*

Interval (s)	Average Energy (keV)		
	Lowell	271 Precursors	Six Groups
0.17 to 0.37	473(14)	508.6	506.5
0.41 to 0.85	482(12)	501.0	502.2
0.79 to 1.25	506(12)	498.0	499.6
1.2 to 1.9	502(12)	496.6	498.6
2.1 to 3.9	491(13)	494.0	497.3
4.7 to 10.2	478(14)	477.7	485.2
12.5 to 29.0	420(12)	457.7	466.7
35.8 to 85.5	441(17)	476.2	468.5

*The average energy (in keV) is given for the delayed neutrons emitted in various time intervals (given in column 1) following fission of ^{235}U by fast neutrons. The experimental results obtained at Lowell (column 2, [Tan+ 86]) are compared with calculations with the summation method using the initial 271 precursors (column 4), [BE 89]), and the six-group parameters of Table VII.4 (column 5). The values given in parentheses following the Lowell data represent the uncertainty in the last two digits, i.e., 473(14) must be interpreted as 473 ± 14 keV ([BE 89]).

FIGURE CAPTIONS

Fig. II.1 Illustration of the three phases of the fission process from the formation on the initial state (supposed to be spherical on the figure) and scission (two touching fragments). For simplicity, the fission barrier is supposed to present only one hump.

Fig. II.2 Graphical representation of various steps of the fission process: (0) formation of the initial state, (1) scission, (2) fragments acquiring 90% of their total kinetic energy from their mutual Coulomb repulsion, (3) prompt neutron emission, (4) prompt γ-ray emission, and (5) fragments stopping and decaying by delayed processes. The horizontal scale indicates the durations of the various phases of the fission process, whereas the vertical scale indicates the distance between the two fragments [WW 58].

Fig. II.3 Schematic representation on a (N,Z) chart of the formation and decay of the fission fragments by prompt and delayed processes. $n_{\beta i}$ is the number of β-rays emitted by fission product i.

Fig. II.4 Contour lines of the potential energy $V(s_1, s_2)$ and fission path in the representation of the PES with two deformation parameters s_1 and s_2. Two regions of low potential energy are connected by a saddle, and the fission path is indicated by a dashed line.

Fig. II.5 Potential energy surface $V(s_1, s_2)$ represented as a function of two deformation coordinates s_1 and s_2 in the vicinity of the point where $V(s_1, s_2)$ presents a minimum as a function of s_1 and a maximum as a function of s_2. This point is called the saddle point because the shape of the PES looks like that of a saddle in this region.

Fig. II.6 A one-dimensional illustration of the results of fission-barrier calculations obtained with the semiclassical (or hybrid) method:

(a) macroscopic energy $V_M(\{s\})$ as a function of deformation,
(b) shell-energy correction $\Delta E_{sh}(\{s\})$ as a function of deformation, and
(c) double-hump fission barrier obtained when the macroscopic energy is combined with the shell-energy correction for a typical actinide nucleus.

In (a), $V(\{0\})$ is the deformation energy at sphericity. In (b) and (c), the ground-state deformation $\{s_0\}$ is indicated by an arrow. When comparing experimental and calculated barrier heights, one has to take into account the vibrational energy of the ground state in the potential well (roughly equal to 0.5 MeV).

Fig. II.7 Region of the (Z,N) nuclear chart showing the location of all the presently known fission isomers with their half-lives. Two values for the same nucleus indicate the existence of spin isomers in the second minimum ([Hab 89]).

Fig. II.8 Neutron-induced fission cross section for ^{230}Th in the vicinity of the vibrational resonance at about 715 keV. The abscissa represents the excitation energy of the fissioning system. The open circles give the experimental results. The solid line is the result of calculations made in terms of a third minimum of the fission barrier. The dashed line represents the calculated ^{230}Th(d,pf) probability ([Blo 89]).

Fig. II.9 Experimental results of the cross section for neutron-induced subthreshold fission of ^{237}Np. These data clearly show a strong intermediate-structure effect ([Mic 68]).

Fig. II.10 PES for ^{240}Pu obtained with the Hartree-Fock-Bogolyubov method by constraining both the quadrupole and the hexadecapole moments Q_{20} and Q_{40}, respectively. This representation shows the existence of two families of shapes located in the fission and fusion valleys, V_1 and V_2, respectively ([BGG 89]).

Fig. III.1 Effect of the Doppler broadening on the shape of a Breit-Wigner resonance. The solid line represents the shape in

the absence of Doppler broadening, and the dashed line represents the broadened shape for $\beta=1$.

Fig. III.2 Plot of the ratio $f(x) = T_{eff}/T$ of the effective temperature T_{eff} over the actual temperature T as a function of $x = \Theta_D/2T$, where Θ_D is the Debye temperature of the sample ([Mic 89]).

Fig. III.3 Variation of the energy self-shielding factor $f_H(\beta,\zeta)$ as a function of the parameter $\zeta\psi_0$ for several values of the parameter $\theta = \frac{\beta^2}{4}$ ([Soo 62]).

Fig. IV.1 Improvements in the measurements of the ^{239}Pu fission cross section made at Los Alamos National Laboratory (1955), at Argonne National Laboratory (1958), and at Saclay (1968).

Fig. IV.2 Fits to the measured fission and total cross sections of ^{239}Pu in the 50- to 100-eV and 800- to 900-eV intervals ([DSP 90]).

Fig. IV.3 Cumulative sum of the number of observed ^{239}Pu resonances as a function of neutron energy. The staircase line corresponds to the measured data and the straight solid line corresponds to a spacing of 2.4 eV ([DSP 90]).

Fig. IV.4 Level-spacing distribution for the ^{239}Pu resonances observed below 480-eV neutron energy. The histogram corresponds to the observed spacings. The solid line represents the calculated level-spacing distribution resulting from the random superposition of two uncorrelated level-spacing distributions for the two spin values (J = 0 and J = 1). Each distribution obeys the Wigner law ([DSP 90]).

Fig. IV.5 Integral distribution of the reduced neutron widths for the ^{239}Pu resonances analyzed below 480 eV. The histogram corresponds to the observed resonances. The solid line corresponds to a Porter-Thomas distribution calculated with 216 levels, which results in an average spacing of 2.17 eV. Note that small levels must be added

to the observed ones to fit the experimental histogram ([DSP 90]).

Fig. IV.6 Integral distribution of the fission widths for the ^{239}Pu resonances analyzed below 480 eV. The experimental data (histogram) can be fitted by the sum of two calculated khi-square distributions (•) corresponding to the 1^+ fission channel (small fission widths) and to the 0^+ fission channels (large fission widths). The parameters used in the calculations are given in Table IV.3 ([DSP 90]).

Fig. IV.7 Ratio of the ^{239}Pu fission cross section, as measured by Weston and Tod ([WT 84]), to the same cross section as evaluated by the ENDF/B-VI standards subcommittee.

Fig. IV.8 Results of several measurements of the ^{239}Pu fission cross section in the MeV region ([YM 91]). The experimental results were obtained by Lisowski et al. ([Lis+ 88]) and Meadows ([Mea 88]). The dotted curve connects the solid squares, which are the results of the covariance analysis performed for reactions for standards in the ENDF/B-VI evaluated data file.

Fig. V.1 Measured ^{235}U fission cross section $\sigma_{nf}(E_n)$, multiplied by $\sqrt{E_n}$, obtained from the measurement described in the text (+) and from previous measurements (*) ([DSP 73]). The solid line represents the evaluated values in the file ENDF/B-V, normalized to σ_{nf} = 587.6 barns for thermal neutrons ([WD 86]).

Fig. V.2 Shape of the ^{235}U fission cross section $\sigma_{nf}(E_n)$, as measured at the ILL for neutron energies between 6 and 60 μeV. The dots give the measured values of $\sigma_{nf}(E_n)\sqrt{E_n}$ in relative units, and the solid line is a qualitative fit to the data. The measured flux distribution of the very cold neutrons used in the measurement is also plotted ([Wag+ 88]).

Fig. V.3 The neutron energy dependence of η for ^{235}U. The open circles represent the data obtained with the Geel linear accelerator used as a pulsed neutron source. The solid

line represents the reference shape, and the dashed line represents the shape proposed from integral experiments ([San 87], [Wei+ 90]).

Fig. V.4 The neutron energy dependence of η for ^{235}U. The open circles represent the data obtained from measurements at the ILL. The solid line represents the reference shape, and the dashed line represents the shape proposed from integral experiments ([San 87], [Wei+ 90]).

Fig. VI.1 Independent yields IN for thermal-neutron-induced fission of ^{235}U from A'_p calculations. Sums of the IN values over Z for each A give mass-number yields Y(A). Sums of IN values over A for each Z give charge yields Y(Z). The spikes in the charge yields illustrate the proton odd-even effect, whereby yields for fragments with even-Z values are favored compared with those for fragments with odd-Z values ([Wah 89]).

Fig. VI.2 Mass distribution of the fission products from the neutron-induced fission of ^{235}U by neutrons of different energies (thermal, fast, 14 MeV) ([BBB 89]).

Fig. VI.3 Average masses of the light and heavy fission-product groups as a function of the mass of the fissioning nucleus ([Fly+ 72]).

Fig. VI.4 Schematic of the fission-fragment mass distributions (normalized to 200% fission-fragment yield) for the spontaneous fission of transberkelium isotopes ([Hof 89]).

Fig. VI.5 Location of the fission fragments of the light group for the thermal-neutron-induced fission of ^{235}U. The fission fragments are located according to their charge and neutron numbers, Z and N, respectively. The solid line represents approximately the line of β stability. The dashed line represents a proton-to-neutron ratio equal to that of the fissioning nucleus ([BBB 89]).

Fig. VI.6 Isobaric charge distribution for fission products having mass number A = 93 produced in the thermal-neutron-induced fission of ^{235}U:

- open circles represent measured independent yields,
- closed circles represent measured cumulative yields,
- the solid line represents a calculated Gaussian curve for the independent yields, and
- the dotted line represents a calculated Gaussian curve for the cumulative yields ([Wah 65]).

Fig. VI.7 Illustration of the mode of operation of the LOHENGRIN mass spectrometer ([Mol+ 75]).

Fig. VI.8 Pulse-height spectrum of the residual energy $E_{res} = E - \Delta E$ of monoenergetic fission fragments (having mass A = 97, energy E = 98 MeV, and ionic charge q = 22) after passing through a passive absorber (foil of parylene C) where they loose energy ΔE. The smooth curve is a computer fit to the data ([QRS 79]).

Fig. VI.9 Arrangement for experiments using the fission-fragment recoil mass spectrometer HIAWATHA and the Illinois Advanced Nuclear Reactor ([DW 77]).

Fig. VI.10 Charge yield distribution Y(Z) for the fission products of the thermal-neutron-induced fission of ^{235}U. The solid line results from calculations using the A'_p model. The open circles, the closed circle, and the closed square result from calculations with the Z_p model. The closed circle and the closed square are calculated for Z = 50 and Z = 42, respectively ([Wah 88]).

Fig. VI.11 Independent yields $Y_i(A, Z)$ and mass yields Y(A) for the thermal-neutron-induced fission of ^{235}U, as calculated with the A'_p model. The INs for each Z are connected by dotted lines for odd-Z values; continuous lines for even-Z values; and heavy, continuous lines for Z = 50 and for the complementary charge Z = 42. The charge numbers are shown inside the borders at the bottom. Sums of the INs for each A give the calculated Y(A) shown as the heavy, outer line. Experimental values of the mass distribution ([FGG 75]) are shown as empty squares ([Wah 88]).

Fig. VII.1 β-ray heat $M_b(t)$ multiplied by the cooling time t for the thermal-neutron-induced fission of ^{235}U. The closed circles are the results of integral measurements ([Joh 88]). The open circles are the results of summation calculations described in the text.

Fig. VII.2 β-ray heat $M_b(t)$ multiplied by the cooling time t for the thermal-neutron-induced fission of ^{235}U. The open circles are the results of the summation method described in the text. The solid line represents the results of the summation method using the Japanese data file. The dash-dot line represents the results of the summation method using the ENDF/B-V data file. The dash-dot-dot line represents the results of the summation method using the French data file. Exact references for these calculations can be found in [Rud+ 88].

Fig. VII.3 β-ray burst function b(t) multiplied by the cooling time t for the thermal-neutron-induced fission of ^{235}U. The open circles are the results of the YAYOI integral experiments ([AA 82]). The solid lines are obtained with the summation method using the data from ENDF/B-VI. The flags 0, 1, 2, and 3 correspond to the various contributions a, b, c, and d described in the text.

Fig. VII.4 γ-ray burst function g(t) multiplied by the cooling time t for the thermal-neutron-induced fission of ^{235}U. The open circles are the results of the YAYOI integral experiments ([AA 82]). The solid lines are obtained with the summation method using the data from ENDF/B-VI. The flags 0, 1, 2, and 3 correspond to the various contributions a, b, c, and d described in the text.

Fig. VII.5 Total burst function m(t) multiplied by the cooling time t for the fast-neutron-induced fission of ^{238}U. The open circles are the results of the YAYOI integral experiments ([AA 82]). The solid lines are obtained with the summation method using the data from ENDF/B-VI. The flags 0, 1, 2, and 3 correspond to the various contributions a, b, c, and d described in the text.

Fig. VII.6 γ-ray burst function g(t) multiplied by the cooling time t for the fast-neutron-induced fission of ^{238}U. The experimental points come from the results of the YAYOI integral experiments ([AA 82]). The curves come from calculations using the summation method with different data files indicated on the figure.

Fig. VII.7 γ-ray burst function g(t) multiplied by the cooling time t for the thermal-neutron-induced fission of ^{239}Pu. The open circles are the results of the YAYOI integral experiments ([AA 82]). The curves are obtained from calculations using the summation method with different values of the γ-ray energy E_γ of ^{232}Tc. The detailed references of the calculations can be found in [RE 91].

Fig. VIII.1 Schematic description of delayed-neutron emission ([Eng+ 88]).

Fig. VIII.2 Location of delayed-neutron precursors on a (Z,N) nuclear chart. These precursors are located to the right of the thick solid line. The fractional abundance is also indicated for each precursor (> 10%, 1 to 10%, 0.1 to 1%) ([BE 89]).

Fig. VIII.3 Results of $\overline{\nu_d}$ for neutron-induced fission in ^{235}U as obtained from measurements for neutron energies 0-4 MeV and 14-15 MeV and from evaluations for thermal neutrons and for a soft fission spectrum ([Bla+ 90]).

Fig. VIII.4 Systematics of $\overline{\nu_d}$ plotted as a function of the parameter $(3Z_F\text{-}A_F) \times \frac{A_F}{Z_F}$ of the fissioning system. The targets (with the type of fission) or the spontaneously fissioning nuclei are indicated for each result ([Tut 79]).

Fig. VIII.5 Comparison of the total delayed-neutron emission rates $n_d(t)$ in the fission induced in ^{235}U by fast neutrons as obtained from the summation method using the six-group parameters of Table VIII.4 and from a measurement following a fast fission pulse ([BE 89]).

Fig. VIII.6 Comparison of the spectra of delayed neutrons in the time interval 0.79 to 1.25 s following fission of ^{235}U

induced by fast neutrons as obtained from a measurement at Lowell ([Tan+ 86]) and from calculations with the summation method using either the six-group parameters of Table VIII.4 or 271 precursors ([BE 89]).

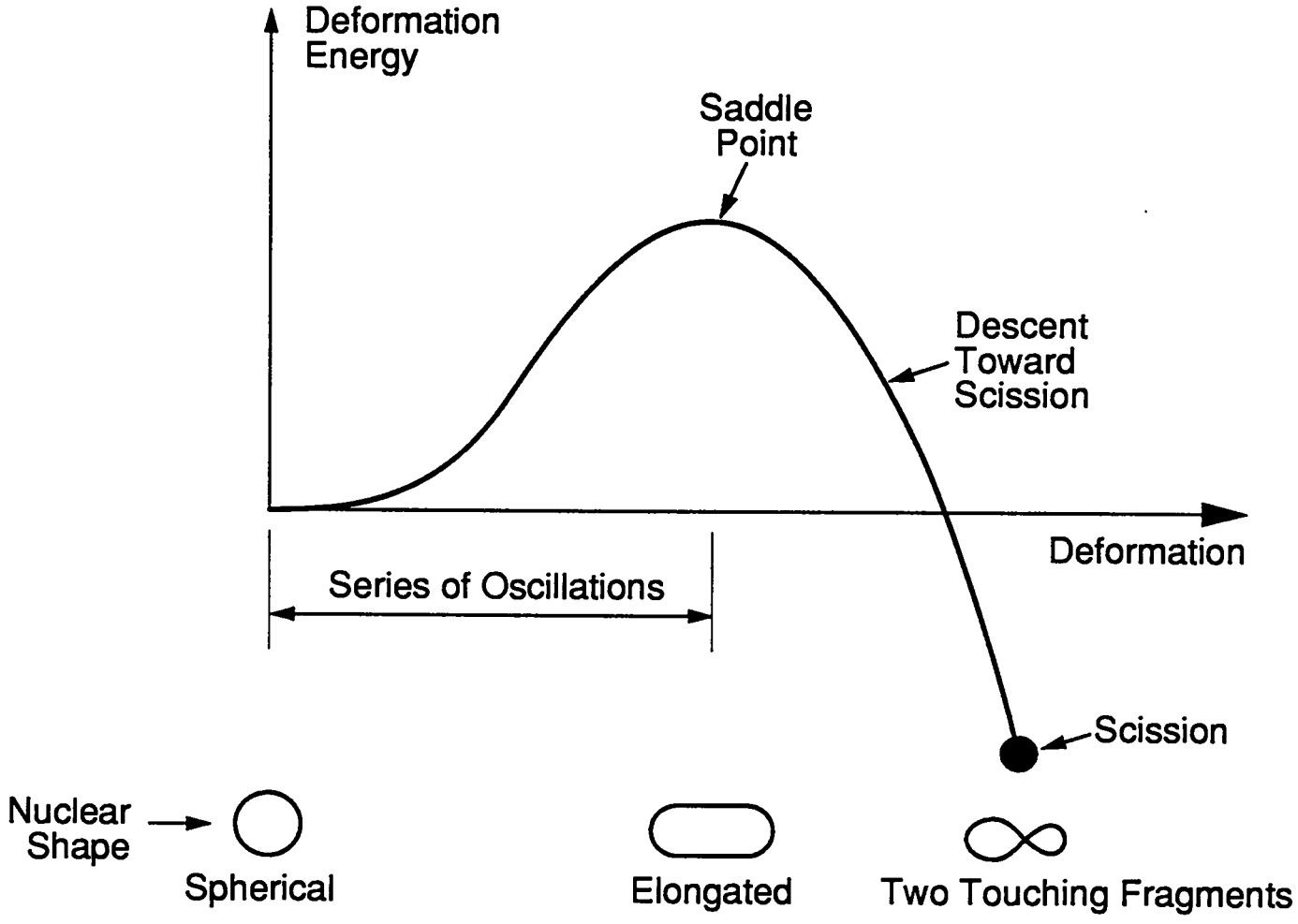
Deformation
Energy
Saddle
Point
Descent
Toward
Scission
Deformation
Series of Oscillations
Scission
Nuclear
Shape
Spherical
Elongated
Two Touching Fragments

Fig. II. 1

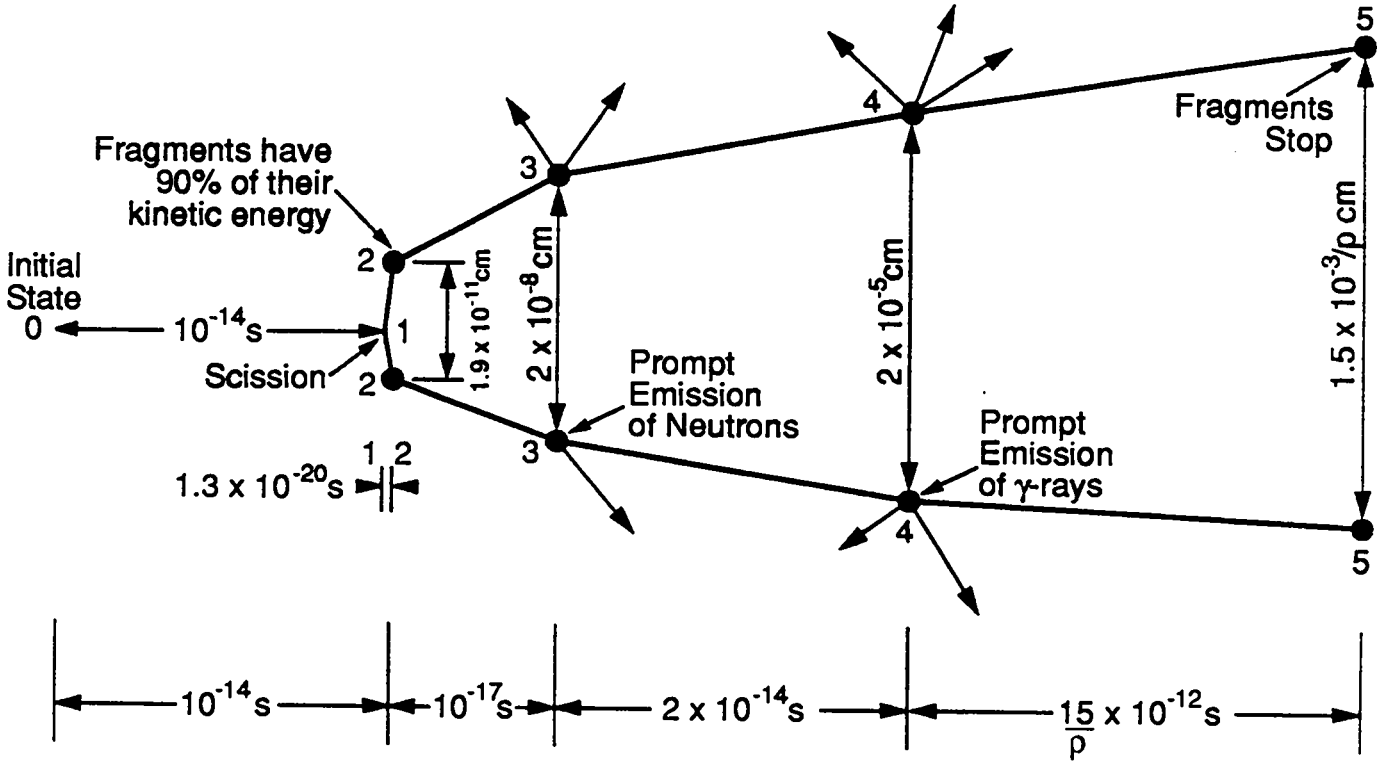
Fragments have
90% of their
kinetic energy
Initial
State
0
10^{-14}s
1
Scission
2
1.9×10^{-11}cm
2×10^{-8}cm
Prompt
Emission
of Neutrons
1.3×10^{-20}s
1 2
3
4
2×10^{-5}cm
Prompt
Emission
of γ-rays
Fragments
Stop
$1.5 \times 10^{-3}/\rho$ cm
5
10^{-14}s
10^{-17}s
2×10^{-14}s
$\frac{15}{\rho} \times 10^{-12}$s

Fig. II. 2

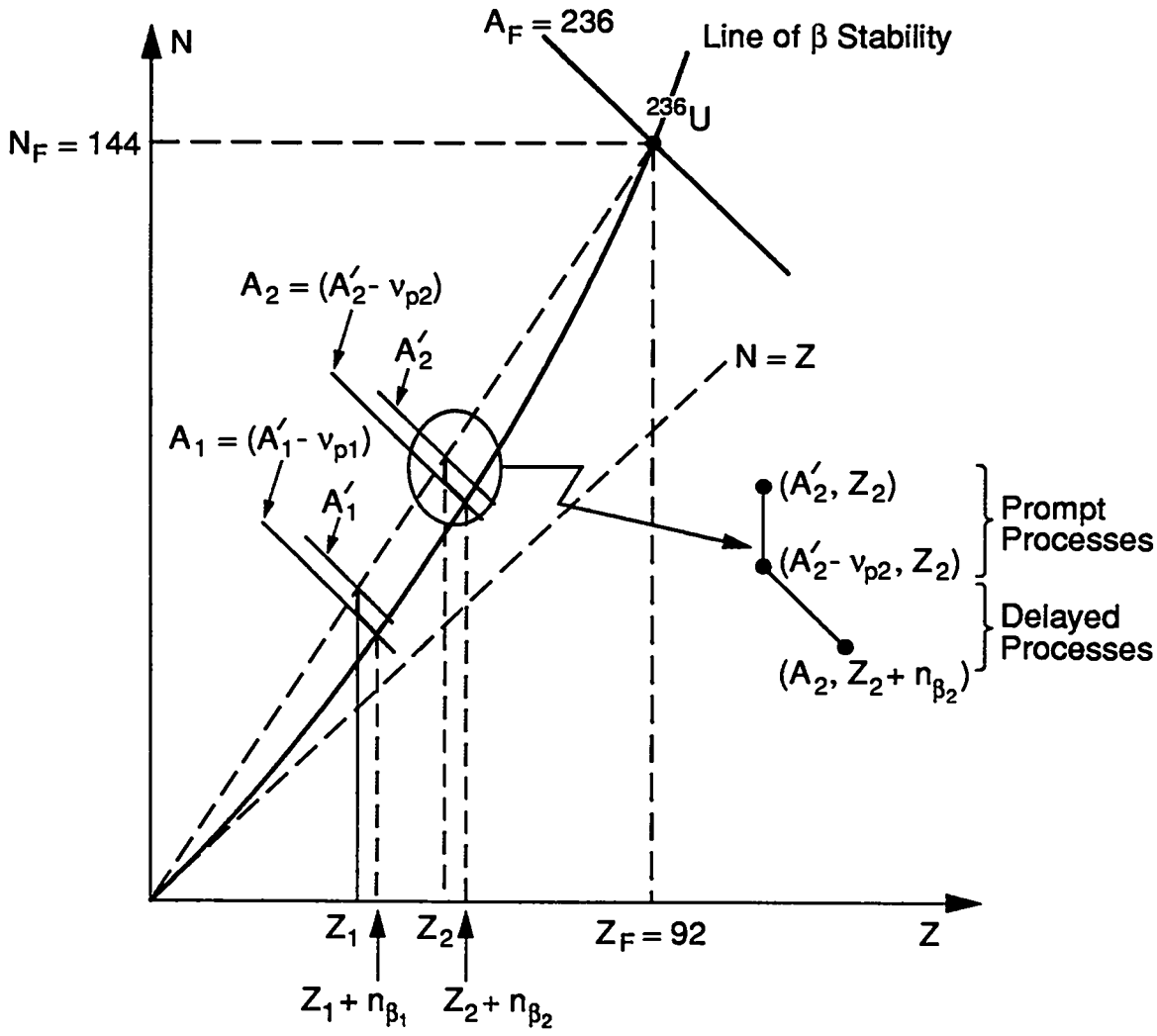
N
$A_F = 236$
Line of β Stability
^{236}U
$N_F = 144$
$A_2 = (A'_2 - \nu_{p2})$
A'_2
N = Z
$A_1 = (A'_1 - \nu_{p1})$
A'_1
(A'_2, Z_2)
$(A'_2 - \nu_{p2}, Z_2)$
Prompt Processes
Delayed Processes
$(A_2, Z_2 + n_{\beta_2})$
Z_1
Z_2
$Z_F = 92$
Z
$Z_1 + n_{\beta_1}$
$Z_2 + n_{\beta_2}$

Fig. II. 3

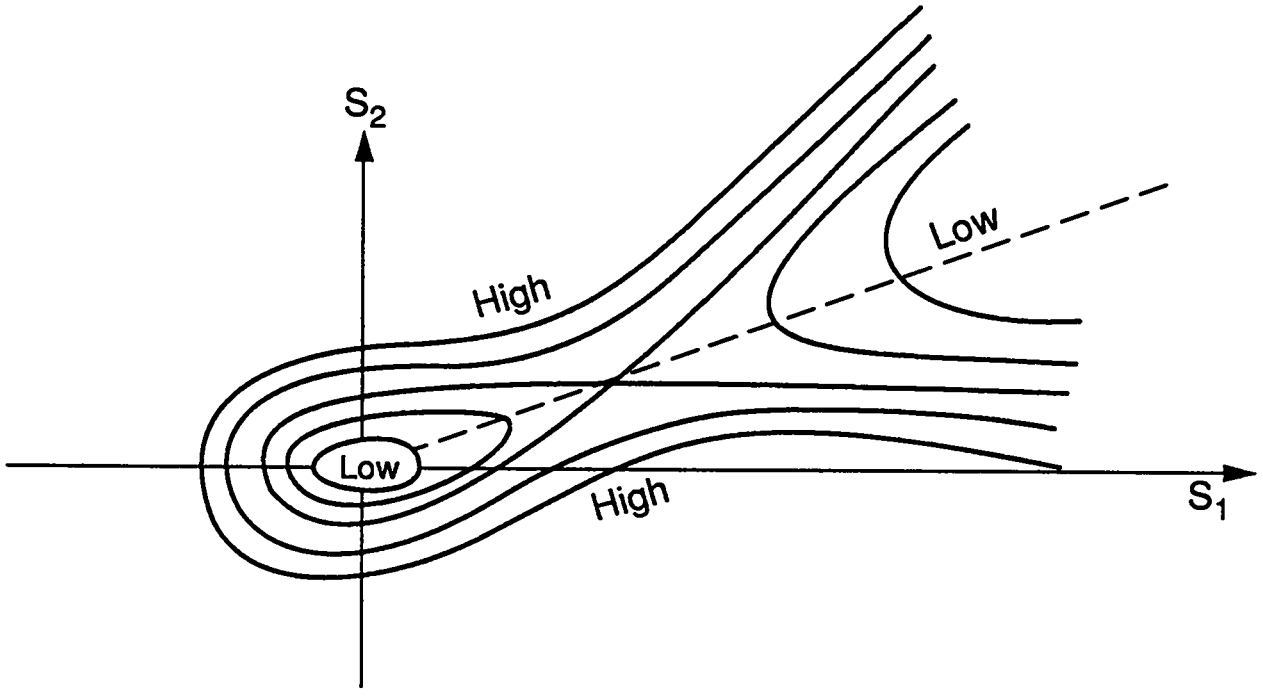

Fig. II. 4

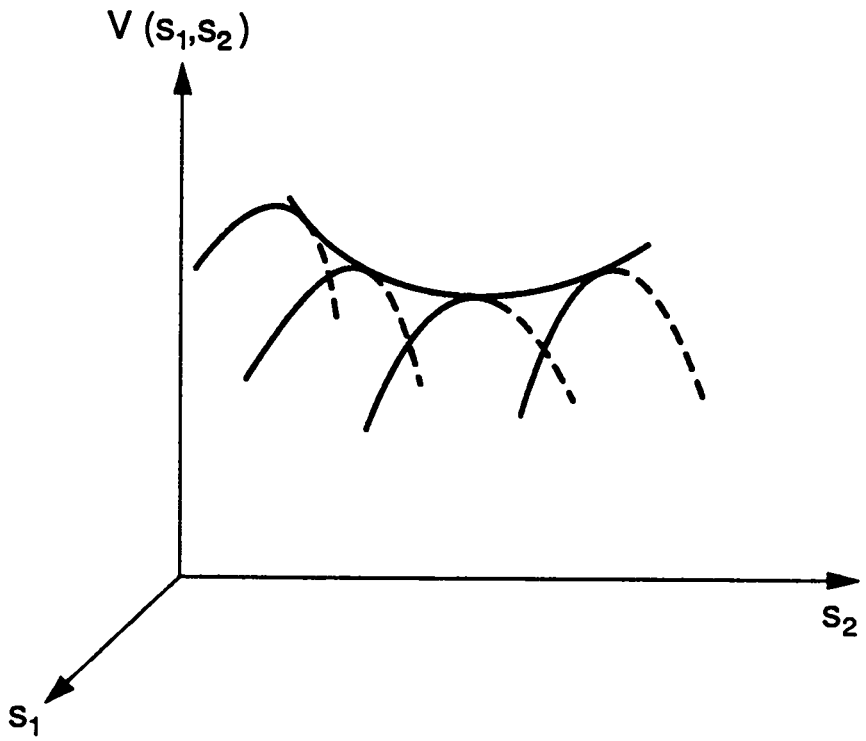

Fig. II. 5

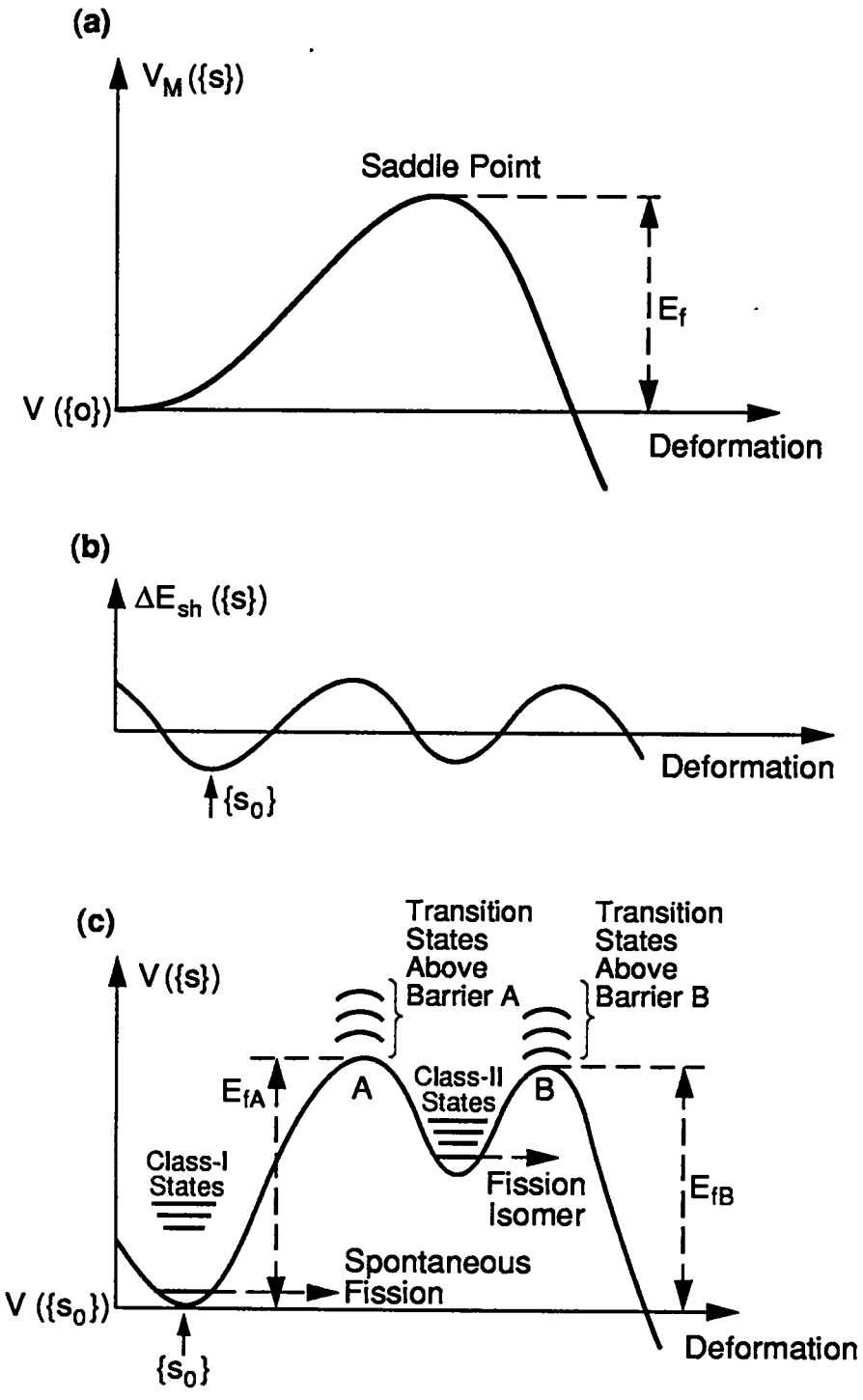
(a)
$V_M(\{s\})$
Saddle Point
E_f
$V(\{o\})$
Deformation
(b)
$\Delta E_{sh}(\{s\})$
Deformation
$\{s_0\}$
(c)
$V(\{s\})$
Transition States Above Barrier A
Transition States Above Barrier B
E_{fA}
A
Class-II States
B
Class-I States
Fission Isomer
E_{fB}
Spontaneous Fission
$V(\{s_0\})$
$\{s_0\}$
Deformation

Fig. II. 6

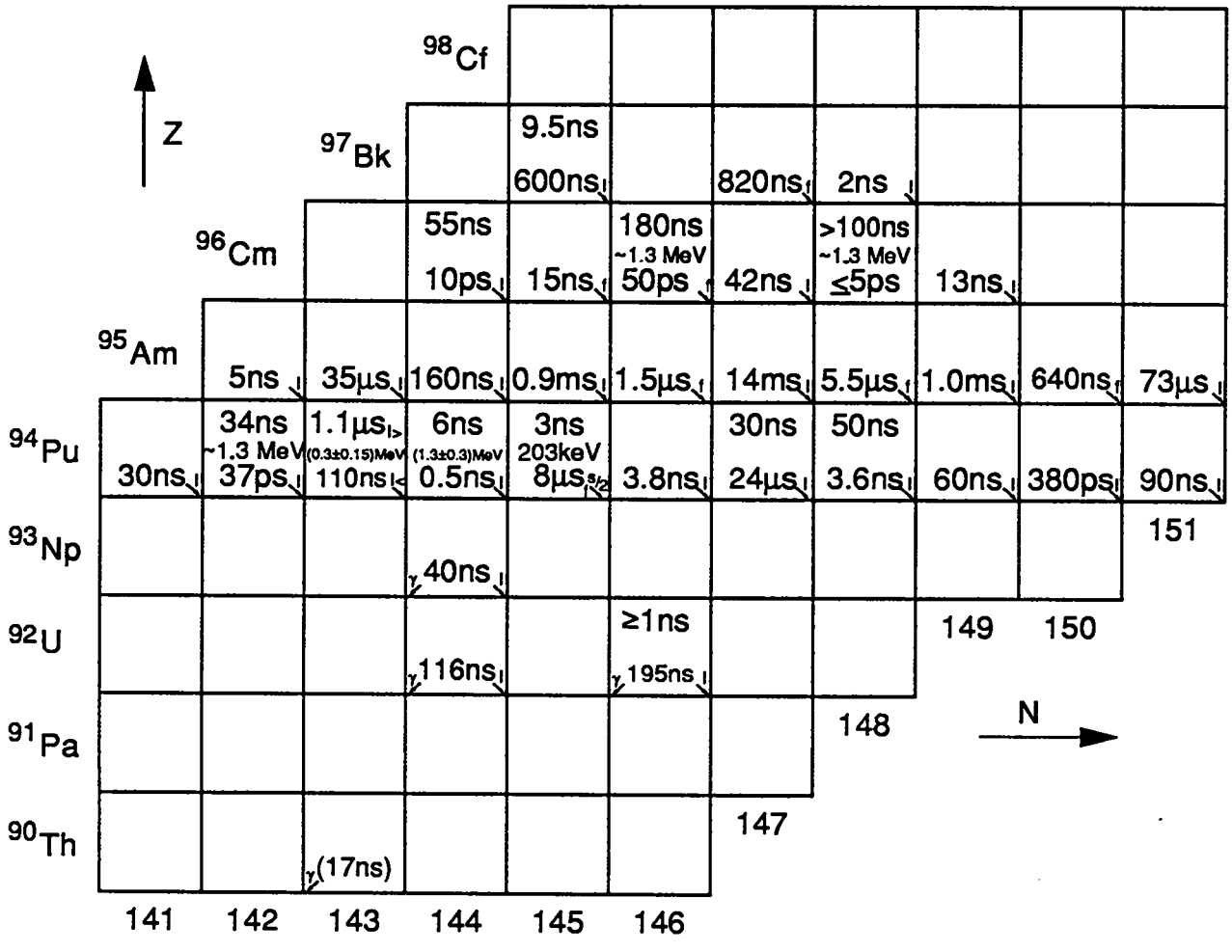
Z
N
98Cf
97Bk
96Cm
95Am
94Pu
93Np
92U
91Pa
90Th
9.5ns
600ns
820ns
2ns
55ns
10ps
180ns
~1.3 MeV
50ps
15ns
42ns
>100ns
~1.3 MeV
≤5ps
13ns
5ns
35μs
160ns
0.9ms
1.5μs
14ms
5.5μs
1.0ms
640ns
73μs
34ns
~1.3 MeV
37ps
1.1μs
(0.3±0.15)MeV
110ns
6ns
(1.3±0.3)MeV
0.5ns
3ns
203keV
8μs
3.8ns
30ns
24μs
50ns
3.6ns
60ns
380ps
90ns
30ns
151
40ns
≥1ns
195ns
116ns
149
150
148
147
(17ns)
141
142
143
144
145
146

Fig. II. 7

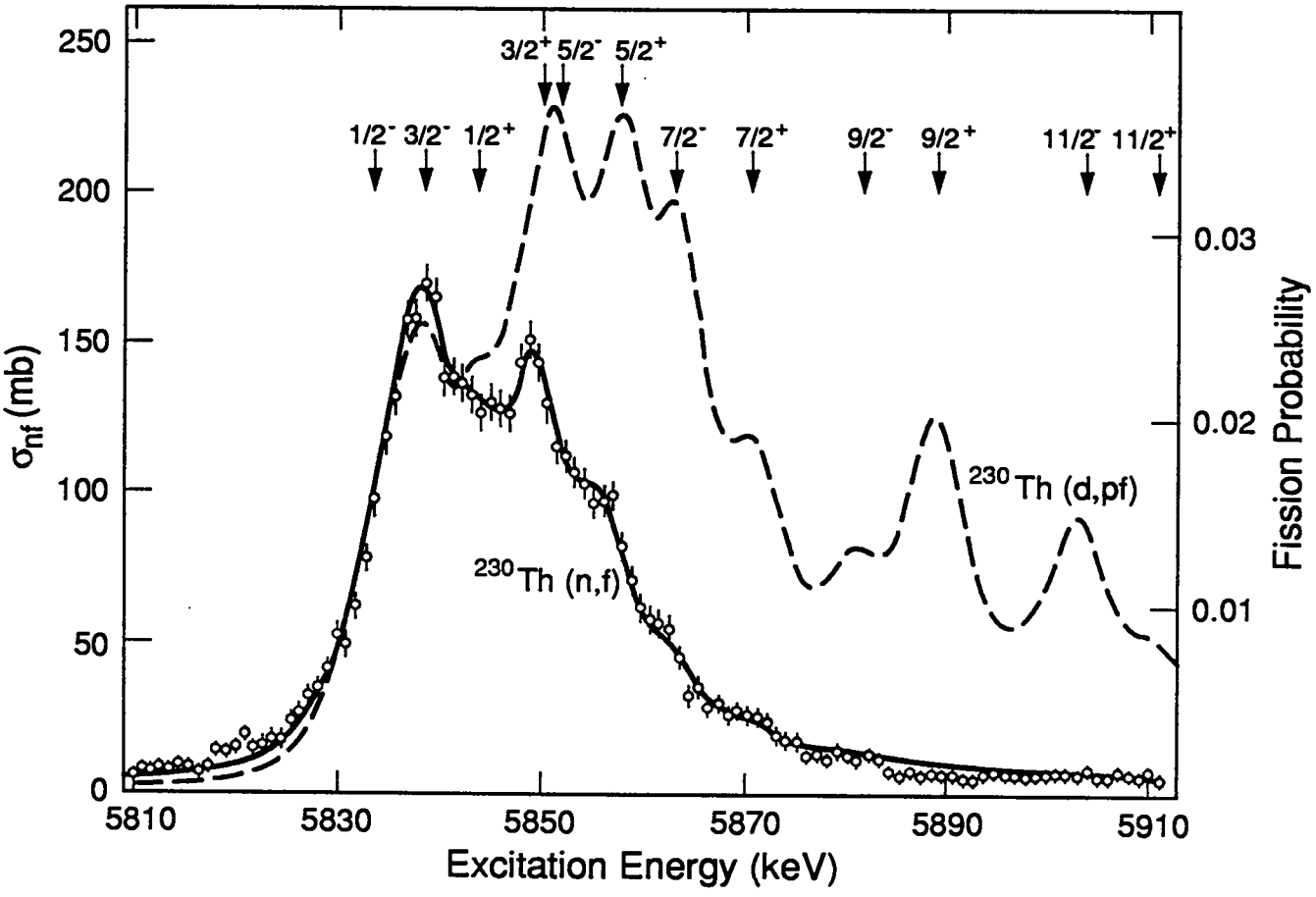
250
200
150
100
50
0
σ_{nf} (mb)
0.03
0.02
0.01
Fission Probability
$3/2^+$ $5/2^-$ $5/2^+$
$1/2^-$ $3/2^-$ $1/2^+$ $7/2^-$ $7/2^+$ $9/2^-$ $9/2^+$ $11/2^-$ $11/2^+$
^{230}Th (d,pf)
^{230}Th (n,f)
5810
5830
5850
5870
5890
5910
Excitation Energy (keV)

Fig. II. 8

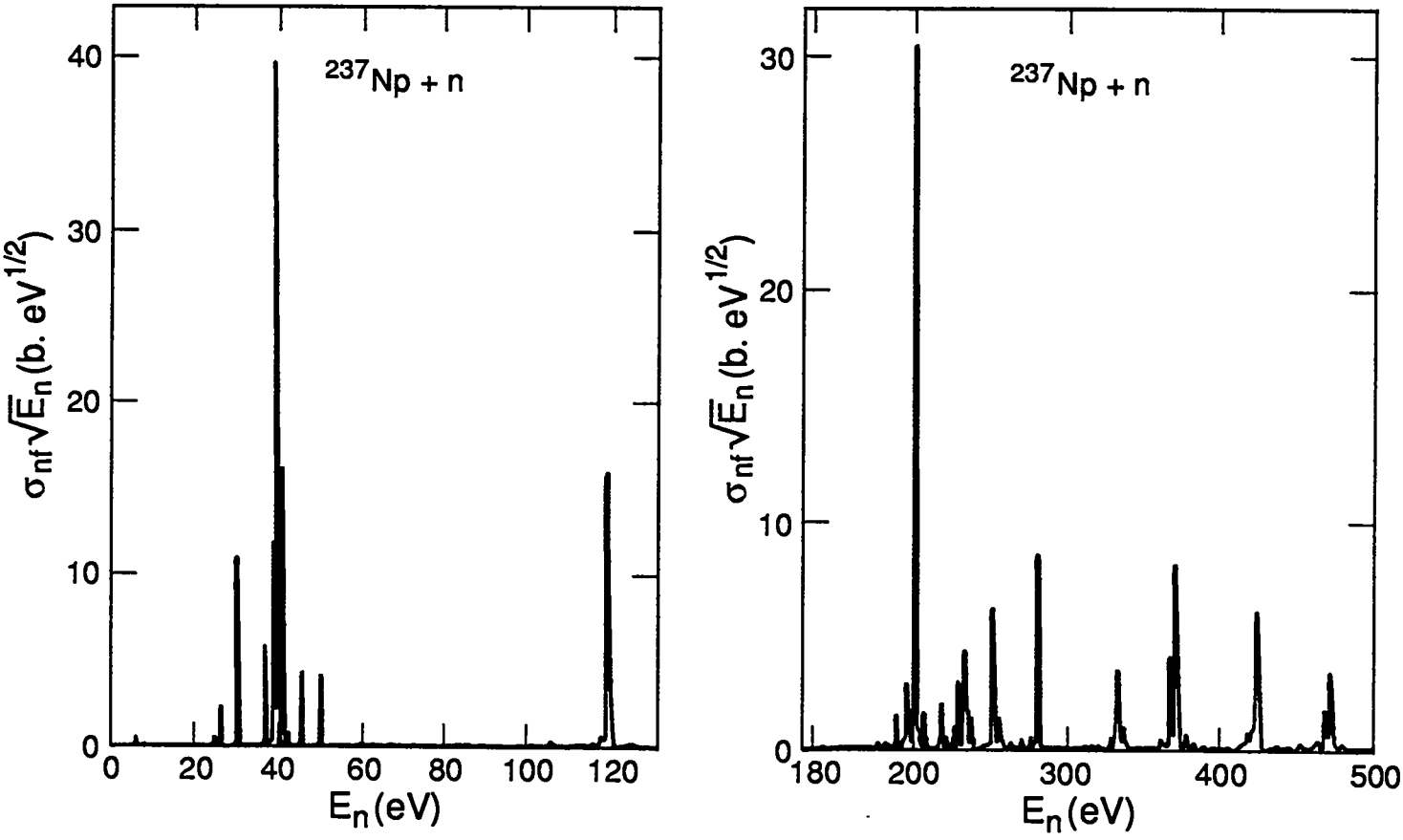
^{237}Np + n
$\sigma_{nf}\sqrt{E_n}$(b. eV$^{1/2}$)
E_n(eV)
0
10
20
30
40
0
20
40
60
80
100
120
^{237}Np + n
$\sigma_{nf}\sqrt{E_n}$(b. eV$^{1/2}$)
E_n(eV)
0
10
20
30
180
200
300
400
500

Fig. II. 9

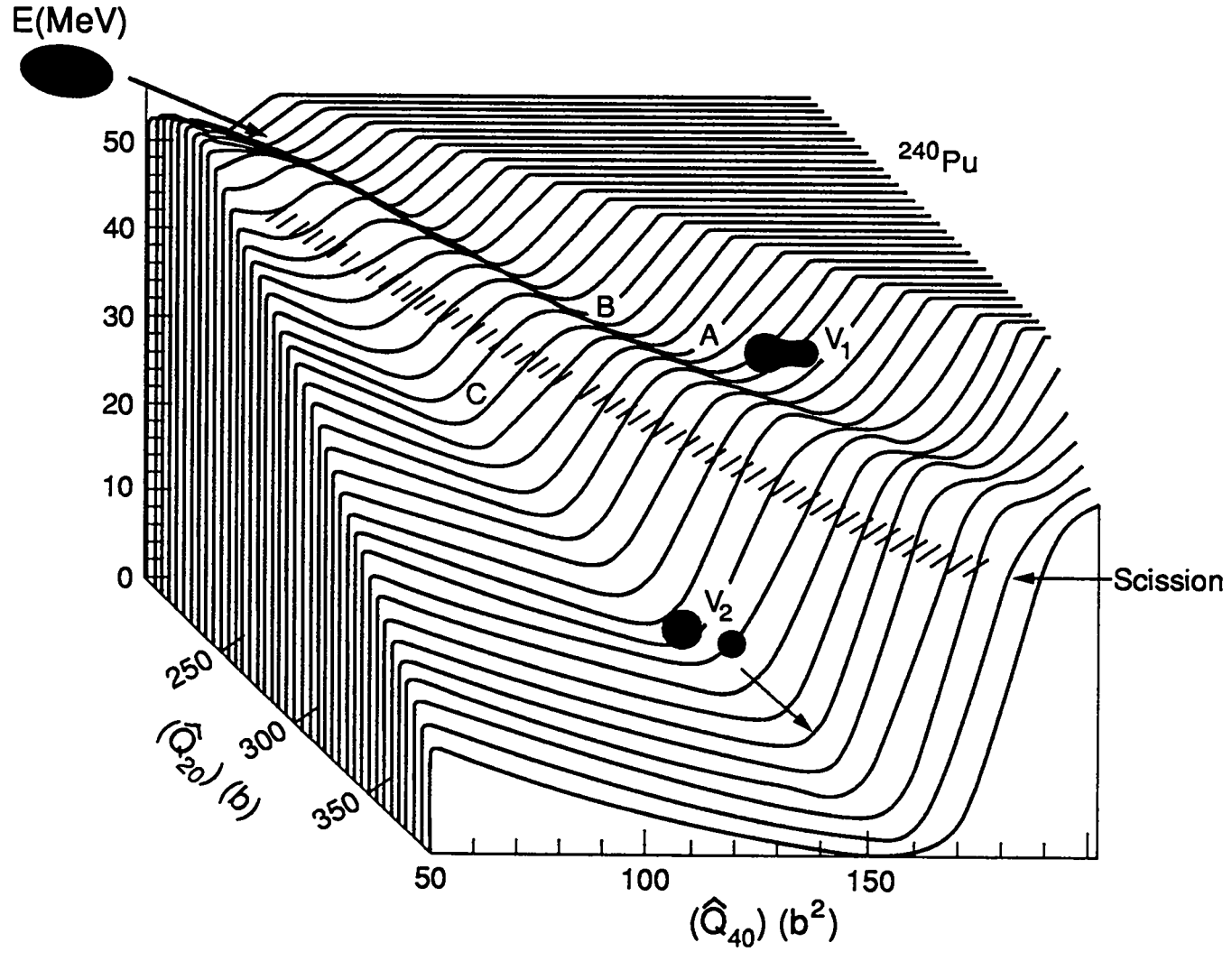
E(MeV)
50
40
30
20
10
0
^{240}Pu
B
A
V_1
C
V_2
Scission
250
300
350
$(\hat{Q}_{20})$ (b)
50
100
150
$(\hat{Q}_{40})$ (b^2)

Fig. II. 10

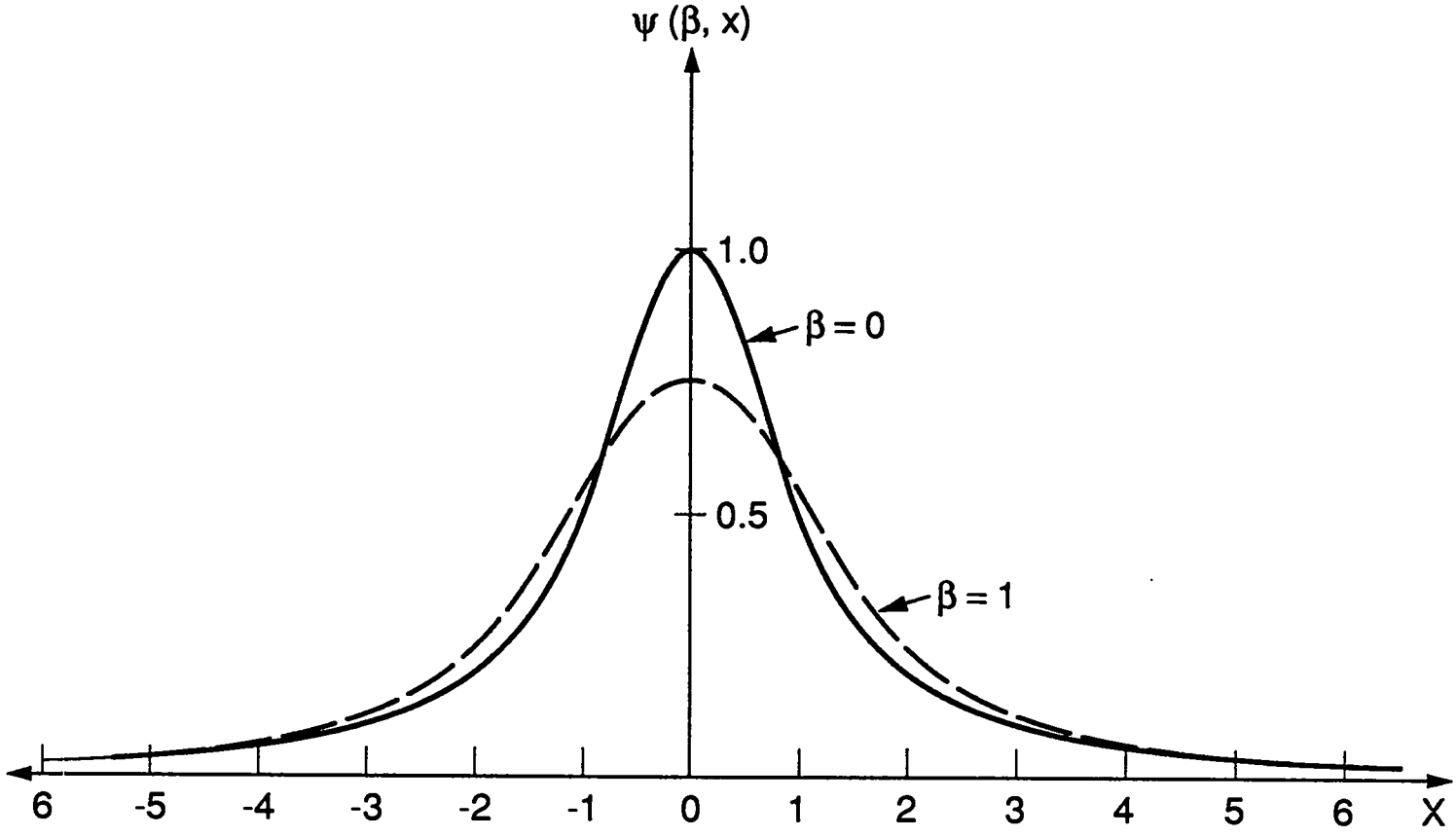

Fig. III. 1

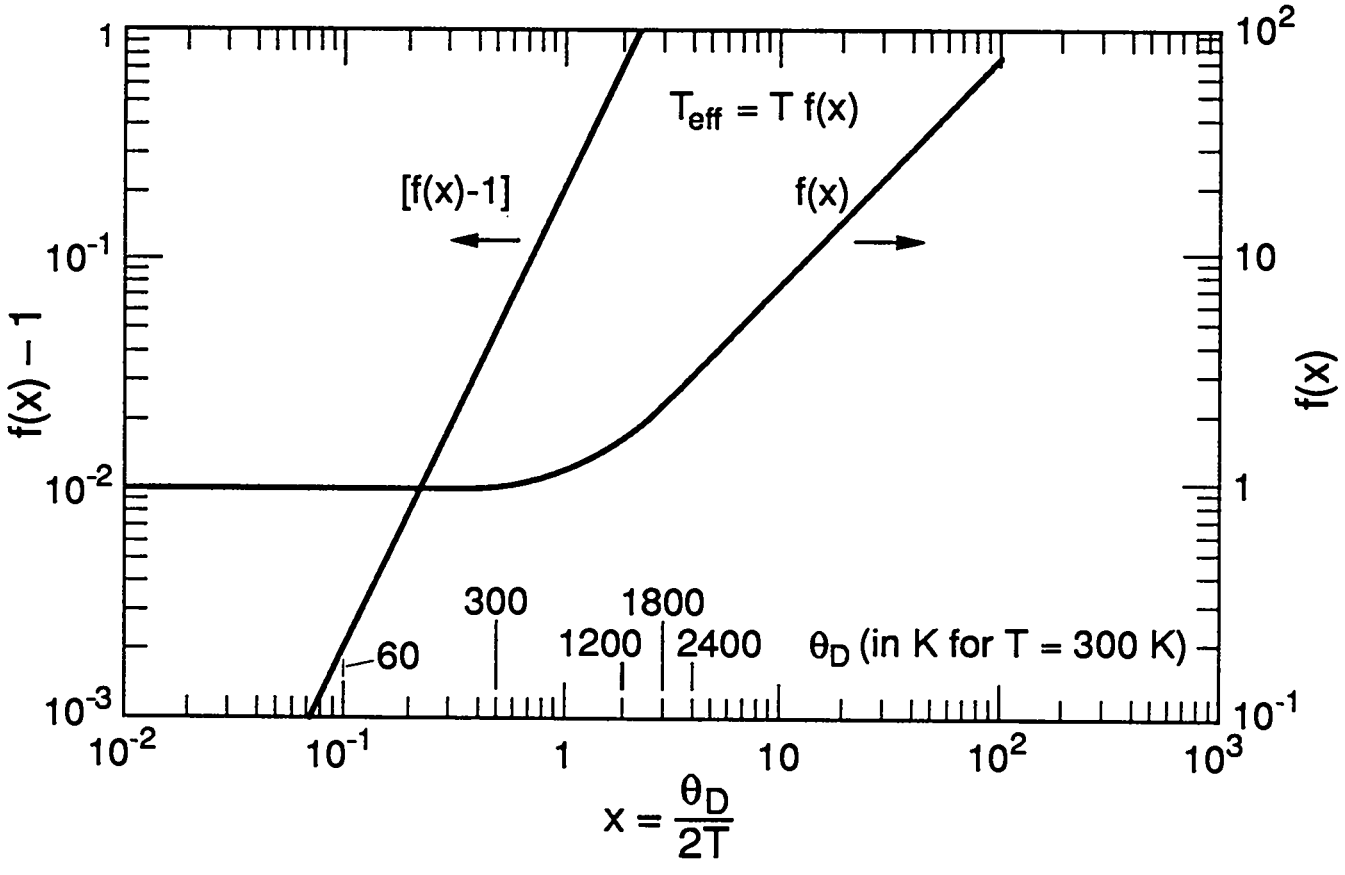
1
10^{-1}
10^{-2}
10^{-3}
f(x) – 1
10^{2}
10
1
10^{-1}
f(x)
T_{eff} = T f(x)
[f(x)-1]
f(x)
60
300
1200
1800
2400
θ_D (in K for T = 300 K)
10^{-2}
10^{-1}
1
10
10^{2}
10^{3}
$x = \frac{\theta_D}{2T}$

Fig. III. 2

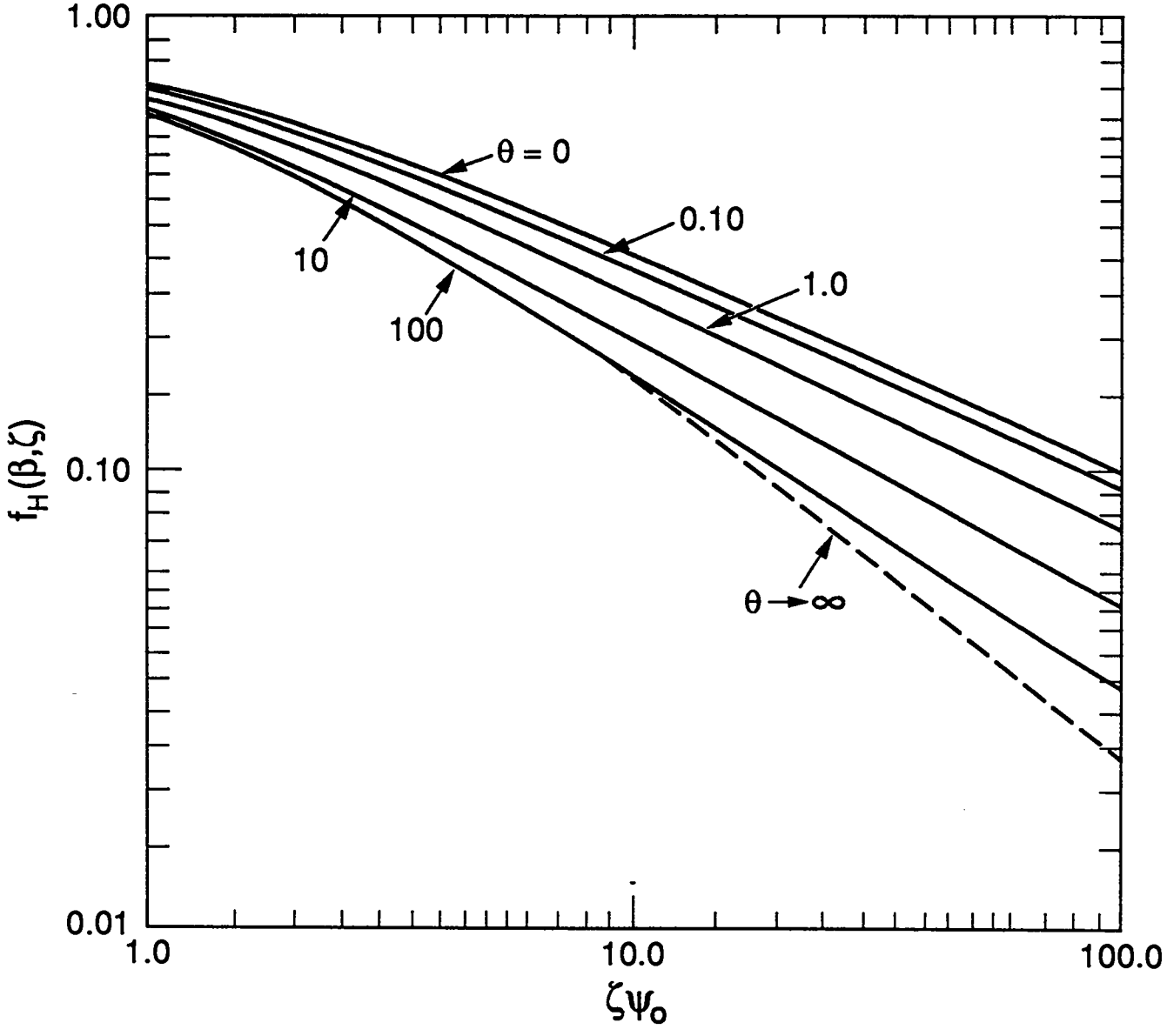

Fig. III. 3

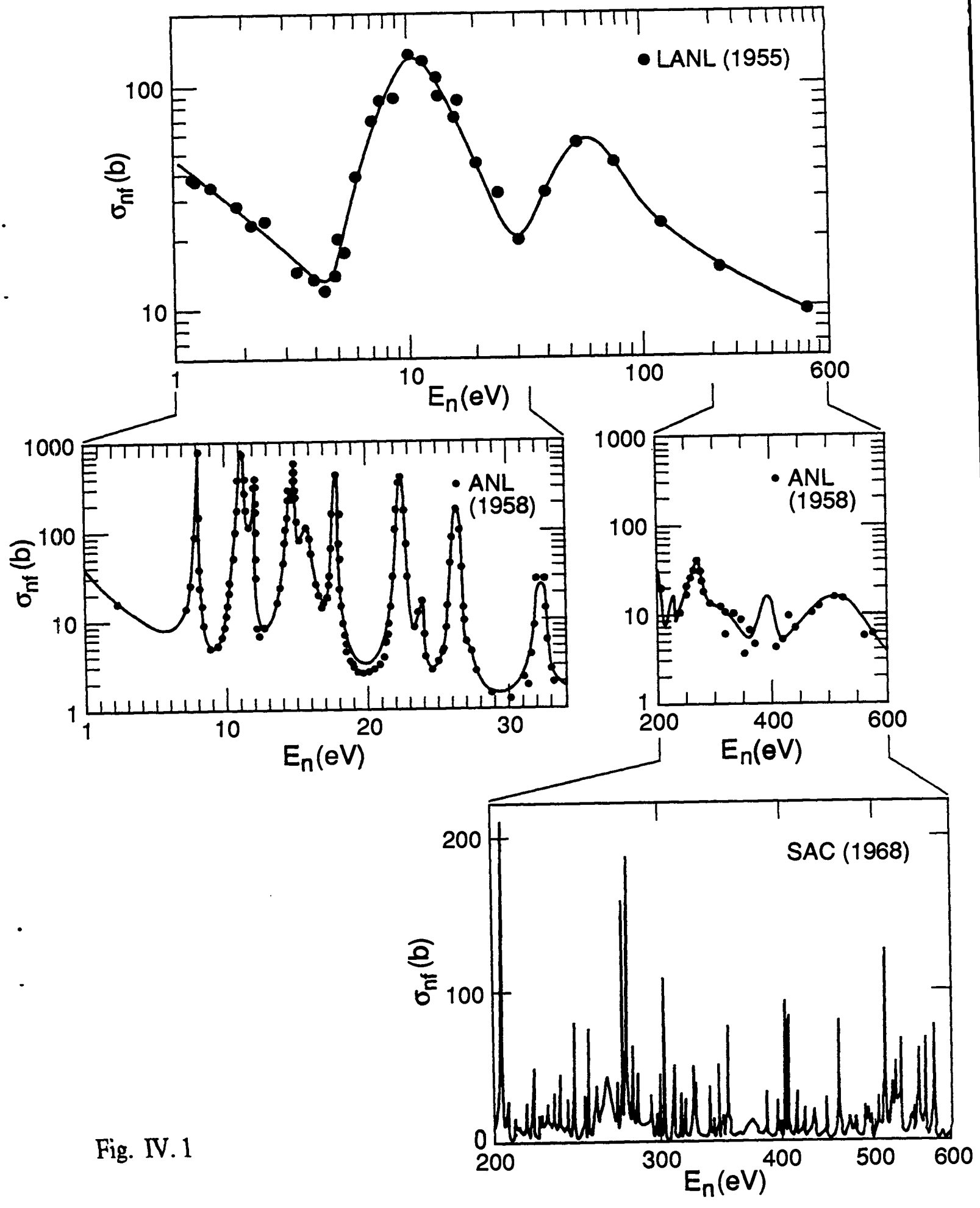
LANL (1955)
100
10
σ_{nf}(b)
1
10
100
600
E_n(eV)
ANL
(1958)
1000
100
10
1
1
10
20
30
E_n(eV)
ANL
(1958)
1000
100
10
1
200
400
600
E_n(eV)
SAC (1968)
200
100
0
σ_{nf}(b)
200
300
400
500
600
E_n(eV)

Fig. IV. 1

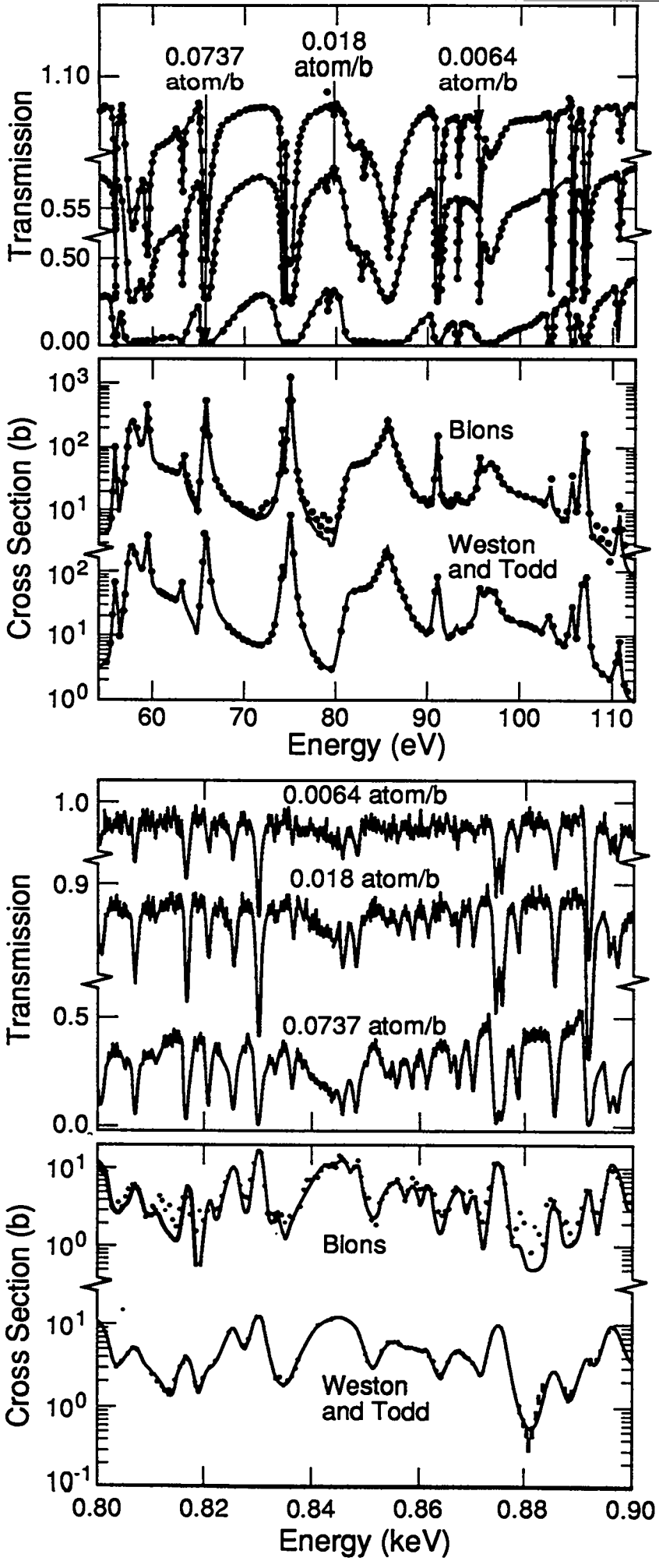
0.0737 atom/b
0.018 atom/b
0.0064 atom/b
Transmission
1.10
0.55
0.50
0.00
Cross Section (b)
Blons
Weston and Todd
Energy (eV)
0.0064 atom/b
0.018 atom/b
0.0737 atom/b
Transmission
1.0
0.9
0.5
0.0
Cross Section (b)
Blons
Weston and Todd
Energy (keV)

Fig. IV-2

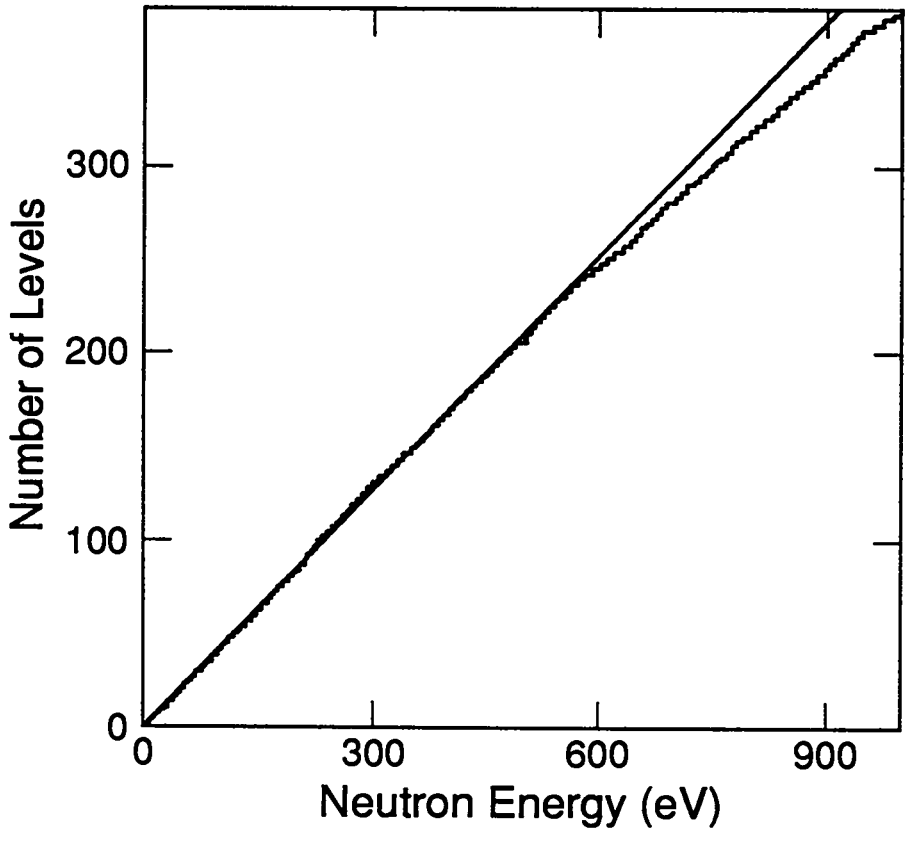

Fig. IV. 3

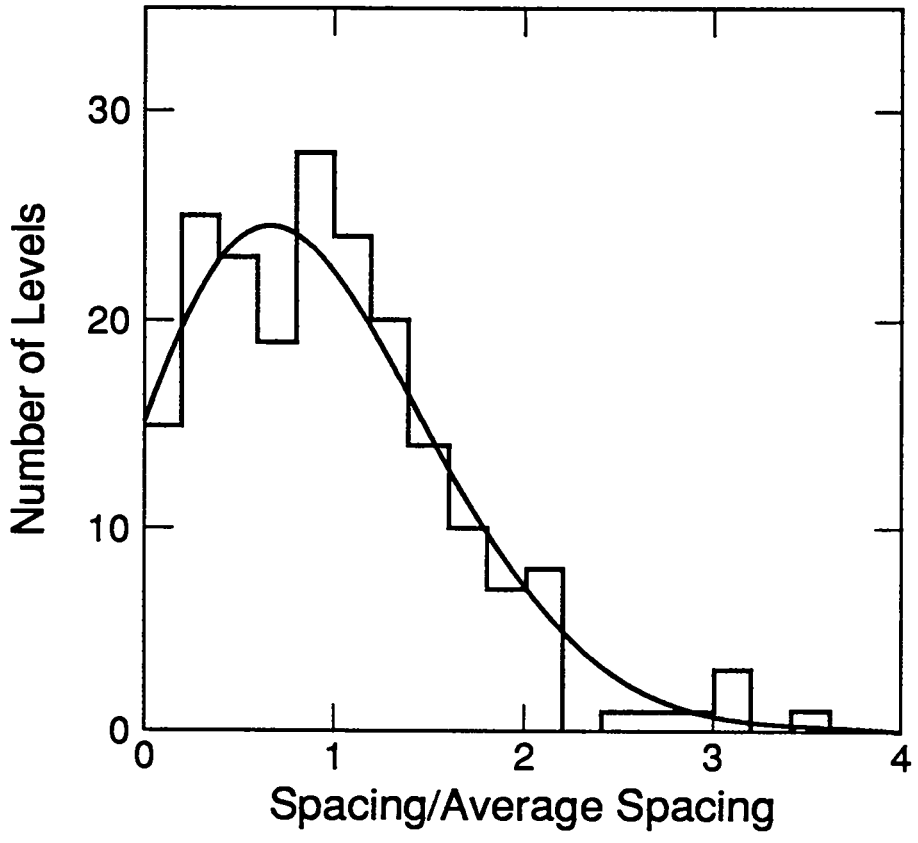

Fig. IV. 4

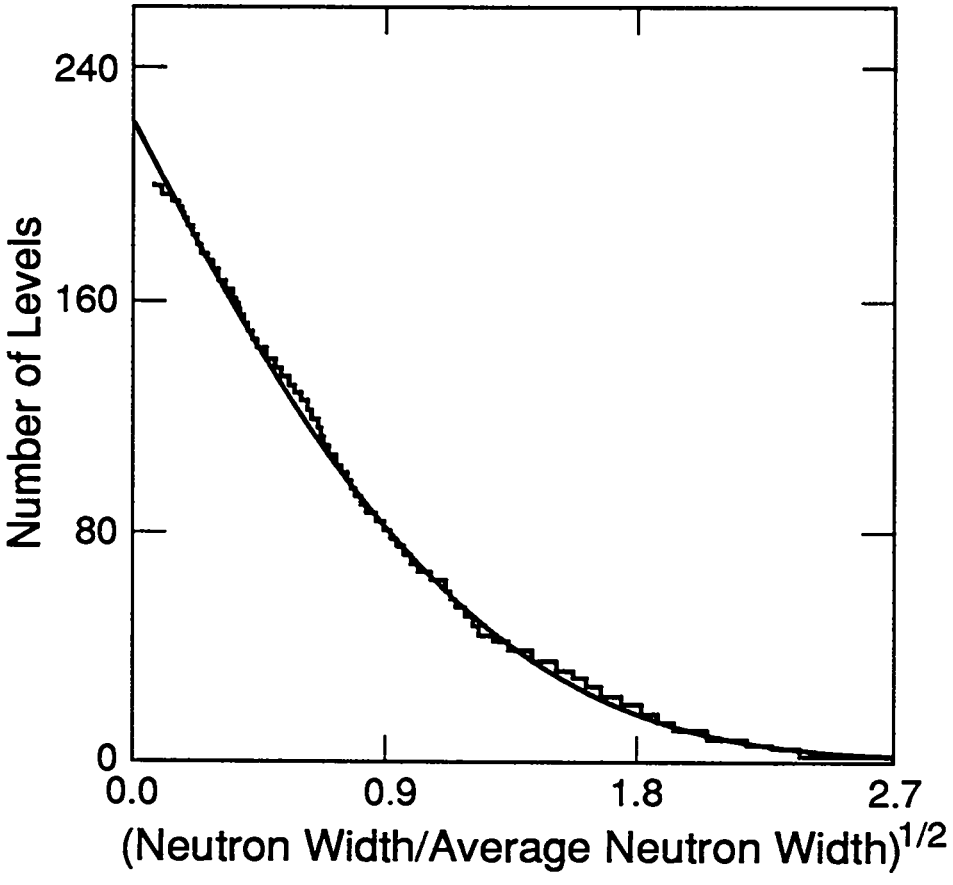
240
160
80
0
Number of Levels
0.0
0.9
1.8
2.7
(Neutron Width/Average Neutron Width)1/2

Fig. IV. 5

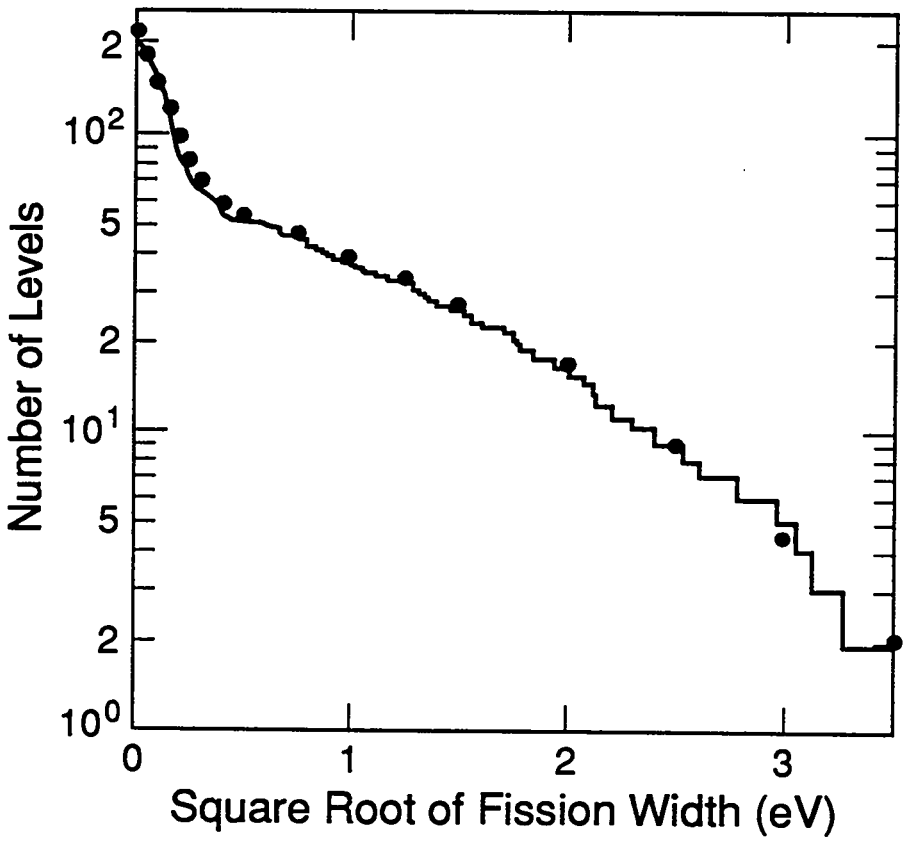
Number of Levels
2
10^2
5
2
10^1
5
2
10^0
0
1
2
3
Square Root of Fission Width (eV)

Fig. IV. 6

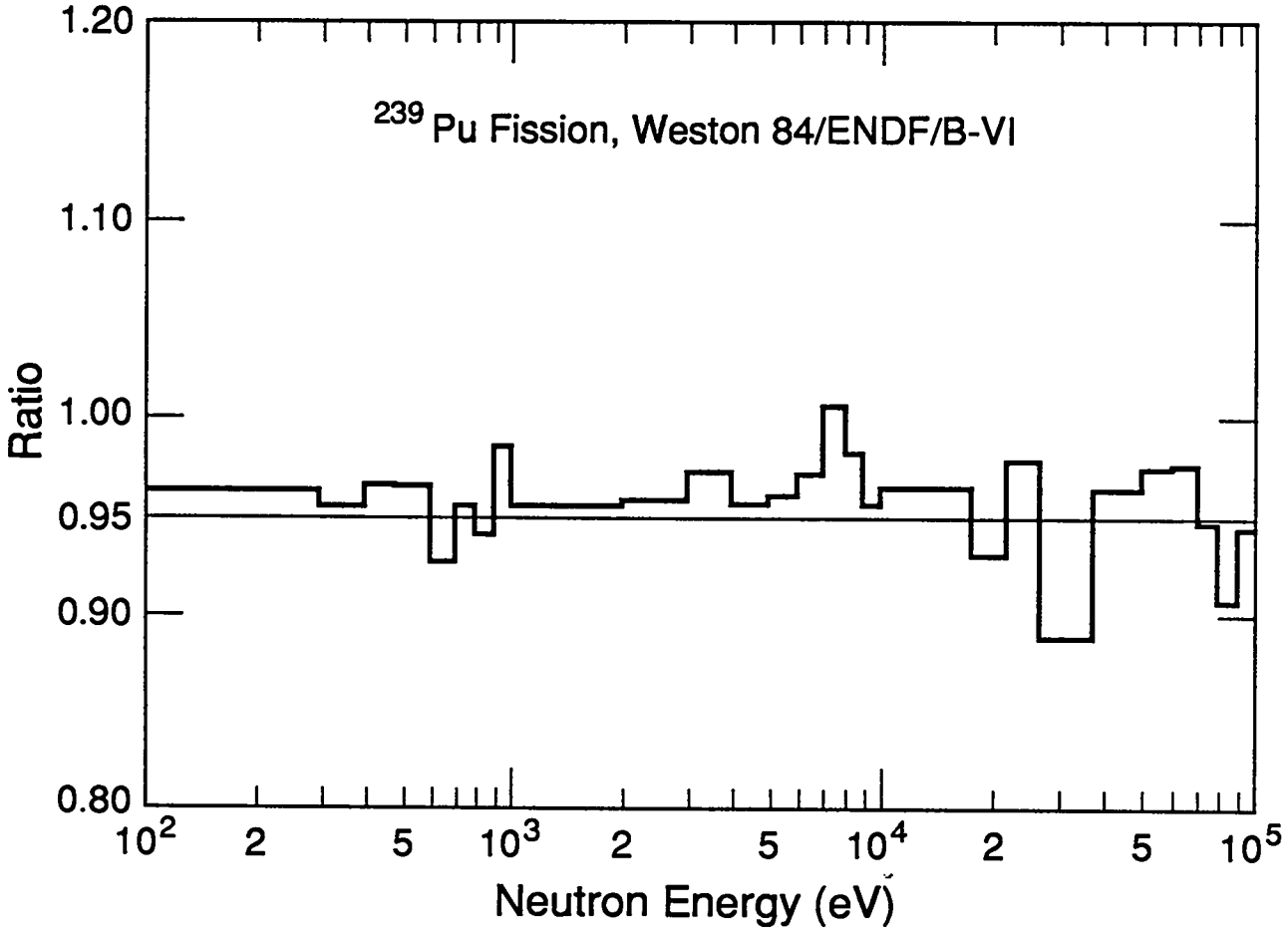
239 Pu Fission, Weston 84/ENDF/B-VI
Ratio
1.20
1.10
1.00
0.95
0.90
0.80
10^2
2
5
10^3
2
5
10^4
2
5
10^5
Neutron Energy (eV)

Fig. IV. 7

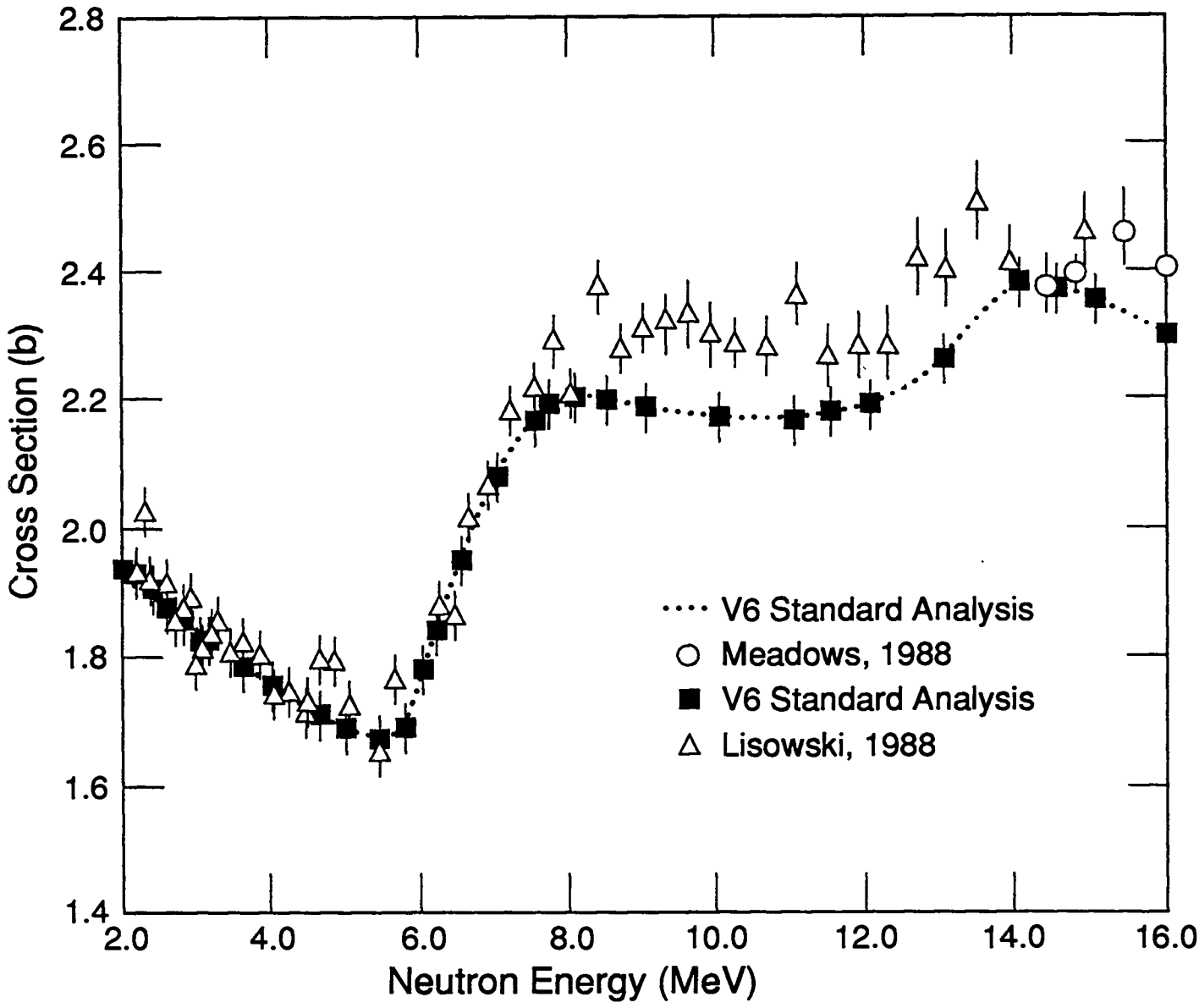
Cross Section (b)
2.8
2.6
2.4
2.2
2.0
1.8
1.6
1.4
2.0
4.0
6.0
8.0
10.0
12.0
14.0
16.0
Neutron Energy (MeV)
V6 Standard Analysis
Meadows, 1988
V6 Standard Analysis
Lisowski, 1988

Fig. IV. 8

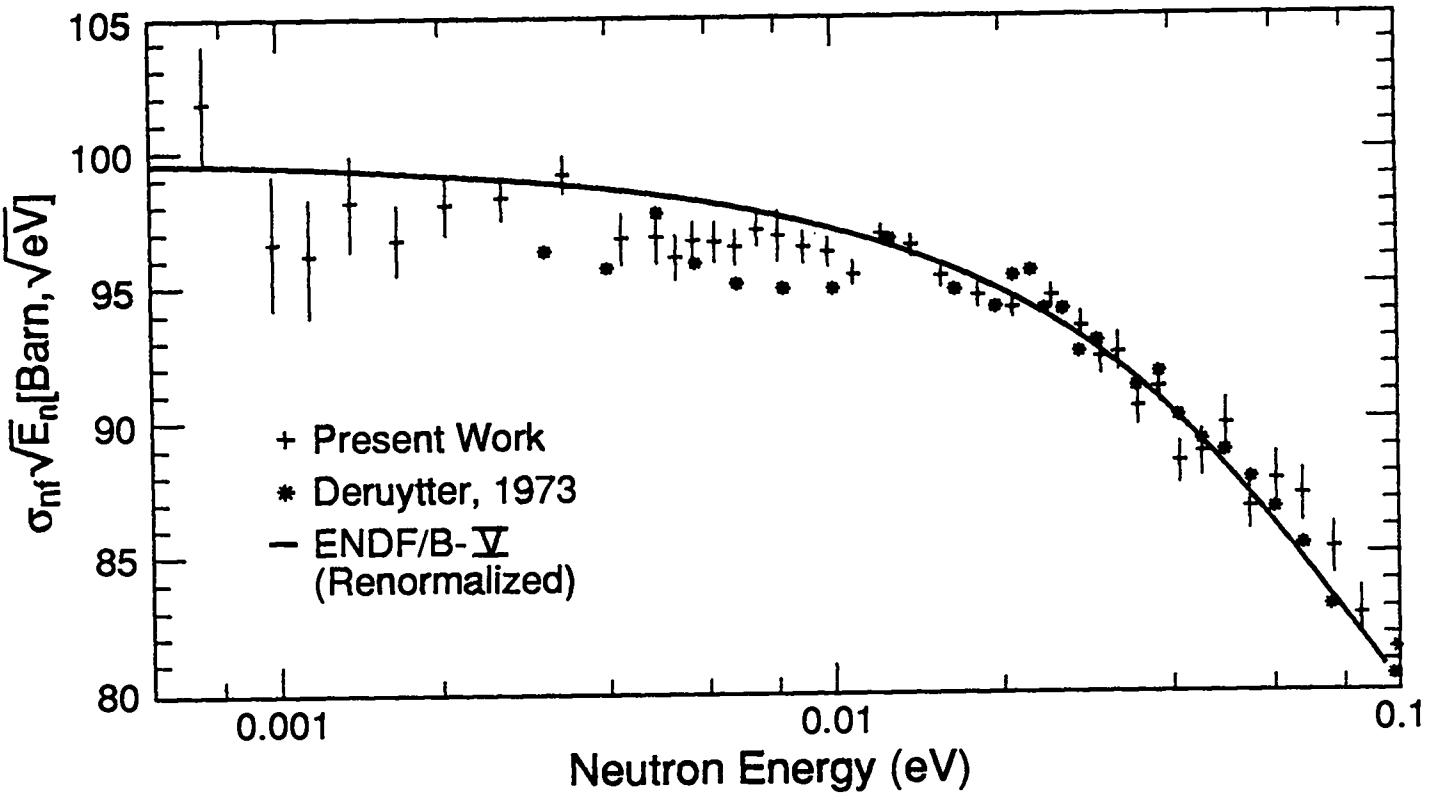
105
100
95
90
85
80
0.001
0.01
0.1
$\sigma_{nf}\sqrt{E_n}$[Barn,$\sqrt{eV}$]
Neutron Energy (eV)
+ Present Work
* Deruytter, 1973
— ENDF/B-V
(Renormalized)

Fig. V. 1

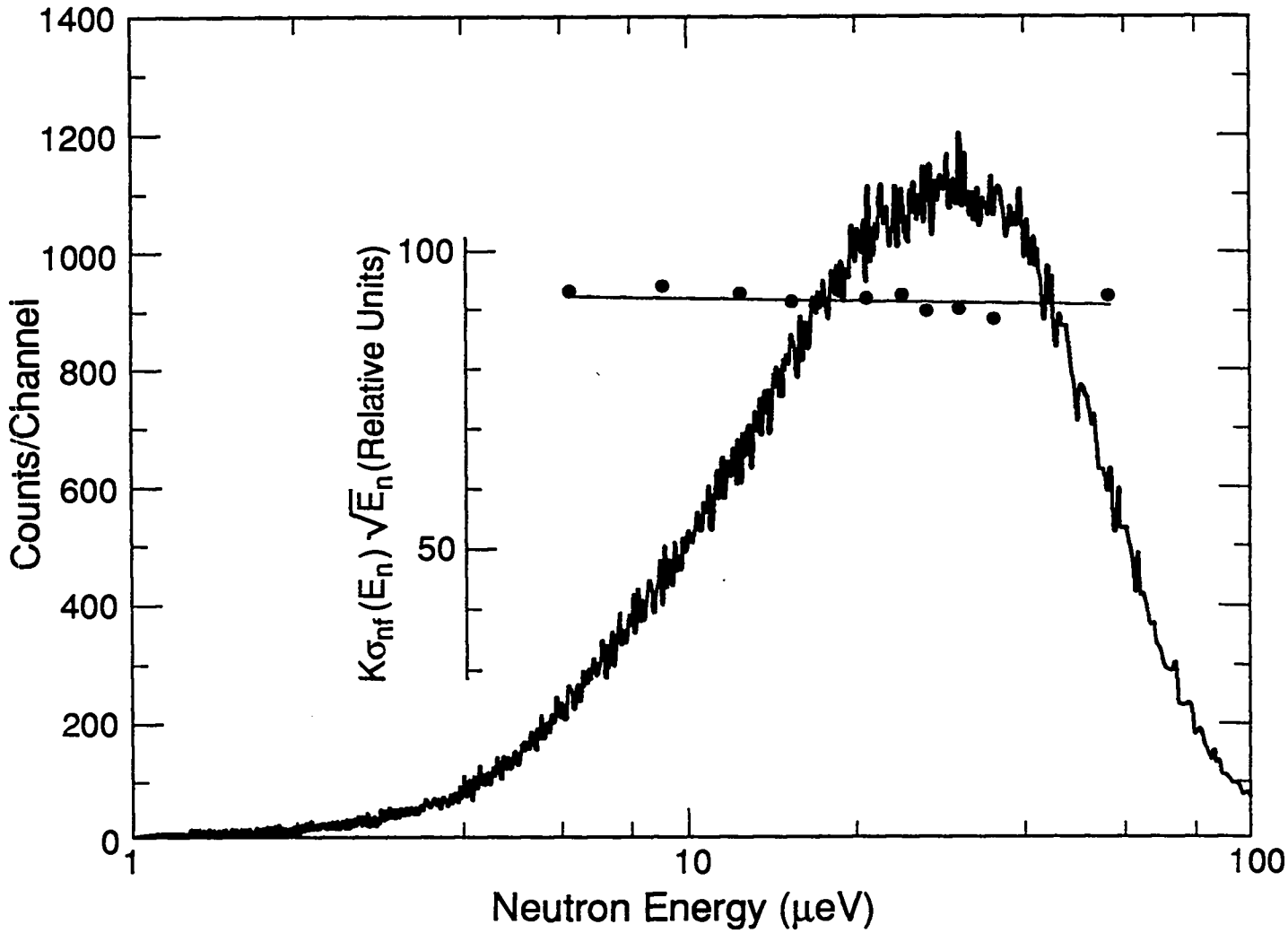
1400
1200
1000
800
600
400
200
0
Counts/Channel
1
10
100
Neutron Energy (μeV)
100
50
$K\sigma_{nf}(E_n)\sqrt{E_n}$ (Relative Units)

Fig. V. 2

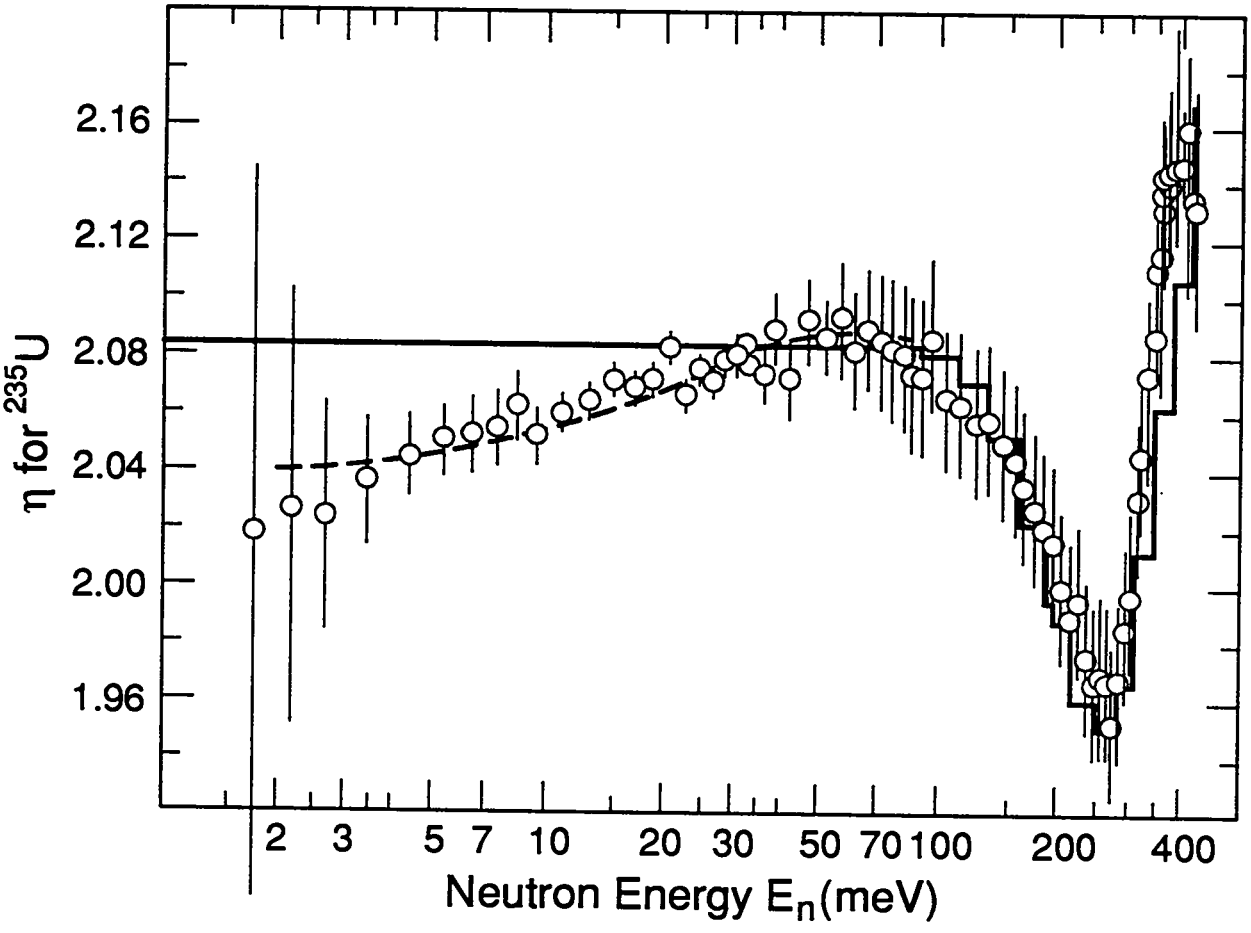
2.16
2.12
2.08
2.04
2.00
1.96
η for ^{235}U
2
3
5
7
10
20
30
50
70
100
200
400
Neutron Energy E_n(meV)

Fig. V. 3

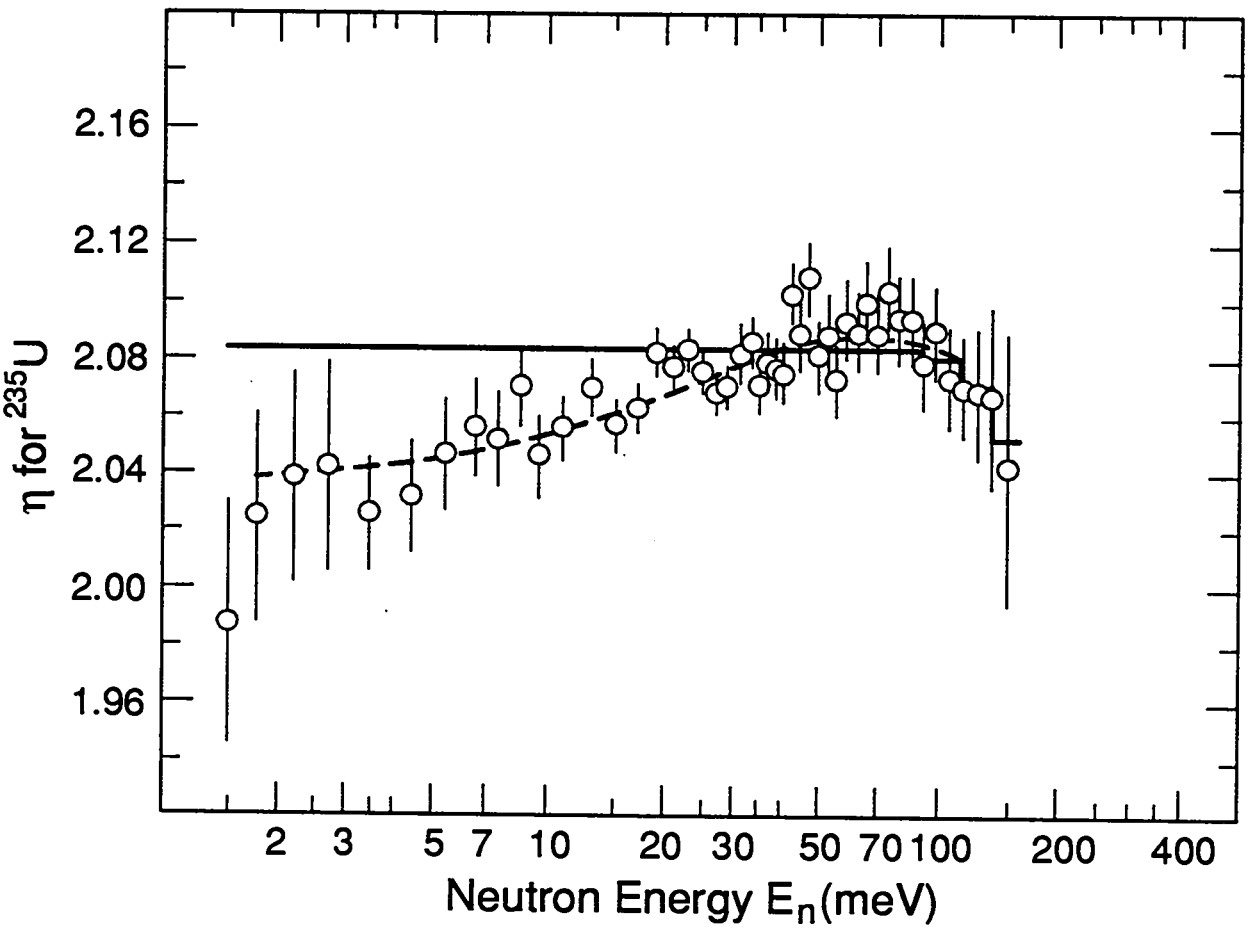
2.16
2.12
2.08
2.04
2.00
1.96
η for ^{235}U
2
3
5
7
10
20
30
50
70
100
200
400
Neutron Energy E_n(meV)

Fig. V. 4

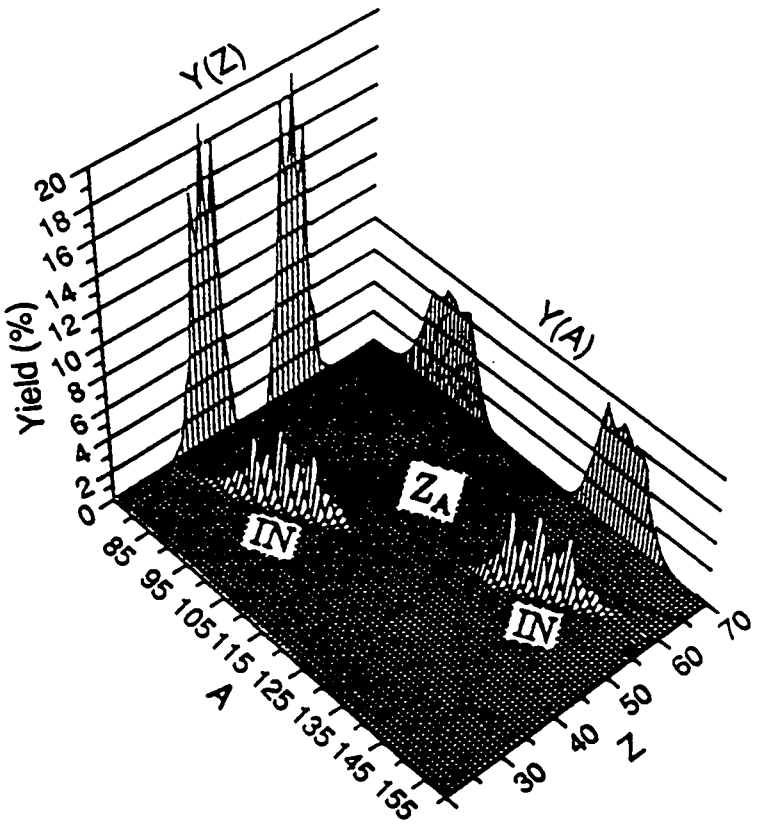
Y(Z)
Y(A)
Yield (%)
0
2
4
6
8
10
12
14
16
18
20
IN
Z_A
IN
85
95
105
115
125
135
145
155
A
30
40
50
60
70
N

Fig. VI. 1

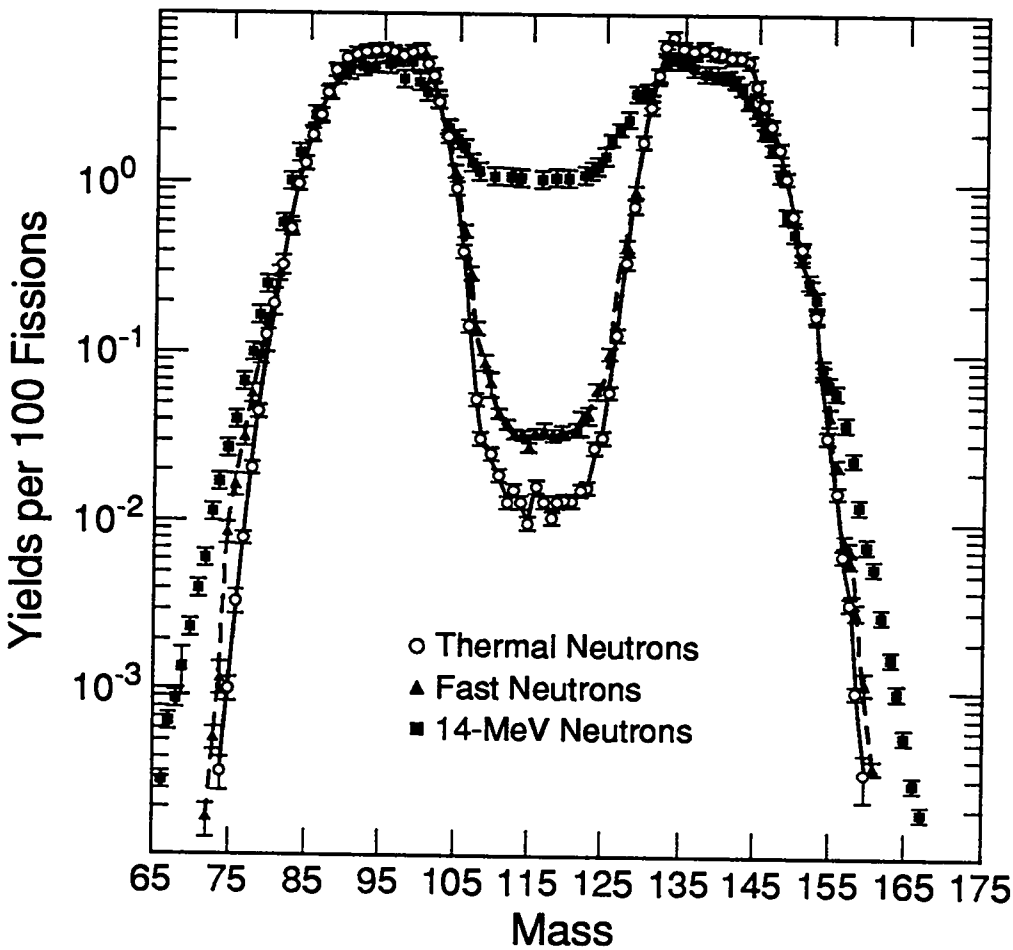
Yields per 100 Fissions
10^0
10^{-1}
10^{-2}
10^{-3}
Thermal Neutrons
Fast Neutrons
14-MeV Neutrons
65 75 85 95 105 115 125 135 145 155 165 175
Mass

Fig. VI. 2

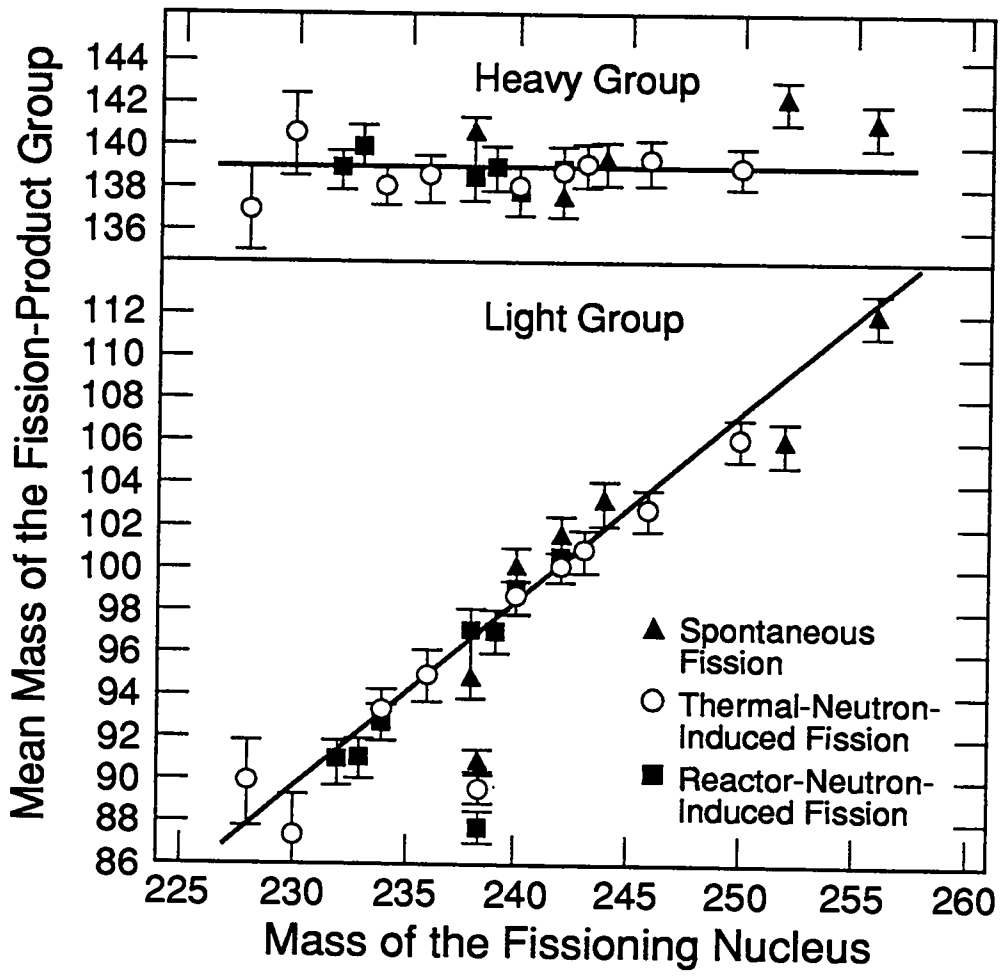
Heavy Group
Light Group
Mean Mass of the Fission-Product Group
Mass of the Fissioning Nucleus
144
142
140
138
136
112
110
108
106
104
102
100
98
96
94
92
90
88
86
225
230
235
240
245
250
255
260
Spontaneous Fission
Thermal-Neutron-Induced Fission
Reactor-Neutron-Induced Fission

Fig. VI. 3

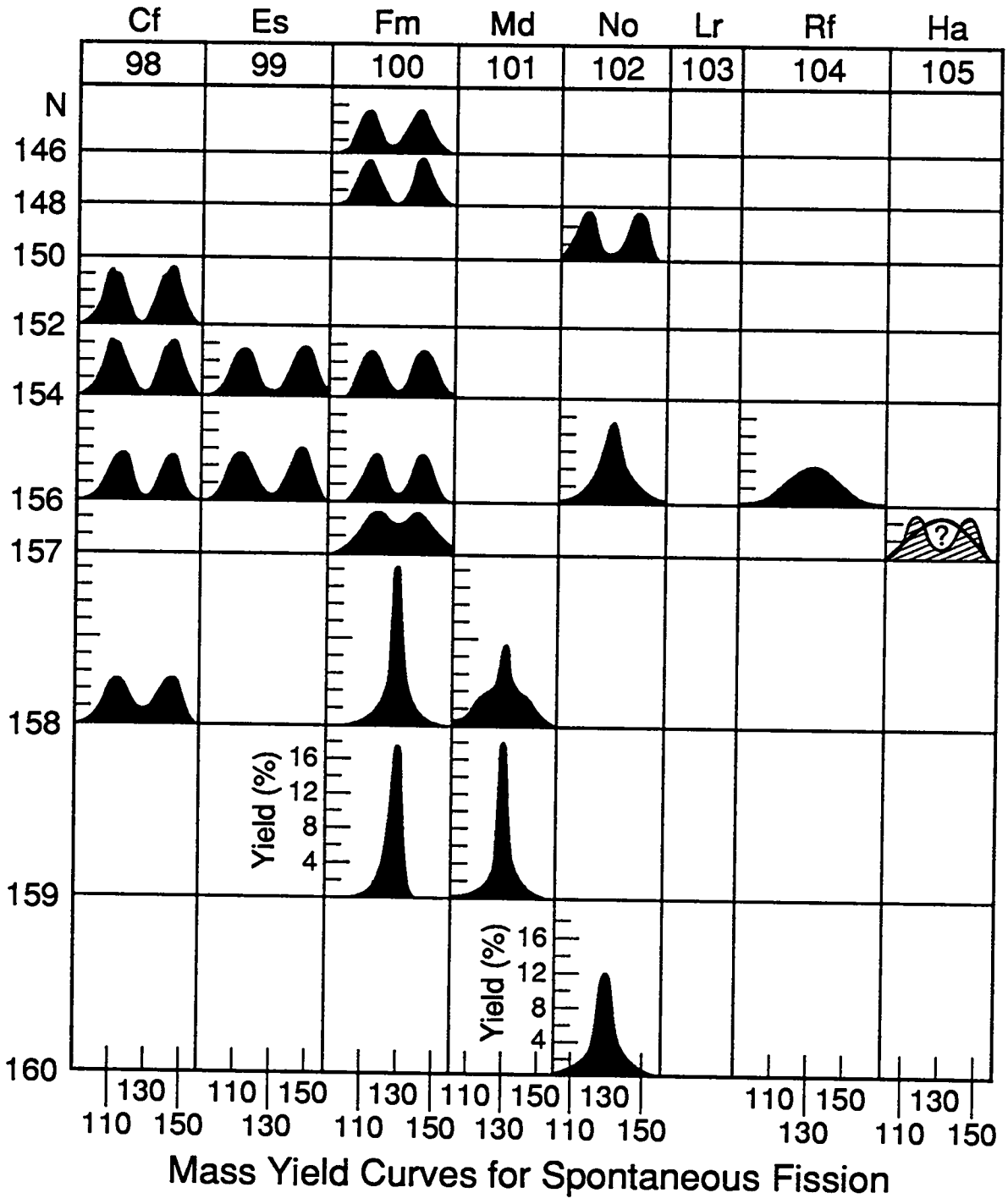
Cf
Es
Fm
Md
No
Lr
Rf
Ha
98
99
100
101
102
103
104
105
N
146
148
150
152
154
156
157
158
159
160
Yield (%)
16
12
8
4
130
110
150
Mass Yield Curves for Spontaneous Fission

Fig. VI. 4

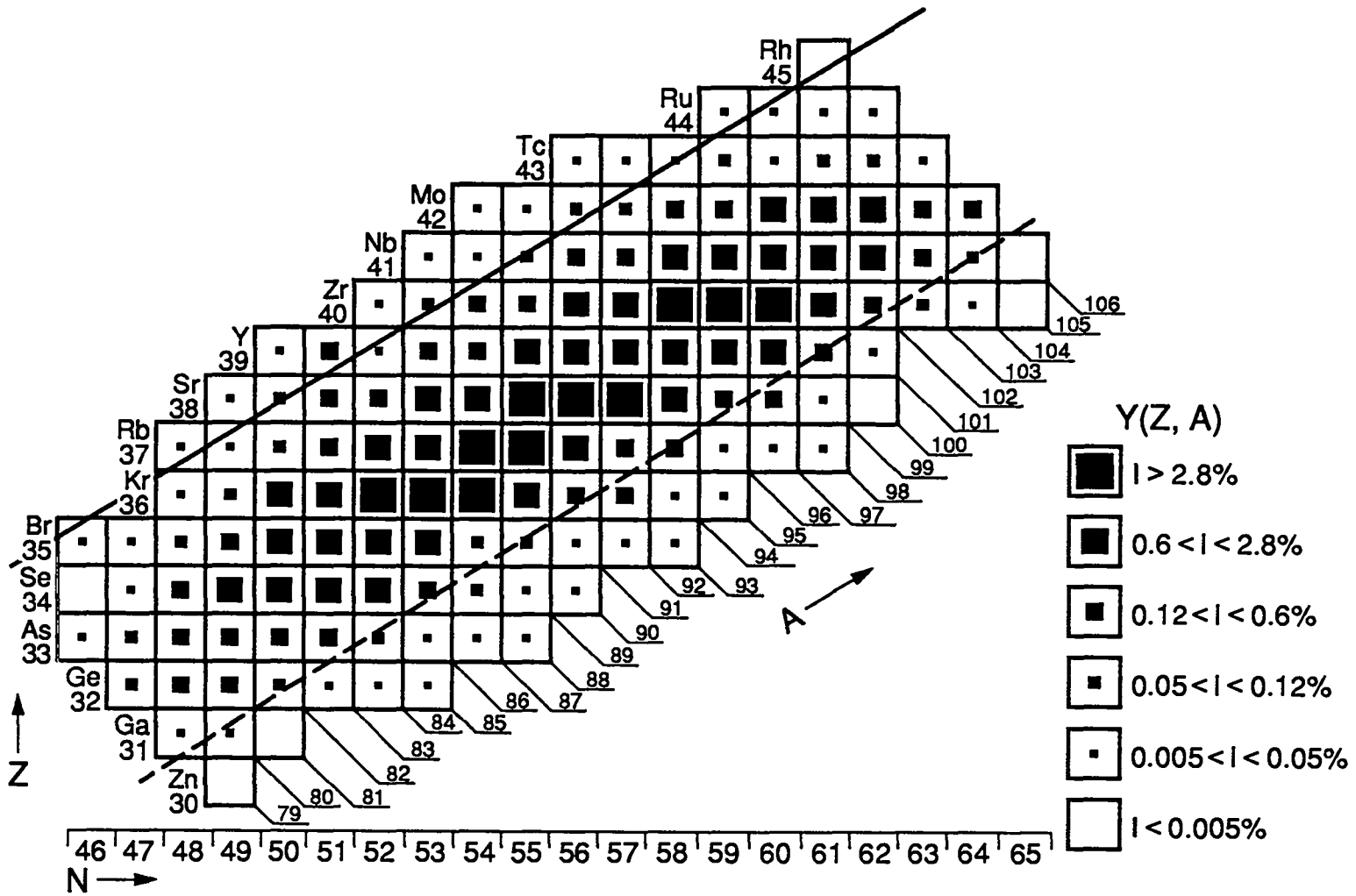
Rh 45
Ru 44
Tc 43
Mo 42
Nb 41
Zr 40
Y 39
Sr 38
Rb 37
Kr 36
Br 35
Se 34
As 33
Ge 32
Ga 31
Zn 30
79
80
81
82
83
84
85
86
87
88
89
90
91
92
93
94
95
96
97
98
99
100
101
102
103
104
105
106
A
Z
N
46 47 48 49 50 51 52 53 54 55 56 57 58 59 60 61 62 63 64 65
Y(Z, A)
I > 2.8%
0.6 < I < 2.8%
0.12 < I < 0.6%
0.05 < I < 0.12%
0.005 < I < 0.05%
I < 0.005%

Fig. VI. 5

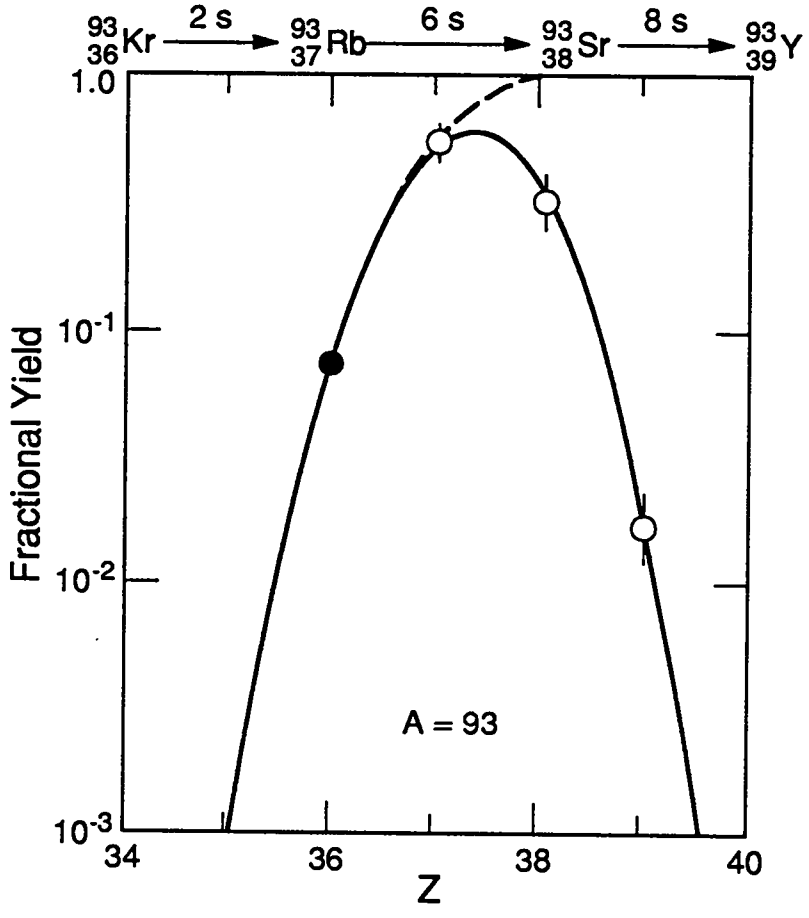
93 36 Kr
2 s
93 37 Rb
6 s
93 38 Sr
8 s
93 39 Y
1.0
10-1
10-2
10-3
Fractional Yield
A = 93
34
36
38
40
Z

Fig. VI. 6

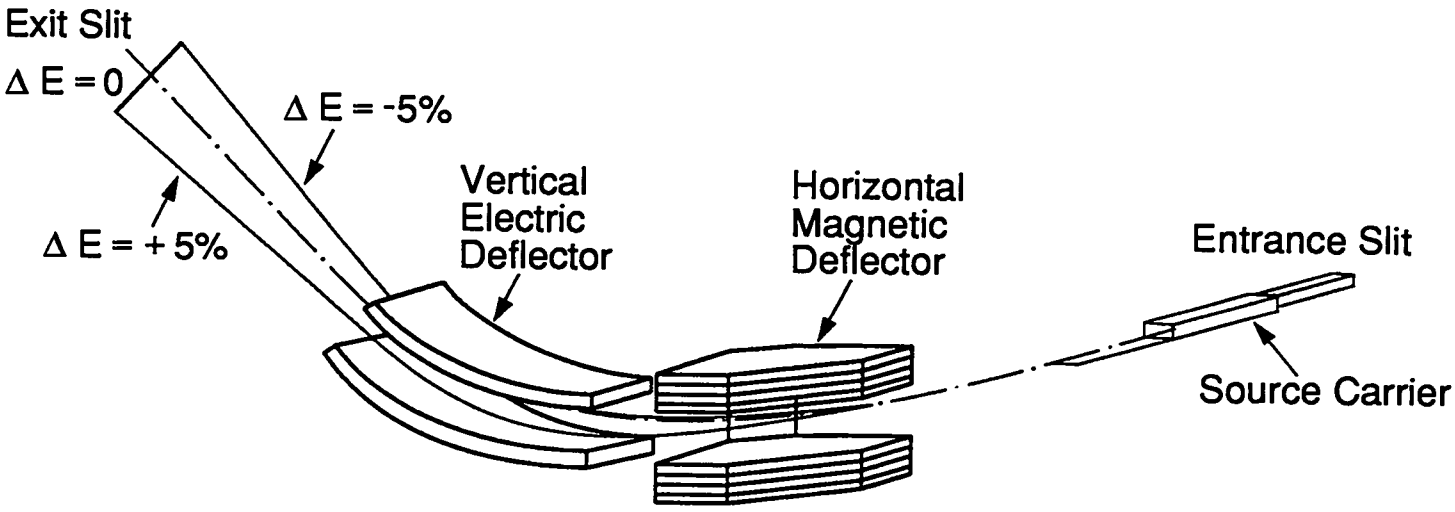
Exit Slit
Δ E = 0
Δ E = -5%
Δ E = + 5%
Vertical
Electric
Deflector
Horizontal
Magnetic
Deflector
Entrance Slit
Source Carrier

Fig. VI. 7

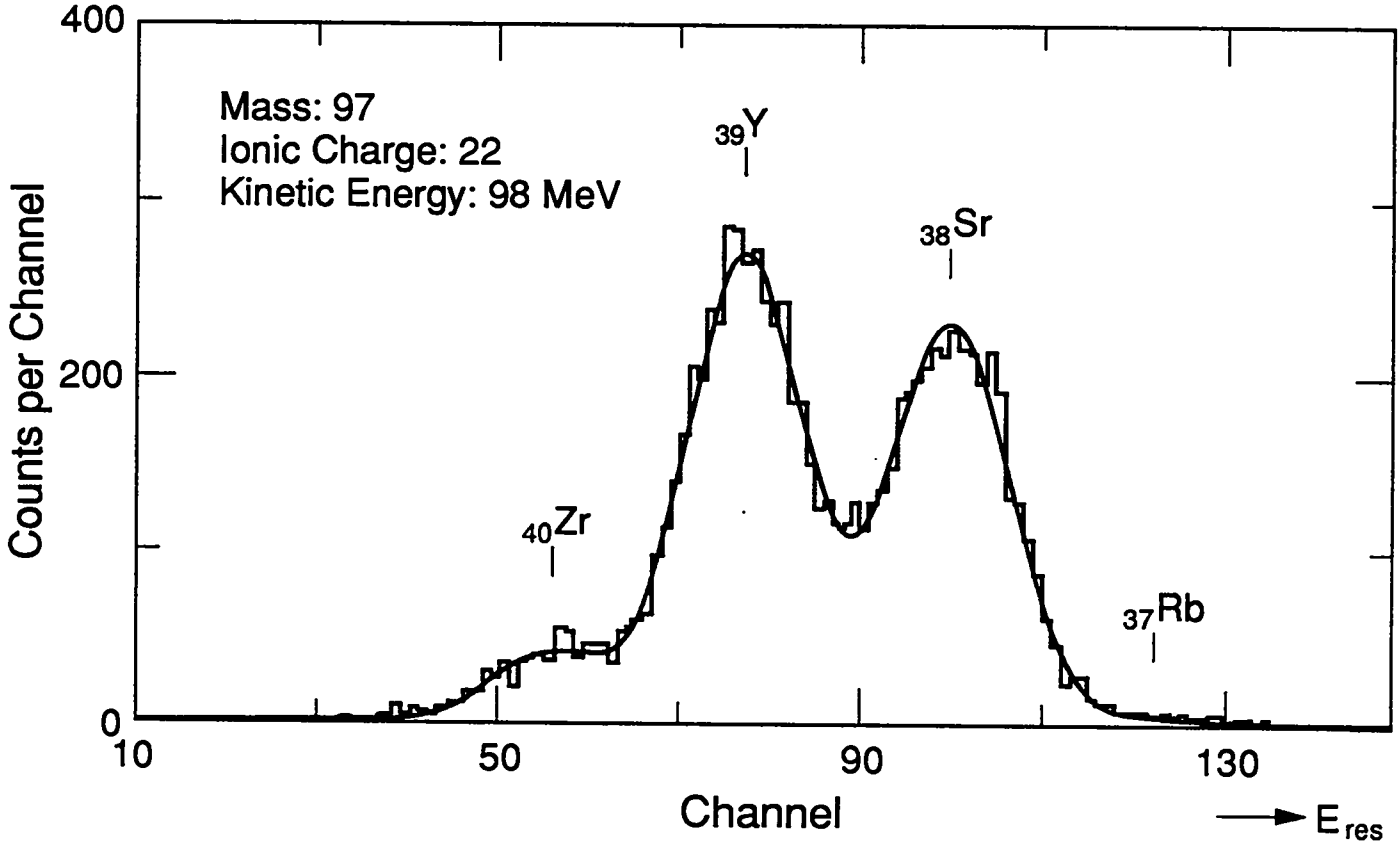
Mass: 97
Ionic Charge: 22
Kinetic Energy: 98 MeV
39Y
38Sr
40Zr
37Rb
Counts per Channel
400
200
0
10
50
90
130
Channel
Eres

Fig. VI. 8

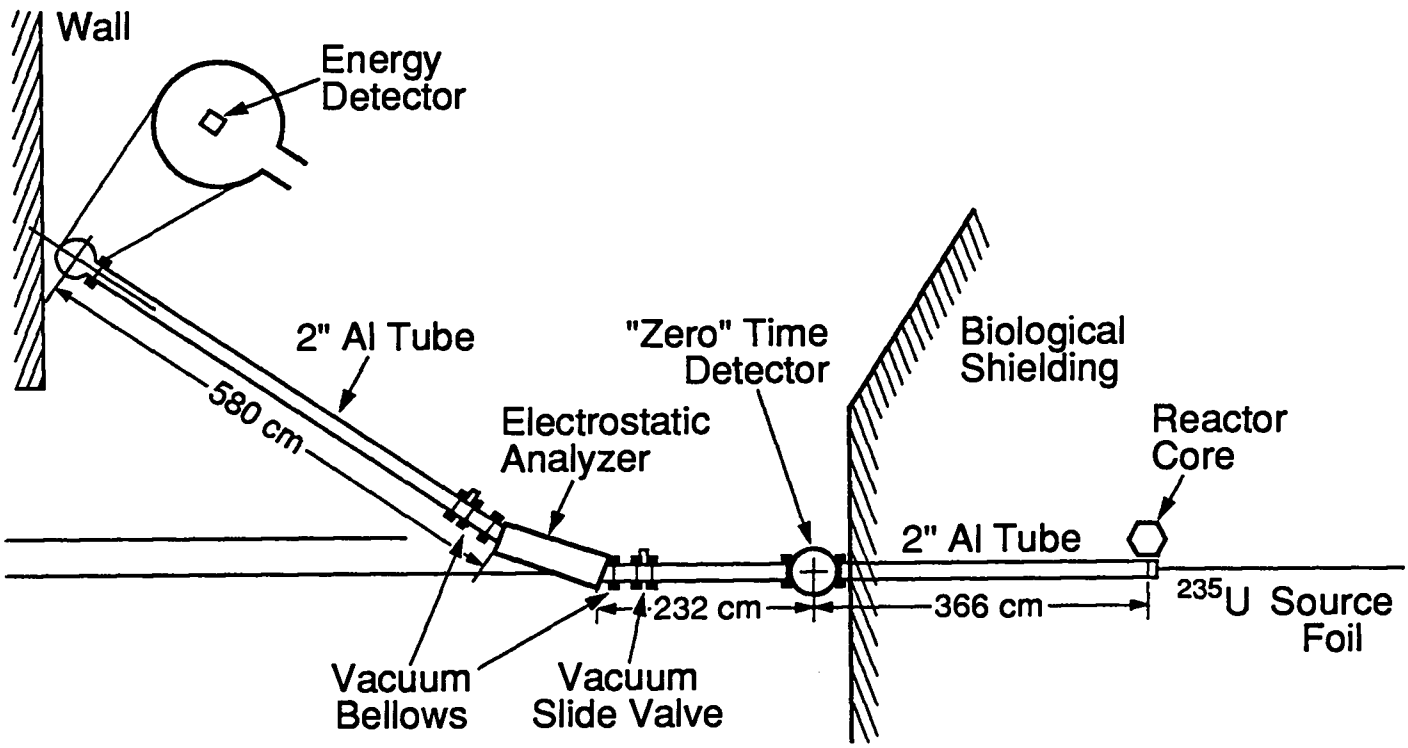
Wall
Energy Detector
2" Al Tube
580 cm
"Zero" Time Detector
Biological Shielding
Electrostatic Analyzer
Reactor Core
2" Al Tube
232 cm
366 cm
^{235}U Source Foil
Vacuum Bellows
Vacuum Slide Valve

Fig. VI. 9

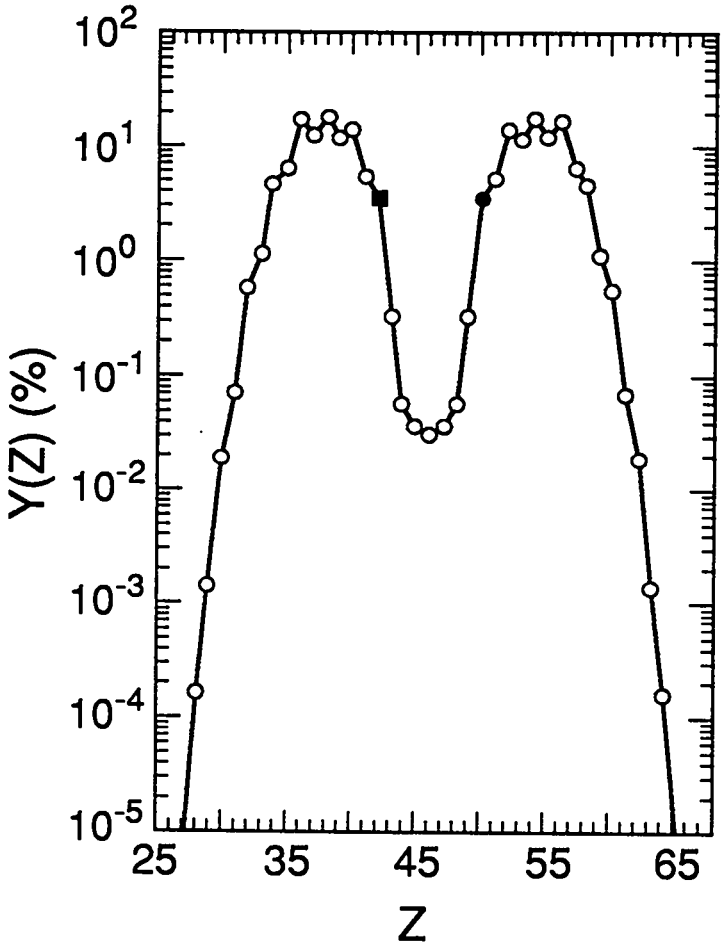

Fig. VI. 10

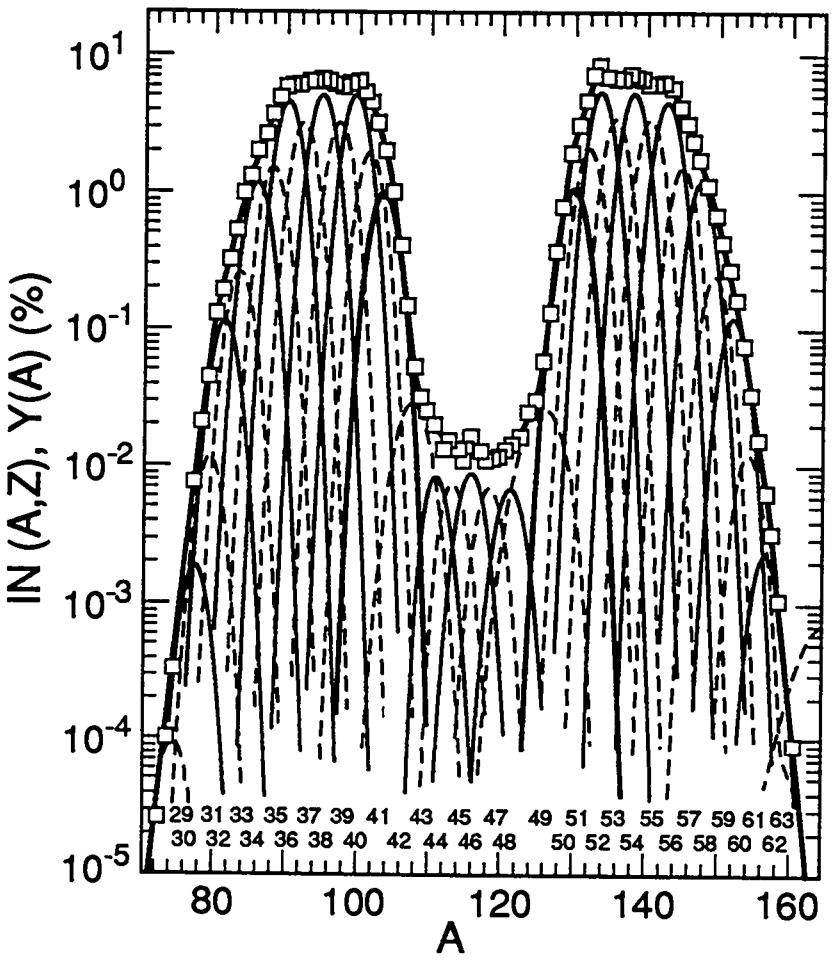
IN (A,Z), Y(A) (%)
10^1
10^0
10^-1
10^-2
10^-3
10^-4
10^-5
29 31 33 35 37 39 41 43 45 47 49 51 53 55 57 59 61 63
30 32 34 36 38 40 42 44 46 48 50 52 54 56 58 60 62
80
100
120
140
160
A

Fig. VI. 11

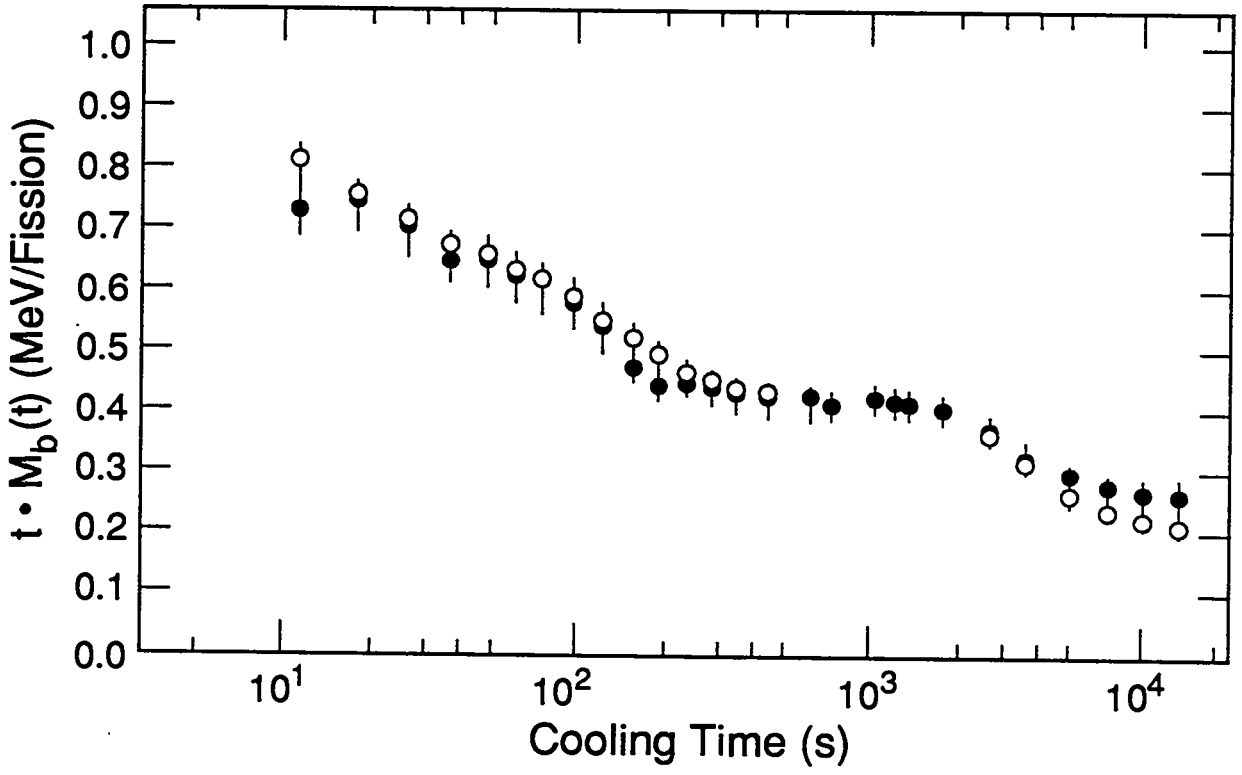
1.0
0.9
0.8
0.7
0.6
0.5
0.4
0.3
0.2
0.1
0.0
t • M_b(t) (MeV/Fission)
10^1
10^2
10^3
10^4
Cooling Time (s)

Fig. VII. 1

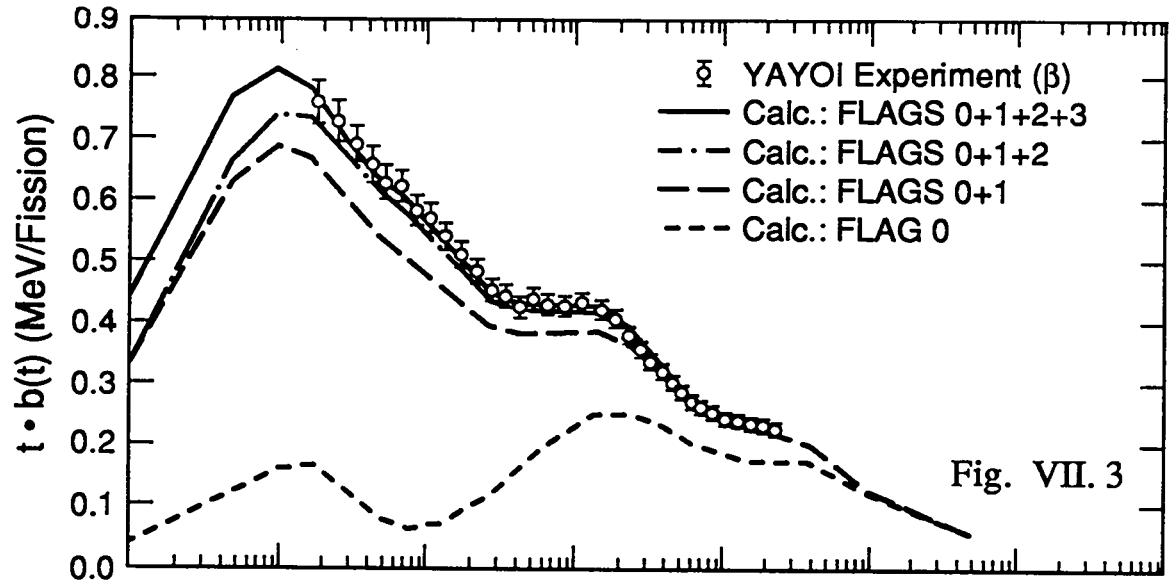

Fig. VII. 3

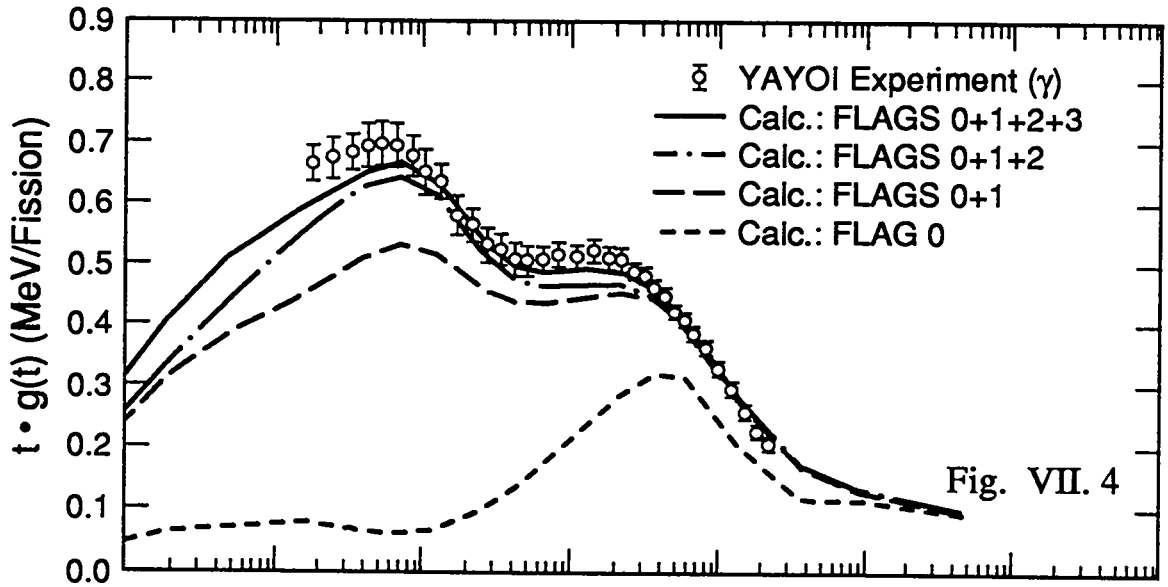

Fig. VII. 4

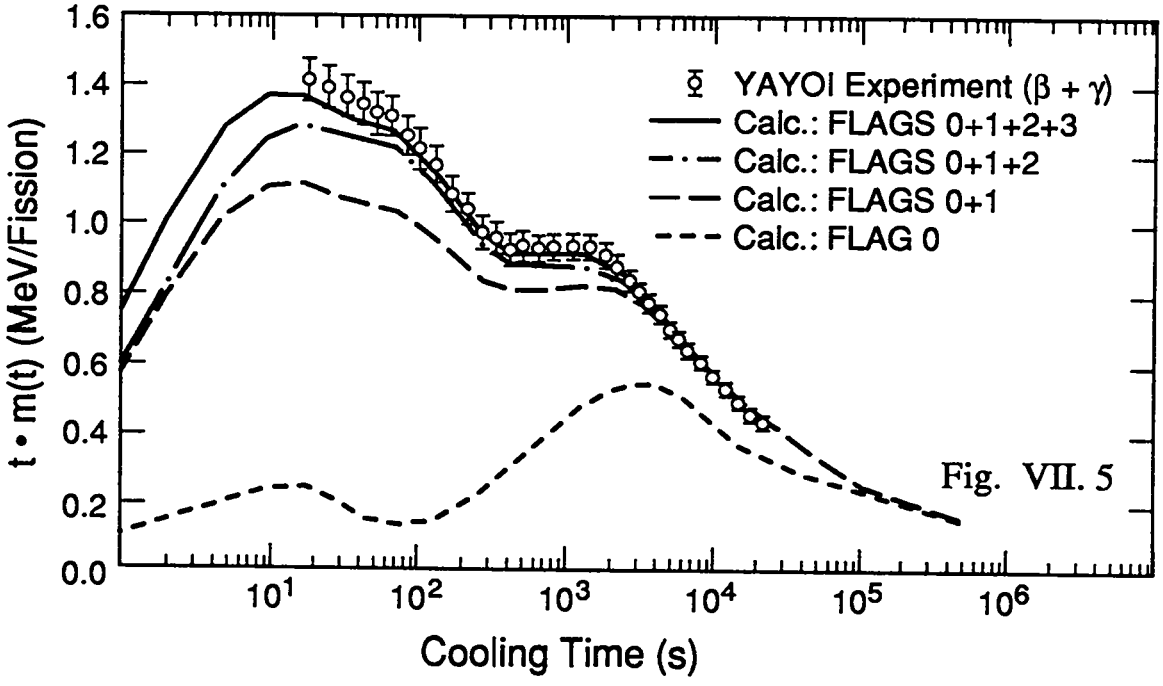

Fig. VII. 5

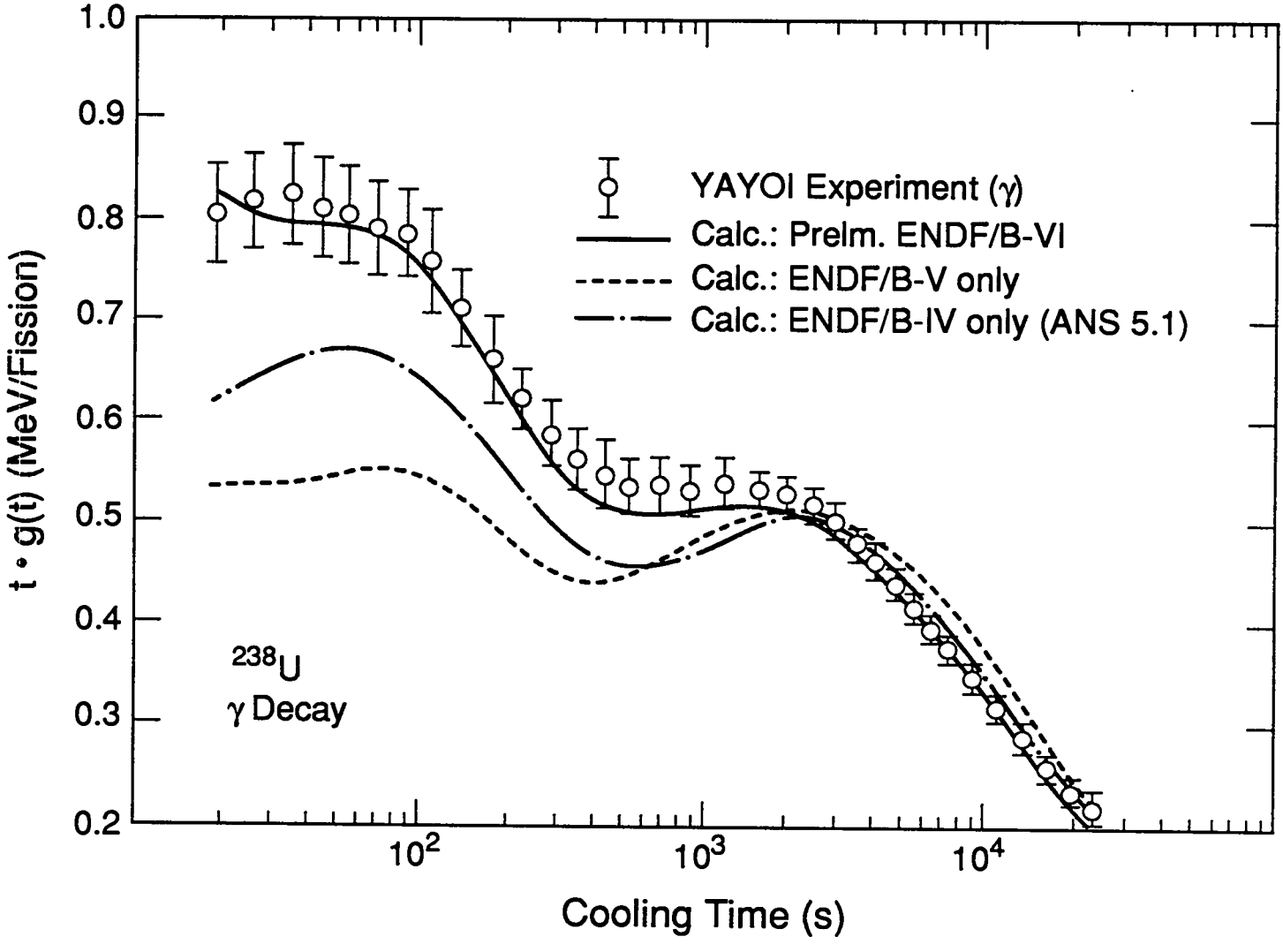
1.0
0.9
0.8
0.7
0.6
0.5
0.4
0.3
0.2
t • g(t) (MeV/Fission)
YAYOI Experiment (γ)
Calc.: Prelm. ENDF/B-VI
Calc.: ENDF/B-V only
Calc.: ENDF/B-IV only (ANS 5.1)
238U
γ Decay
10^2
10^3
10^4
Cooling Time (s)

Fig. VII. 6

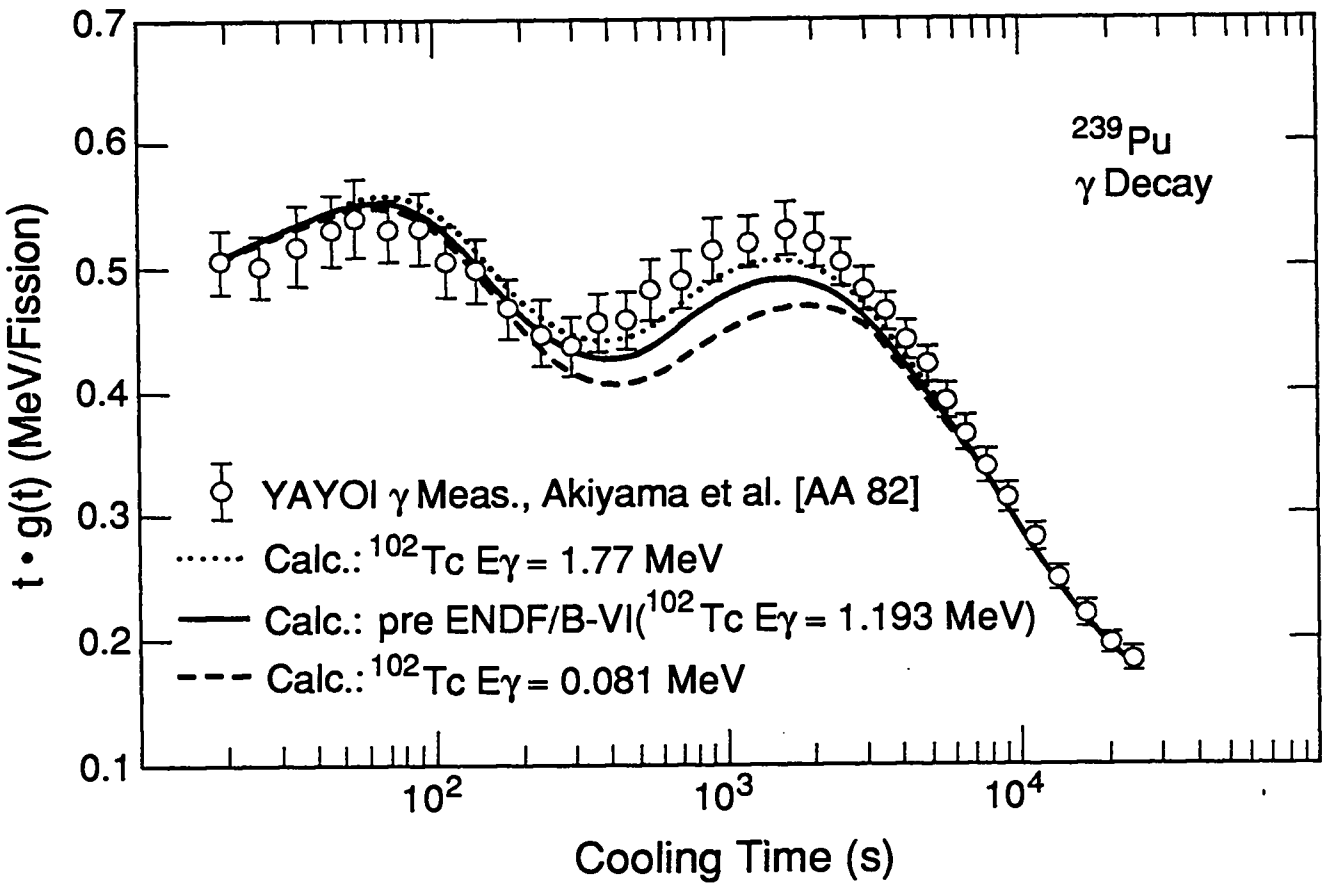
0.7
0.6
0.5
0.4
0.3
0.2
0.1
t • g(t) (MeV/Fission)
239Pu
γ Decay
YAYOI γ Meas., Akiyama et al. [AA 82]
Calc.: 102Tc Eγ = 1.77 MeV
Calc.: pre ENDF/B-VI(102Tc Eγ = 1.193 MeV)
Calc.: 102Tc Eγ = 0.081 MeV
10^2
10^3
10^4
Cooling Time (s)

Fig. VII. 7

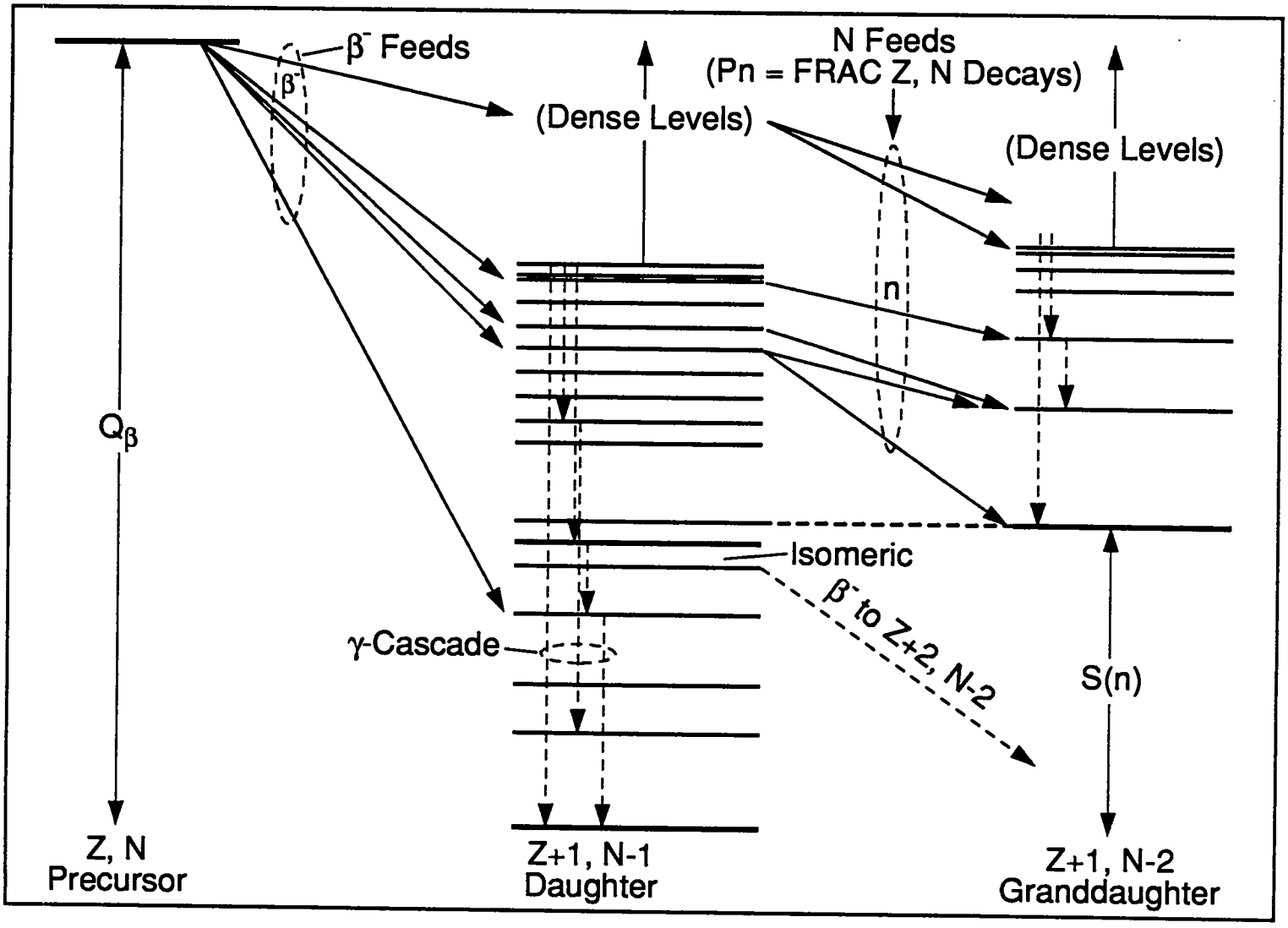
β⁻ Feeds
β⁻
N Feeds
(Pn = FRAC Z, N Decays)
(Dense Levels)
(Dense Levels)
n
Qβ
Isomeric
β⁻ to Z+2, N-2
γ-Cascade
S(n)
Z, N
Precursor
Z+1, N-1
Daughter
Z+1, N-2
Granddaughter

Fig. VIII. 1

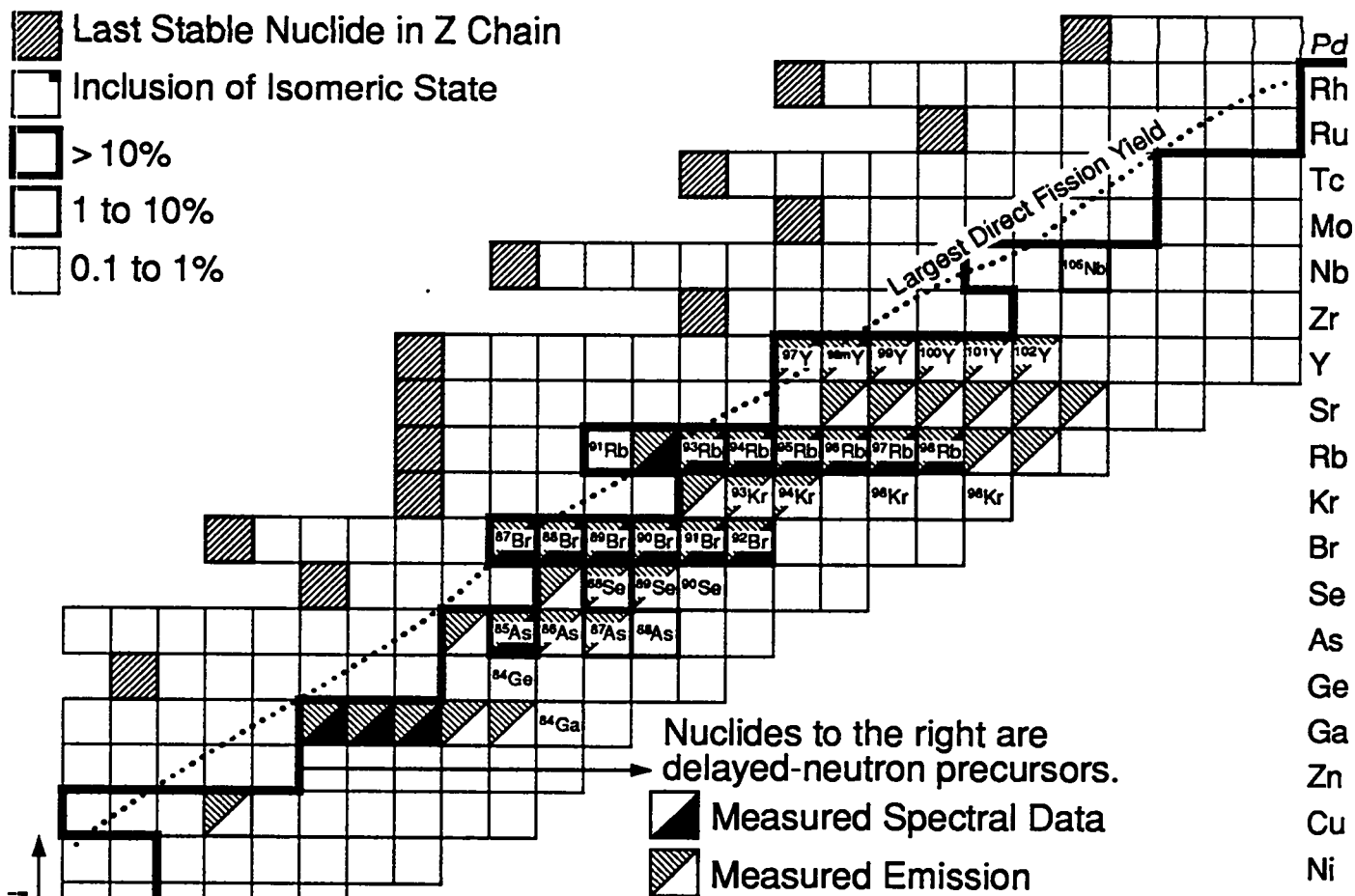
Last Stable Nuclide in Z Chain
Inclusion of Isomeric State
> 10%
1 to 10%
0.1 to 1%
Largest Direct Fission Yield
Nuclides to the right are delayed-neutron precursors.
Measured Spectral Data
Measured Emission Probability, Pn
Z
N
Pd
Rh
Ru
Tc
Mo
Nb
Zr
Y
Sr
Rb
Kr
Br
Se
As
Ge
Ga
Zn
Cu
Ni
Co

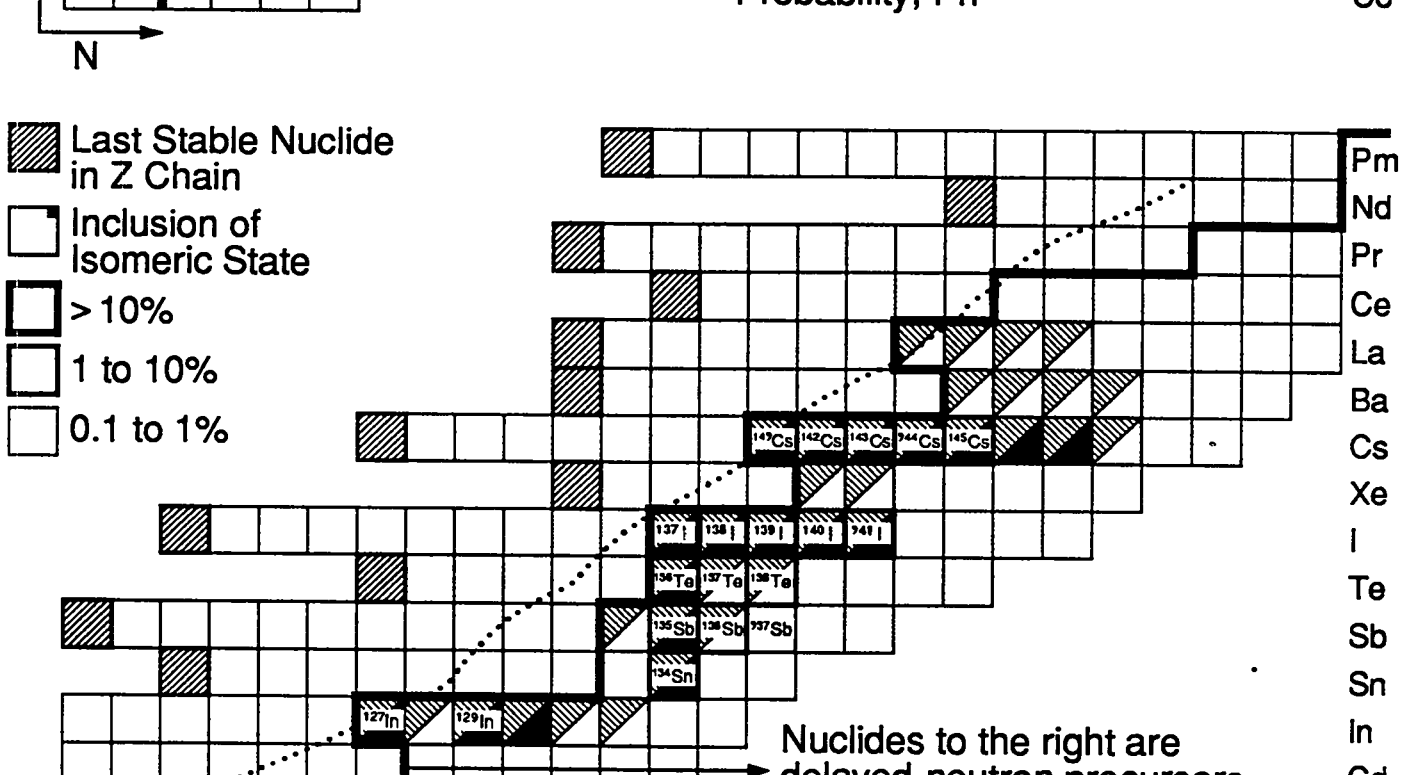
Last Stable Nuclide in Z Chain
Inclusion of Isomeric State
> 10%
1 to 10%
0.1 to 1%
Nuclides to the right are delayed-neutron precursors.
Measured Spectral Data
Measured Emission Probability, Pn
Z
N
Pm
Nd
Pr
Ce
La
Ba
Cs
Xe
I
Te
Sb
Sn
In
Cd
Ag
Pd

Fig. VIII. 2

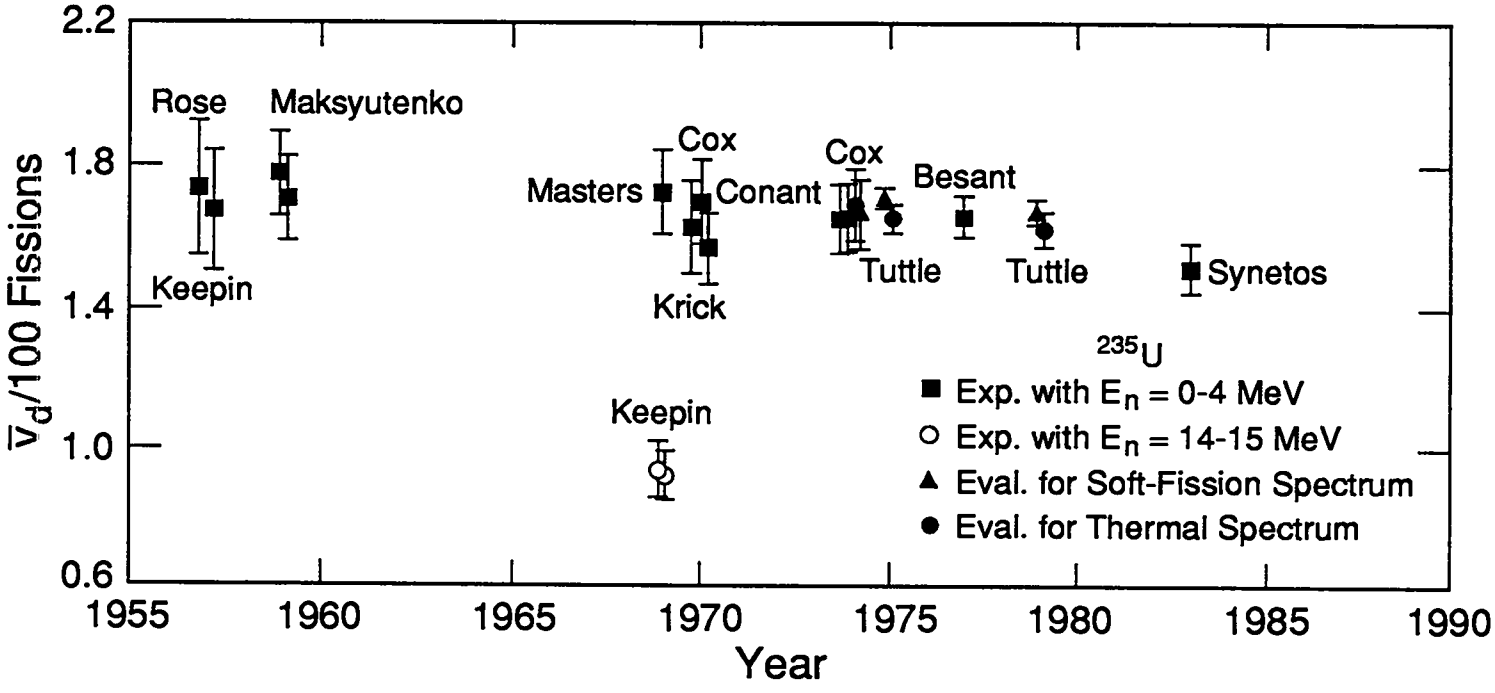
2.2
1.8
1.4
1.0
0.6
$\bar{\nu}_d$/100 Fissions
1955
1960
1965
1970
1975
1980
1985
1990
Year
Rose
Maksyutenko
Keepin
Masters
Cox
Conant
Krick
Cox
Tuttle
Besant
Tuttle
Synetos
Keepin
^{235}U
Exp. with E_n = 0-4 MeV
Exp. with E_n = 14-15 MeV
Eval. for Soft-Fission Spectrum
Eval. for Thermal Spectrum

Fig. VIII. 3

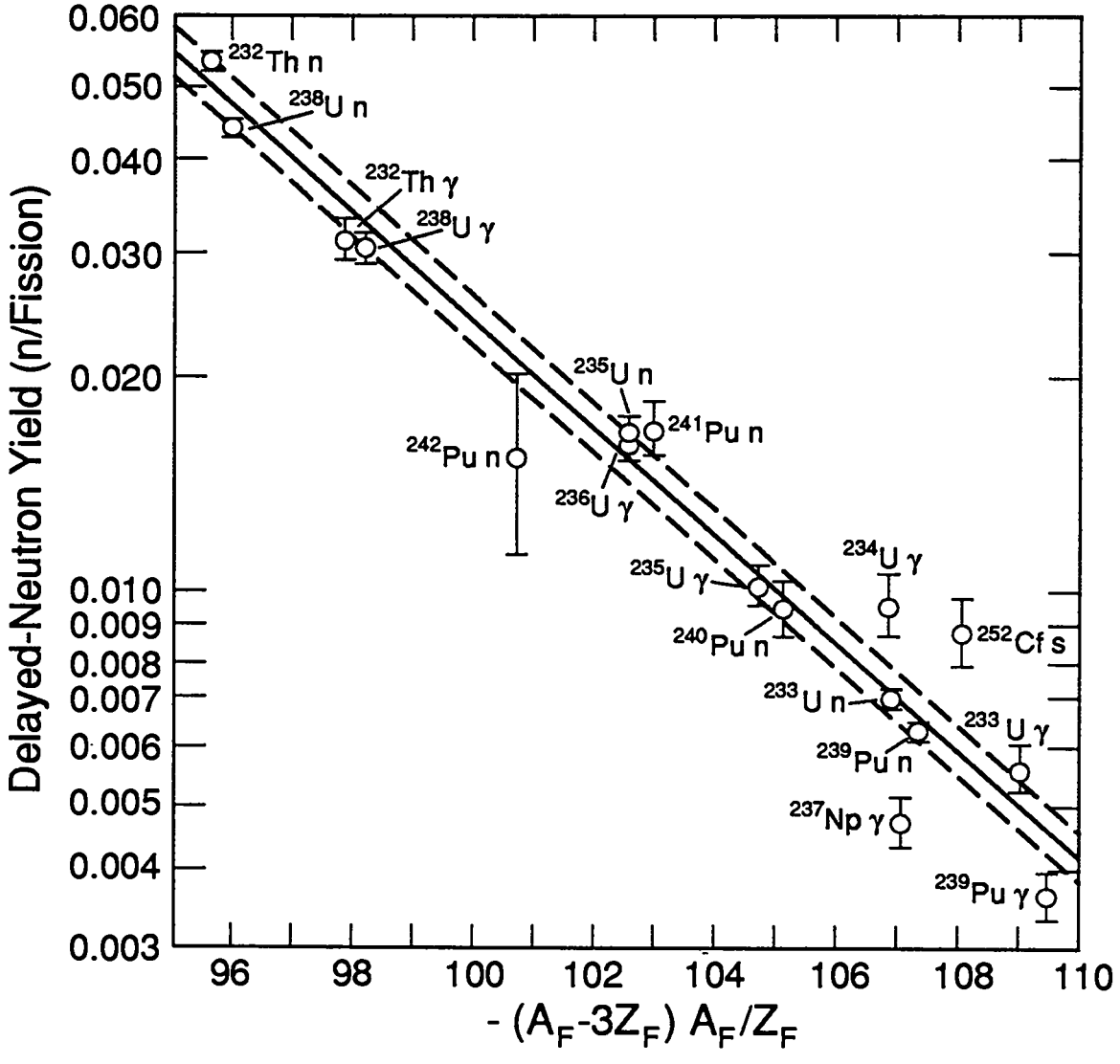
Delayed-Neutron Yield (n/Fission)
0.060
0.050
0.040
0.030
0.020
0.010
0.009
0.008
0.007
0.006
0.005
0.004
0.003
96
98
100
102
104
106
108
110
- (A_F-3Z_F) A_F/Z_F
232Th n
238U n
232Th γ
238U γ
235U n
241Pu n
242Pu n
236U γ
234U γ
235U γ
240Pu n
252Cf s
233U n
233U γ
239Pu n
237Np γ
239Pu γ

Fig. VIII. 4

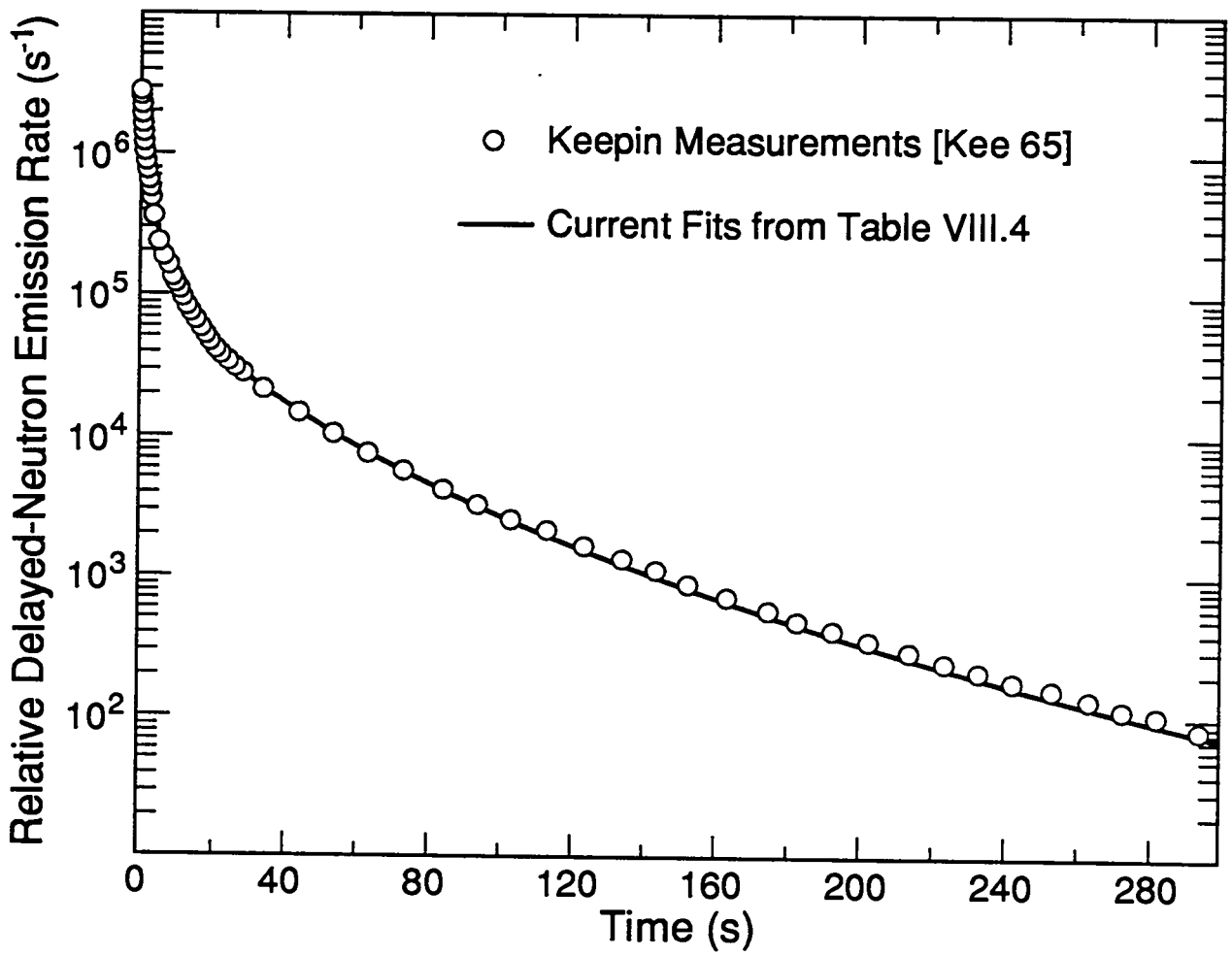
Relative Delayed-Neutron Emission Rate (s^{-1})
10^6
10^5
10^4
10^3
10^2
Keepin Measurements [Kee 65]
Current Fits from Table VIII.4
0
40
80
120
160
200
240
280
Time (s)

Fig. VIII. 5

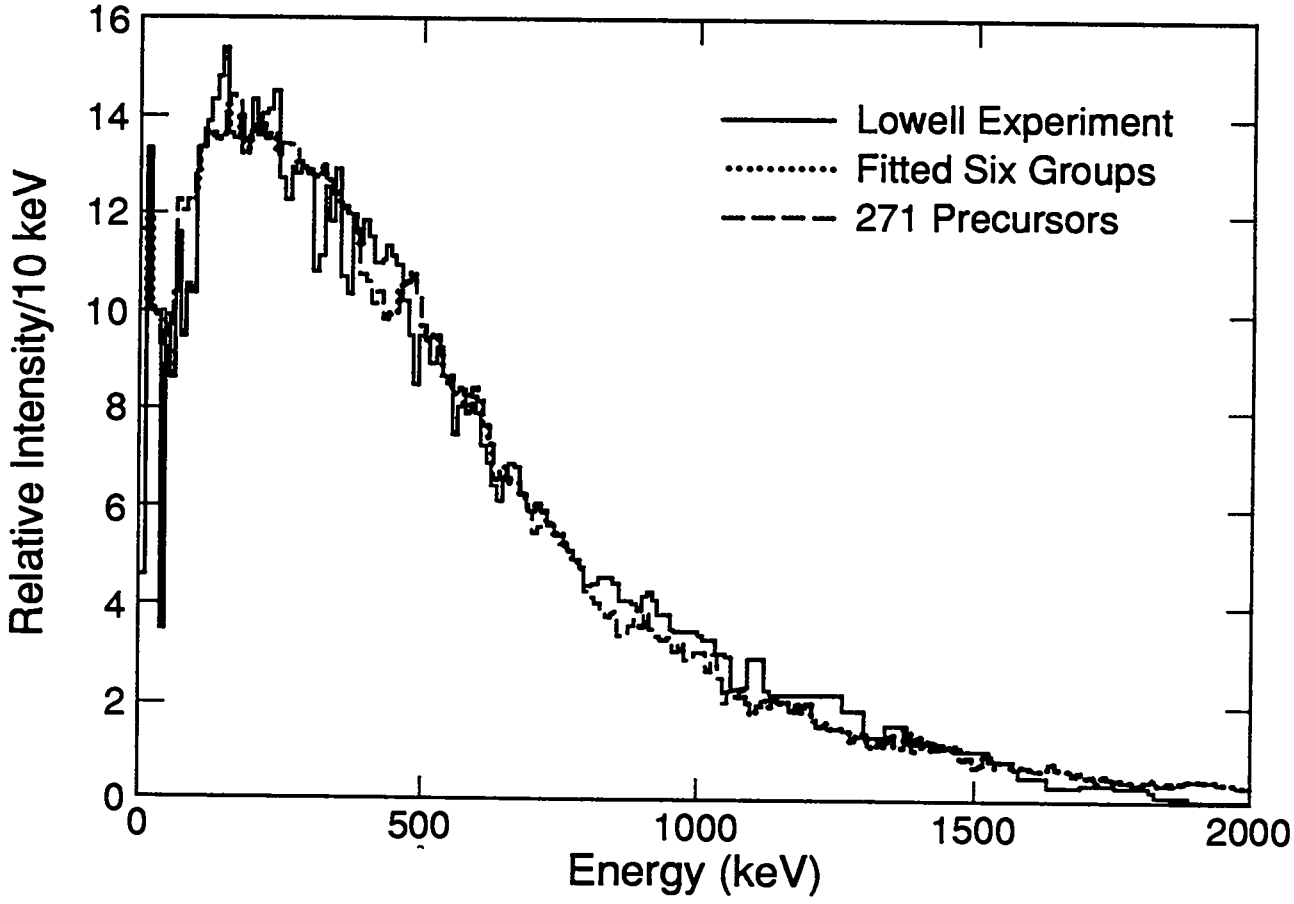
Relative Intensity/10 keV
Energy (keV)
Lowell Experiment
Fitted Six Groups
271 Precursors
0
2
4
6
8
10
12
14
16
0
500
1000
1500
2000

Fig. VIII. 6